UNIVERSIDADE DE LISBOA
FACULDADE DE CIÊNCIAS
DEPARTAMENTO DE GEOLOGIA

Factors impacting multi-layer plume distribution in CO_2 storage reservoirs

Andrea Callioli Santi

Mestrado em Geologia
Especialização em Estratigrafia, Sedimentologia e Paleontologia

Dissertação orientada por:
Professor Doutor Nuno Lamas de Almeida Pimentel
Dr. Philip Ringrose, Equinor Energy AS, Norway

2018

Acknowledgements

First of all I wish to express my deepest gratitude to Philip Ringrose for the incredible opportunity of developing a master's thesis with Equinor in such an exciting topic and the valuable guidance and support throughout this year.

I would like to thank the Sleipner CO_2 storage team in Equinor Anne-Kari Furre, Peter Zweigel, Bamshad Nazarian and Britta Paasch for the expert insights and interesting discussions. Grethe Tangen and Odd Andersen from SINTEF for the feedback and support of the modelling work performed on this project.

I am grateful to Professor Nuno Pimentel for the technical inputs and guidance in developing this master's thesis with the Department of Geology of the Faculty of Science of the University of Lisbon from Norway.

Thanks to Equinor Energy AS and the Sleipner partnership for the dataset and permission to publish this material. Also to Halliburton for granting an academic license for the Permedia CO_2 toolkit software for the development of this thesis.

On a personal note, I would like to thank my family and in-laws for the encouragement and support.

Abstract

The Sleipner Carbon Capture and Storage project in the North Sea has been injecting CO_2 underground into a saline formation for permanent storage for over 22 years. Equinor Energy AS, the field operator, and the license partners have injected about 18 million metric tons (Mt) of CO_2 by the end of 2018 into the Utsira Formation at depths around 800 to 1100 m below sea level.

The Sleipner CO_2 storage reservoir comprises mostly unconsolidated sands with high porosities (36%) and high permeabilities (Darcy range) under near hydrostatic pressure conditions. An intensive geophysical monitoring program has been implemented since CO_2 injection commenced in 1996. Nine bright reflections were already identified in the first time-lapse repeat survey in 1999 indicating that the CO_2 ascended more than 200m vertically from the injection point to the caprock. The CO_2 plume is evidently layered and asymmetric with a vertical stack distribution indicating that it encountered and breached a series of thin shale barriers (about 1m thick) within the storage site. The thin shale layers within the Utsira Formation acting as baffles to the CO_2 migration were identified on well data but too thin to be resolved on seismic. Core and cutting samples of the caprock above the storage reservoir have indicated threshold pressures around 1.7 MPa. In order for the CO_2 to break through the shale layers within the reservoir and form a vertical stack of thin plume layers, their threshold pressures need to be significantly smaller than the sampled caprock.

Despite the high quality time-lapse seismic surveys imaging of the areal distribution of the CO_2 plume in Sleipner, to date no published dynamic model has accurately replicated the layered morphology or flow behaviour of the plume. This is due to challenges around the underlying flow physics of CO_2 and uncertainties in geological assumptions. Equinor has previously released benchmark reservoir models of Sleipner focusing on the uppermost plume layer (Singh et al., 2010). This master's thesis objective was to define the full Sleipner multi-layer reservoir model in order to analyse the key factors controlling gravity-dominated flow in CO_2 storage reservoirs, based on assumptions from Cavanagh et al. (2015).

Fundamental aspects of the plume remain uncertain such as layer thickness, plume temperature profile (which impacts CO_2 densities) and gas saturations for the plume layers. These uncertainties are inherited from the remote geophysical monitoring of the CO_2 storage reservoir and the broadly constrained fields of pressure, temperature and saturation (Cavanagh and Haszeldine, 2014).

Two main reservoir models were built in the Permedia software for the Sleipner CO_2 storage in this study, a simple and a map-based approaches. The simple approach defined constant values for the reservoir properties and the map-based assigned lateral distributions to the reservoir properties corresponding to the areal distribution of the CO_2 layers observed in seismic. Invasion percolation was applied to simulate the CO_2 migration which assumes a flow domain dominated by gravity and capillary forces over viscous forces, similar to the expected in Sleipner.

Using iterative experimentation in an Invasion Percolation (Permedia tool) simulator, values of shale threshold pressure (Pth) were modified until a satisfactory match was achieved. It was established that the multi-layer plume was very sensitive to the choice of Pth and the best match was obtained by using lower threshold pressures which could indicate pore sizes associated with silt-rich shales. A sensitivity analysis of the poorly constrained parameters, temperature (and related CO_2 densities) and gas saturations, was performed to assess their impact on the CO_2 migration simulation. Other models are also possible, such as incorporation of chimneys (leakage points), which need to be investigated in future studies.

Key-words: Geological carbon storage; Sleipner; invasion percolation simulation; threshold pressures; multi-layered CO_2 plume.

Resumo

A captura e armazenamento geológico de dióxido de carbono é considerada uma solução essencial para atingir os objetivos do Acordo de Paris sobre as alterações climáticas, visando manter o aumento da temperatura média mundial bem abaixo dos 2°C em relação aos níveis pré-industriais. De acordo com a International Energy Agency (IEA), a captura e armazenamento de carbono – CCS (sigla em inglês para Carbon Capture and Storage) é a única tecnologia com capacidade para reduzir as emissões de CO_2 em larga escala, necessária para alcançar os objetivos de longo prazo na mitigação do aquecimento global. O CCS consiste na captura de CO_2 de grandes fontes estacionárias, como centrais termo-elétricas e instalações industriais, seguida de sua compressão, transporte por gasodutos ou navios e injeção para armazenamento geológico em formações rochosas com alta porosidade.

O campo de Sleipner está localizado a cerca de 250 km da costa da Noruega, na parte central do Mar do Norte. O projeto de captura e armazenamento é combinado com o desenvolvimento e produção deste campo de gás. O campo é dividido em Sleipner Oeste e Leste, sendo que a produção do Sleipner Oeste apresenta conteúdos altos de CO_2 para o mercado consumidor. O CO_2 é entretanto separado e injetado numa grande formação salina localizada acima do campo Sleipner Leste, a cerca de 800 metros abaixo do fundo oceânico. O CO_2 tem sido injetado para armazenamento permanente por mais de 22 anos em Sleipner, sendo este o primeiro projeto de captura e armazenamento de CO_2 em larga escala no mundo. A Equinor Energy AS, empresa operadora, e empresas parceiras injetaram na Formação Utsira (depósitos marinhos do Miocénico) cerca de 18 milhões de toneladas métricas (Mt) de CO_2 até ao final de 2018. A sequência de lutitos (*shales*) do Grupo Nordland depositada acima da Formação Utsira foi comprovada como uma rocha selante efetiva para o reservatório de armazenamento de CO_2 (Singh et al., 2010).

O reservatório Sleipner de armazenamento de CO_2 é composto principalmente por arenitos mal consolidados com excelentes propriedades - porosidades em torno de 36% e permeabilidades em torno de 1 a 5 Darcy. Este reservatório está sob condições de pressão próximas a hidrostáticas, com salinidade das águas intra-formacionais com valores similares aos da água do mar. Desde o início do projeto em 1996, um programa intensivo de monitorização geofísica foi implementado. O Sleipner foi monitorizado com levantamentos geofísicos aproximadamente a cada 2 anos, o que permitiu a delineação de uma imagem detalhada da distribuição e dinâmica da pluma de CO_2. No primeiro levantamento sísmico 4D (*time-lapse seismic*) em 1999, apenas 3 anos após o início da injeção, foram identificados 9 refletores com fortes contrastes de impedância acústica (*bright reflectors*), o que indica que o CO_2 ascendeu verticalmente mais de 200 metros, do ponto de injeção até a rocha selante (*caprock*). A distribuição vertical da pluma de CO_2 é evidentemente assimétrica e em camadas, indicativa do encontro e migração através de uma série de finas barreiras de *shales* (com cerca de 1 metro de espessura) dentro do reservatório. Estas finas camadas de *shales* que agiram como barreiras semi-permeáveis (*baffles*) à migração de CO_2 foram identificadas em dados de poço mas, com exceção da unidade Thick Shale (com cerca de 6.5 metros de espessura) que separa a Formação Utsira da unidade arenosa Sand Wedge localizada logo abaixo da rocha selante, não foi possível realizar uma correlação devido às grandes distâncias entre os poços nem identificá-los na sísmica devido à resolução. Estima-se que cada camada de CO_2 apresentará espessuras entre 7 e 20 metros, com extensão lateral de 1 a 3 quilómetros (Cavanagh et al., 2015). Cada camada de CO_2 apresenta um pronunciado

alongamento na direção norte-sul, indicativo da forte influência da topografia da rocha selante e da unidade Thick Shale.

A migração vertical do CO_2 é resultante do grande contraste entre as densidades da água (presente nos poros da formação rochosa, *brine*) e do CO_2. Quando o CO_2 atinge uma barreira com rochas de baixa permeabilidade, ele acumula-se abaixo desta barreira, com o preenchimento de pequenas armadilhas ou estruturas (*traps)* em conformidade com sua topografia. O CO_2 migra através destas barreias de baixa permeabilidade quando a pressão exercida pelo fluido de CO_2 supera a pressão limite para invasão do CO_2 (*threshold* ou *displacement pressures*) da rocha de baixa permeabilidade. Amostras de testemunho e *cuttings* da rocha selante (*caprock*) acima do reservatório indicaram pressões limite para invasão do CO_2 de cerca de 1.7 MPa. Para o CO_2 conseguir migrar através das camadas de *shales* do reservatório e formar uma pluma composta por um empilhamento vertical de camadas finas, as pressões limite para invasão do CO_2 precisam de ser significativamente menores que o valor indicado pelas amostras da rocha selante.

Apesar da alta qualidade das imagens da distribuição espacial da pluma de CO_2 em Sleipner, adquiridas por levantamentos sísmicos 4D, até hoje nenhum modelo dinâmico publicado reproduziu com sucesso a morfologia em camadas ou o comportamento do fluxo da pluma de CO_2. Isto é devido aos desafios relacionados com a física inerente aos fluxos de CO_2 e às incertezas relacionadas com as interpretações geológicas. A Equinor publicou anteriormente modelos do reservatório Sleipner de armazenamento de CO_2, para referência da comunidade científica, com foco na camada superior da pluma, uma vez que as interpretações das estruturas correspondentes ao topo do reservatório foram realizadas no levantamento sísmico 3D, com menos incertezas relacionadas com os efeitos do CO_2 (Singh et al., 2010). A presente Tese de Mestrado definiu o modelo do reservatório completo com a incorporação das 9 camadas de CO_2 para analisar os fatores principais que controlam o fluxo dominado por gravidade em reservatórios de armazenamento de CO_2, com base em suposições de acordo com Cavanagh et al. (2015).

Alguns aspectos fundamentais da pluma permanecem incertos, tais como a espessura das camadas (dependentes das pressões limite para invasão do CO_2 das unidades *shale*), o perfil de temperatura da pluma (o qual impacta as densidades do CO_2) e a saturação em gás das camadas da pluma (parâmetro difícil de distinguir acima de 30%). Estas incertezas são devidas às características intrínsecas da monitorização sísmica remota e da ampla variação possível dos parâmetros pressão, temperatura e saturação num reservatório (Cavanagh & Haszeldine, 2014).

O desenvolvimento desta Tese de Mestrado incorporou a construção de dois modelos principais do reservatório de CO_2 Sleipner no *software* Permedia, um com uma abordagem simples e o outro baseado em mapas. A abordagem simples consistiu na definição de valores constantes para as propriedades do reservatório, enquanto a abordagem por mapas definiu distribuições laterais para as propriedades das rochas do reservatório conforme a distribuição espacial das camadas de CO_2 observada em sísmica com significativo alongamento norte-sul. O método de percolação por invasão (*invasion percolation*) foi aplicado para simular a migração de CO_2, o qual assume um fluxo dominado pelas forças da gravidade e da capilaridade sobre a viscosidade, de modo similar ao processo interpretado para o reservatório Sleipner.

As pressões limite para invasão do CO_2 (*threshold* ou *displacement pressures*) foram estimadas por experimentação, através da sistemática redução do valor medido nas amostras da rocha selante até que a distribuição das 9 camadas de CO_2 empilhadas verticalmente fosse reproduzida. As pressões limite para invasão do CO_2 (*threshold* ou *displacement pressures*) efetivas para as unidades *intra-shales* e as correspondentes permeabilidades indicaram que seus valores reduzidos poderiam ser devidos a uma maior dimensão da generalidade das gargantas dos poros (*pore throat sizes*), associada à presença de *shales* mais ricas em silte. Uma análise de sensibilidade dos parâmetros com alta incerteza - temperatura (e consequentes

densidades de CO_2) e saturações do CO_2 - foi realizada para avaliar os seus impactos na migração de CO_2 e identificar os fatores-chave que contribuem para a distribuição da pluma de CO_2 em múltiplas camadas. Estudos futuros devem investigar outros modelos possíveis, especialmente com a incorporação de áreas com alta permeabilidade interpretadas como "chaminés" (*chimneys, leakage points*) em sísmica.

Contents

Figures

I. Introduction

1. Why CO_2 storage?

It is a worldwide consensus that reduction in global greenhouse gas emissions is crucial for the sustainable development of modern human civilization (Ringrose, 2017). The consumption of fossil fuels started with the industrial revolution in the beginning of the 19th century and rapidly increased after 1950 (Figure 1), resulting in substantial emissions of carbon dioxide (CO_2). High rates of CO_2 emissions to the atmosphere is a well-known significant contributor to global warming and ocean acidification (Cavanagh and Haszeldine, 2014).

Economic development of human society has been driven by energy from fossil fuels with current global fossil fuel consumption around 82% of the world energy supply according to the International Energy Agency (IEA, 2016a *In* Ringrose,2017). Considering that two-thirds of the current greenhouse gas emissions come from the energy sector, a transition to low-carbon energy systems is therefore an urgent priority.

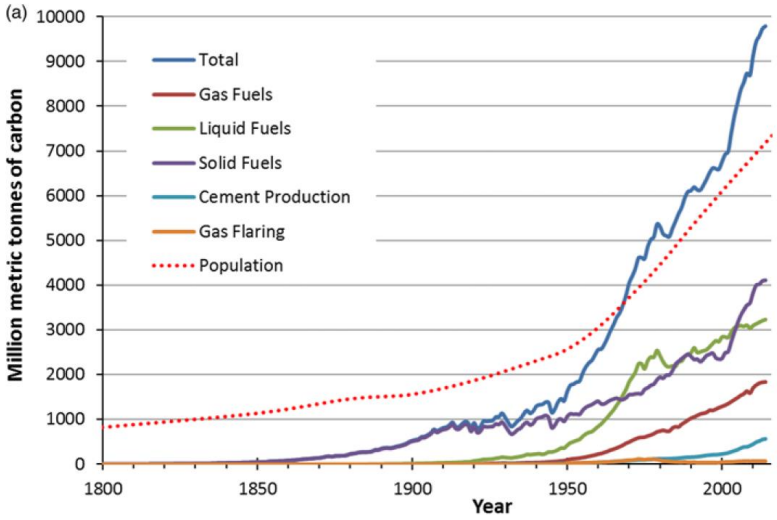

Figure 1 - Global CO_2 emissions from 1800 to 2014 from combustion of fossil fuel, cement manufacture, gas flaring and global population (Sources: carbon emissions data from cdiac.ornl.gov, with years 2012 – 2014 based on data from BP statistical review; population data from www.census.gov In Ringrose, 2017). To convert the CO_2 emissions from million metric tonnes of carbon to mass of CO_2 multiply by the molecular ratio 3.667.

Carbon Capture and Storage (CCS) is a technology proposed by the G8 and the International Energy Agency as an essential solution to reduce CO_2 emissions in order to mitigate climate change (Cavanagh and Haszeldine, 2014). It consists on the capture of CO_2 from large stationary sources (power stations, industrial plants) which is then compressed, transported by pipeline or ships and injected for geological storage into porous rock formations deep below the land or sea surface (Cavanagh and Haszeldine, 2014). Saline aquifers and depleted oil and gas fields are considered the most viable injection targets (Bandilla et al., 2014). Deployment of CCS with CO_2 used for enhanced oil recovery (EOR) is also an important option for large scale storage given the potential benefit of increased revenues (Senior et al., 2010). CCS technology has been largely applied to remove CO_2 from natural gas processing, coal-fired power plants, as well as ethanol, fertilizer and hydrogen production plants (Ringrose, 2017). It is now also emerging as a primary mean to

decarbonize industrial processes, especially cement and steel manufactures. In addition, when combined with biomass-fired power plants it provides a major pathway into negative emissions (GCCSI, 2017).

The Paris Agreement limits the increase in global average temperature to well below 2°C above pre-industrial levels. The European Union has called for CO_2 emissions reductions of 80% below 1990 levels by 2050, which is equivalent to 80 Gt (metric gigaton) of CO_2 being kept out of the atmosphere. In order to reach this target, a transition into a low-carbon energy system will be required which consists of a combination of renewables, increased efficiency and Carbon Capture and Storage. CCS alone is expected to account for 12.2 Gt of CO_2 emissions avoided by 2050, which implies average injection rates of 400 Mt/year (Gasda et al., 2016).

There are currently 18 large-scale CCS projects in operation worldwide with a collected capacity to capture and store about 32 Mtpa (million metric tonnes per annum) of CO_2 according to the Global CCS Institute project database (https://www.globalccsinstitute.com/projects/large-scale-ccs-projects). This capacity should increase to 100 Mtpa by 2030, taking into account the CCS projects currently in the planning stages. This is still way beyond what would be required in order to meet the large-scale greenhouse reduction goal set by the Paris Agreement. Therefore, strategies to scale up CCS deployment have an urgency in development by governments, policy makers and private sectors (Ringrose et al., 2017).

The Sleipner Carbon Capture and Storage project in the North Sea was the first commercial CO_2 storage site in the world. CO_2 has been captured from the produced gas and re-injected it into an underlying saline formation since 1996. Equinor (formerly Statoil), the field operator, and Sleipner partners have injected about 18 million metric tons (Mt) of CO_2 by the end of 2018 into the Utsira Formation, a Miocene aged shallow marine sandstone formation, at a depth of 800-1100 m below sea level in the Sleipner area. Overlying the sandstones is the Nordland Group shale sequence that has proven to be an effective seal for the CO_2 storage site (Singh et al., 2010).

Sleipner has been monitored with geophysical surveys approximately every 2 years as well as gravimetric and electromagnetic surveys, defining a detailed image of the CO_2 plume distribution and dynamics (Cavanagh, 2013). From 1996 to 1999, the CO_2 plume ascended more than 200 m vertically from the injection point, breaching a series of thin shale barriers within the storage site, forming nine vertically stacked CO_2 layers, each estimated about 7-20 m thick and extending laterally for a few hundred meters (Cavanagh et al., 2015). These intraformational shales within the main Utsira Sand unit are too thin to be resolved seismically (about 1 m thick) except for the uppermost barrier about 6.5 m thick. This thick shale barrier is overlain by a shallower sand unit beneath the caprock. Each CO_2 layer has a pronounced north-south elongation appearing to be strongly influenced by the mapped topography of the caprock and underlying thick shale barrier, in a similar manner to the flat oil-water contacts of many hydrocarbon fields.

Cavanagh and Haszeldine (2014) and Cavanagh et al. (2015) published a successful match to the observed CO_2 multi-layered plume distribution with a basin modelling approach which simulated the gravity-dominated migration of a buoyant fluid using a capillary percolation method. The invasion percolation approach considers that the CO_2 backfills against each shale barrier and breaks through when the buoyant force of the CO_2 exceeds the capillary threshold of the shale barrier. This thesis defines the storage reservoir model capturing the multi-layer plume distribution for the latest Sleipner published data (up to 2010) assuming a flow domain dominated by capillary and gravity forces. There are significant aspects of the plume which are poorly understood due to the uncertainties inherent in remote geophysical monitoring of gas plumes. The impact of these factors' possible ranges on the CO_2 plume migration within the storage reservoir is assessed in this study.

2. Project Scope and Objectives

The work hereby presented corresponds to the final thesis for the Master in Geology with specialization in Stratigraphy, Sedimentology and Palaeontology of the Department of Geology of the Faculty of Science of the University of Lisbon.

This master's thesis goal was to define the full Sleipner multi-layer model to analyse the key factors controlling gravity-dominated flow in CO_2 storage reservoirs. The dataset utilized is published and provided by Equinor Energy AS. The reservoir storage modelling work was fully performed in the Permedia CO_2 toolkit software. The Permedia Research Group is part of Halliburton and provided a single-user academic license for the development of this project.

The MSc thesis development timeframe is summarized on Table 1 based on the main tasks and technical reviews at the Equinor office which are described as follows. The project started in January 2018 with the evaluation of previous modelling work performed in the field (PR) and the scientific basis for this study (SB). Familiarization with the Permedia CO_2 software (PE) was achieved by reviewing online tutorials available and contacting the Permedia software support team via email to clarify specific questions and concerns. The Sleipner dataset was delivered remotely in March for initial input and QC in Permedia (IN). More detailed information of the field and dataset was provided at the Equinor office in Trondheim, Norway on the 16th April (E1).

A 3D model was built (MO) consisting of a geological framework extending from the base of the Utsira Formation below the injection point to the caprock with nine alternating sandstone and shales intervals based on assumptions made in previous studies (Cavanagh and Haszeldine, 2014 and Cavanagh et al., 2015). Data analysis of the input reservoir and fluid properties (DA) was carried out in order to define a vertical stack of CO_2 plume layers as a result of percolation. The reservoir model was calibrated by adjusting the threshold pressures of the intraformational shales in order to represent the distribution observed on the time-lapse seismic (CA).

Different reservoir modelling approaches were applied and tested considering the input data available, software functionalities and published studies of the field (AP). A sensitivity analysis of key factors of the plume that have limited data constrain was performed to define their impacts on CO_2 migration in a multi-layer model (SE).

The interpretation of the results required the review of field reports and papers on threshold pressures and permeability anisotropies for low permeability rocks (RE). These results were also compared to previous CO_2 storage modelling studies performed in Sleipner (CO).

The project progress and results were presented for review by technical experts at the Equinor office on the 28th June (E2), an intensive work week from the 6th to the 10th August (E3) and on the 24th August (E4) as shown on Table 1. After each review, the project was updated before moving on to the next task based on the feedback provided. The task of writing the thesis (WR) was developed mainly after the bulk modelling work was finalized.

Table 1- MSc thesis development weekly timetable with milestones (technical reviews at the Equinor office in Trondheim and project delivery) displayed with diamonds. WR corresponds to the task of writing the thesis. Some tasks were performed in parallel to other tasks.

	Jan					Feb				Mar				Apr				May				Jun				Jul					Aug				Sep				Oct					Nov			
	1	2	3	4	5	6	7	8	9	10	11	12	13	14	15	16	17	18	19	20	21	22	23	24	25	26	27	28	29	30	31	32	33	34	35	36	37	38	39	40	41	42	43	44	45	46	47	48
Main Tasks	1-5	8-12	15-19	22-26	29-2	5-9	12-16	19-23	26-2	5-9	12-16	19-23	26-30	2-6	9-13	16-20	23-27	30-4	7-11	14-18	21-25	28-1	4-8	11-15	18-22	25-29	2-6	9-13	16-20	23-27	30-3	6-10	13-17	20-24	27-31	3-7	10-14	17-21	24-28	1-5	8-12	15-19	22-26	29-2	5-9	12-16	19-23	26-30
1. PR																																															
2. SB																																															
3. PE																																															
4. IN																																															
5. E1																♦																															
6. MO																																															
7. DA																																															
8. E2																										♦																					
9. CA																																															
10. E3																																♦																
11. AP																																															
12. SE																																															
13. CO																																															
14. RE																																															
15. E4																																		♦														
16. WR																																															

3. Field Location and History

The Sleipner field is located in the central part of the North Sea about 250 km off the coast of Norway, close to the border with the UK (Norwegian block 15/9, Production License 046) (Figure 2). The Sleipner West gas field was discovered in 1974 and put on stream in 1996, in a combined development with the Sleipner East condensate gas field which was proven in 1981 and started production in 1993. The decision made by Equinor Energy AS (field operator – formerly Statoil) and the license partners (LOTOS E&P Norway AS, ExxonMobil E&P Norway and KUFPEC Norway AS) to store geologically the captured CO_2 was based on willingness to mitigate air pollution, implement new technology, CO_2 tax incentive and state requirements (Furre et al., 2017).

The Carbon Capture and Storage project is part of the gas field development. The CO_2 content of the gas stream in Sleipner East is within market specifications (less than 2.5 %) but Sleipner West gas has a CO_2 content in the range of 4-9%, which must be reduced to meet customer requirements. The CO_2 from the Sleipner West gas field is therefore separated and then injected into a large saline formation above the Sleipner East field, about 800m below the seafloor (Figure 3). The Sleipner A production and drilling platform is at 80m water depth. The Utsira Formation was chosen due to its extensive size, excellent reservoir properties, shallow depth and consequent low well and topside costs. The seal to the reservoir is provided by a 700m thick caprock. The carbon dioxide injection at the Sleipner field was the world's first industrial scale CO_2 injection project designed specifically as a greenhouse mitigation measure.

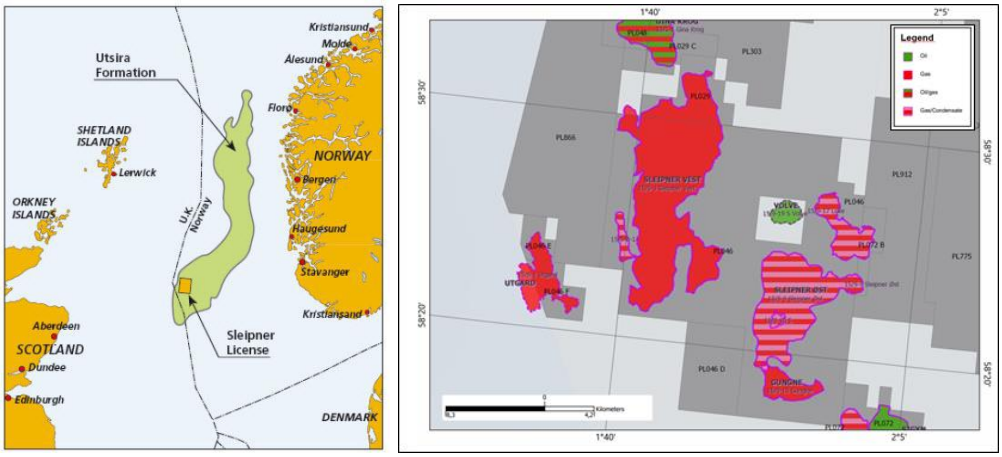

Figure 2– Left: Location map showing areal extent of the Utsira Formation and the Sleipner licence. Right: Sleipner field (West/Vest and East/Øst) license – PL046, block 15/9 (courtesy of the Norwegian Petroleum Directorate - NPD).

The CO_2 is injected via a deviated well (15/9-A-16), near horizontal at the injection point, in a dense phase at a depth of about 1012m below sea level. Injection commenced in 1996 with a roughly stable annual rate of about 0.9 Mt. Approximately 18 million tonnes (Mt) of carbon dioxide have been injected by the end of 2018. Initial development plans for Sleipner West estimated the amount of CO_2 to be injected over the field's expected life of 25 years to be about 25 Mt. Since 2014, CO_2 from the Gudrun gas field (about 50km to the North) which is tied-back to Sleipner A has also been processed via the Sleipner CCS facility providing an additional 100,000-200,000 tonnes of CO_2 per annum.

Extensive geophysical and environmental monitoring programmes have been deployed without indication of any CO_2 release from the storage unit (Furre et al., 2017). Due to costs and added risks, early on the project it was decided not to drill a dedicated monitoring well but to focus on the use of remote geophysical monitoring methods. The monitoring of the CO_2 plume growth within the Utsira Formation includes a baseline 3D seismic survey and eight time-lapse (4D) seismic surveys, four seabed micro gravimetric surveys, one electromagnetics survey and two seabed imaging surveys. Wellhead pressure and flow rate is monitored continuously and have remained stable from production start-up (Furre et al., 2017).

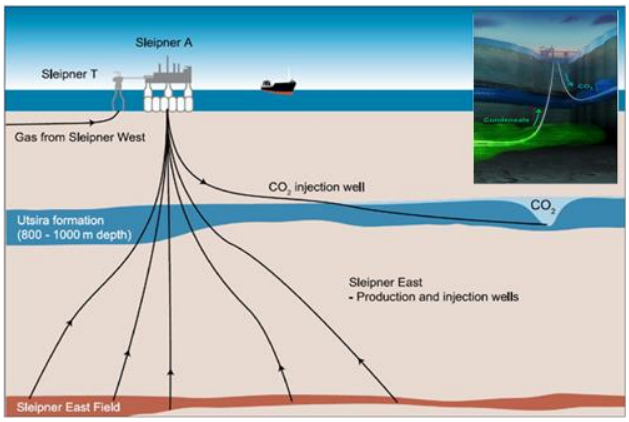

Figure 3- Simplified diagram of the Sleipner CO_2 Storage Project (IPCC, 2005). CO_2 is removed from the well stream at Sleipner T and injected into the Utsira Formation via a dedicated injection well (15/9-A-16) at Sleipner A facility.

II. Geological Framework and CO_2 Storage

1. Regional Geology

1.1. South Viking Graben

The North Sea Basin is composed of several major Mesozoic graben and highs, dominated by the Viking graben to the north and the Central graben to the south (Gregersen et al., 1997). The Sleipner field is located on the eastern flank of the south Viking Graben, northern North Sea (Figure 4).

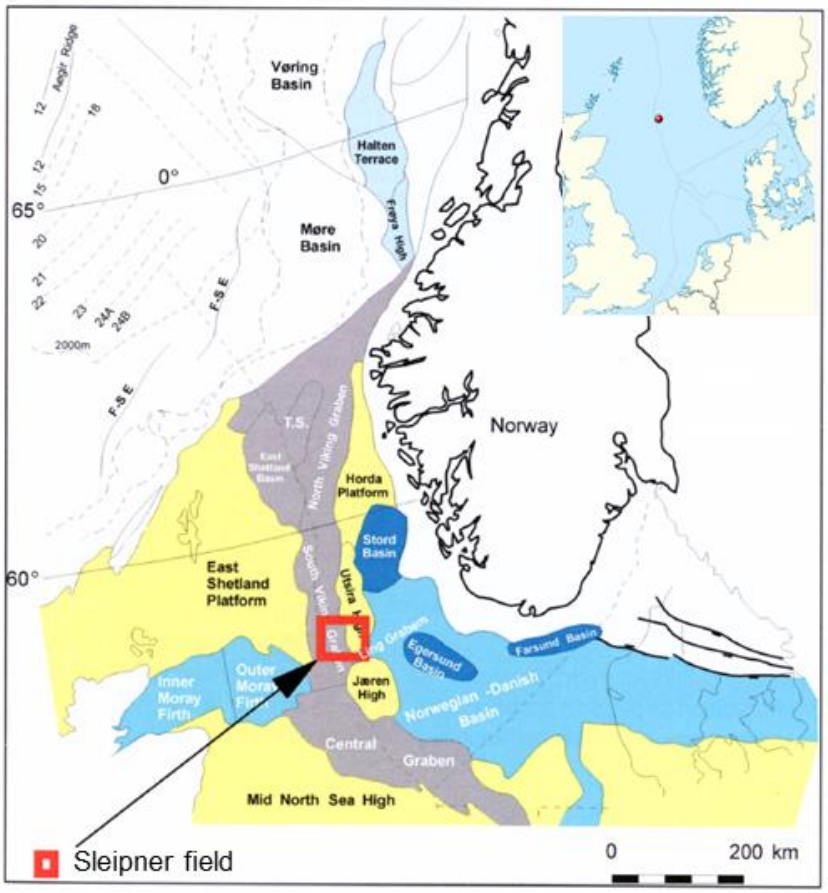

Figure 4 - Regional structure map of the northern North Sea and Norwegian continental margin, with the outline of Sleipner field (modified from Kennett, 2008).

From the Permian and throughout the Mesozoic, extensional tectonism dominated the northern North Sea (Gregersen et al., 1997). The north to south trend of the asymmetric Viking graben was developed due to the spread of rifting from arctic areas southwards into the North Sea during the Late Jurassic (Kennett, 2008). This extensional phase was characterized by rapid fault-controlled subsidence, the formation of a series of graben and half-graben basins and clastic syn-rift sedimentation (Fyfe et al., 2003). According to Gregersen et al. (1997), extensional tectonism died out in the Early Cretaceous with the North Sea basin entering a prolonged period of post-rift thermal subsidence and sediment filling supplied by the surrounding

topographic highs. Deposition of thick mud-rich clastic sequences dominated the post-rift sedimentary basin fill corresponding to the Shetland, Rogaland, Hordland and Nordland Groups (Ziegler, 1981).

The Cenozoic era presented six phases of uplift affecting the basin margin and surrounding British and Scandinavian land-shelf areas. These uplifts enhanced erosion of surrounding provenance which resulted in major episodes of siliciclastic sedimentation, mainly during the Palaeocene, Eocene, Oligocene and Miocene, which Galloway et al. (1993) interpreted as onlap defined megasequences. From the Oligocene to Middle Miocene, the northern North Sea basin continued to subside forming a shallow marine sag-basin with deposition of the mud-dominated Hordaland Group (Figure 5) (Head et al., 2004). Three sand-dominated units are also present in the Hordland Group, the Frigg, Grid and Skade formations. Only the Skade Formation is observed in the Hordaland succession in the Sleipner area.

According to Ziegler (1981), the regionally extensive Middle Miocene Unconformity (MMU) marks the top of the Hordaland Group and is particularly prominent on the eastern flank of the basin. It has been interpreted to be a response to uplift of the western Norwegian margin and tilting of the Horda platform, with consequent sub-aerial exposure of the basin margins and a temporary hiatus in sediment supply (Fyfe et al., 2003; Gregersen at al., 1997). A glacial-eustatic sea level fall associated with polar ice cap expansion is interpreted at this time by these authors. Connection between the Norwegian-Greenland Sea and the North Sea became restricted with shallowing and denudation of the uplifted areas resulting in deposition of sand from the rivers draining the Shetland platform to the west and the Norwegian North Sea margin to the east (Fyfe et al., 2003). These sands are the main component of the Utsira Formation in the Viking graben, corresponding to the basal part of the mud-dominated Nordland Group (Gregersen et al. 1997; Fyfe et al., 2003).

Subsidence of the basin during the Pliocene with input from European delta systems from the south-east resulted in large deposition of argillaceous sediments and re-establishment of connection to the Norwegian-Greenland Sea (Fyfe et al., 2003). The Quaternary was dominated by high subsidence and deposition of glaciomarine sediments (Justwan, 2006).

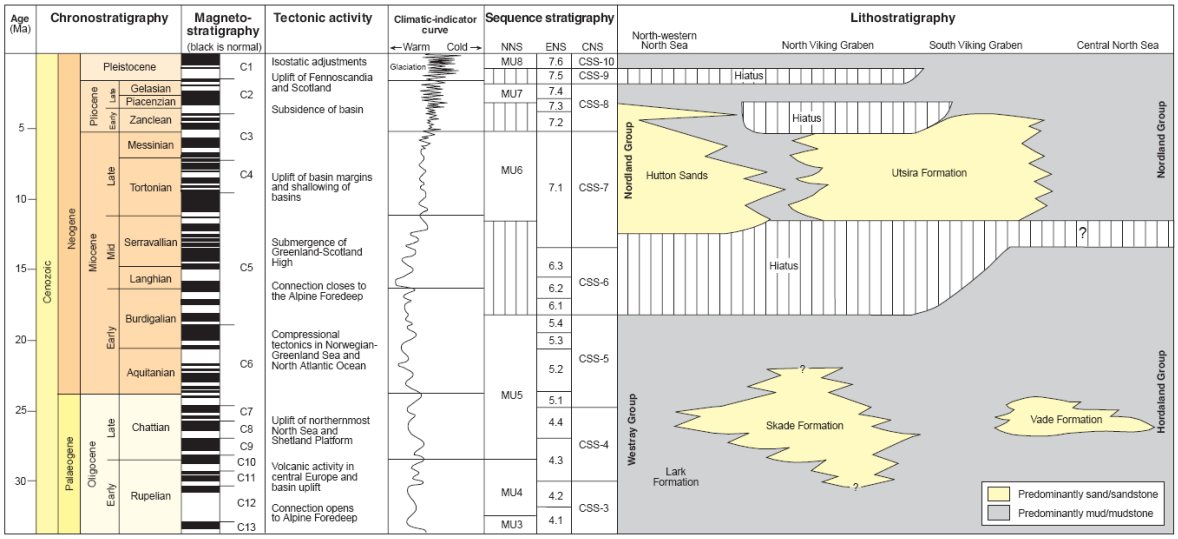

Figure 5- Stratigraphic correlation chart for the Cenozoic Hordaland and Nordland Groups. Sequence stratigraphic schemes: NNS = Northern North Sea; ENS = Eastern North Sea; CNS = Central North Sea (Fyfe et al., 2003).

1.2. Utsira Formation

The Utsira Formation was first defined by Deegan and Scull (1977) and is interpreted as a basin-restricted deposit which constitutes the basal part of the Upper Cenozoic Nordland Group in the northern North Sea (Gregersen et al., 1997; Zweigel et al., 2004), unconformably overlying the Hordaland Group shales (Figure 6). It is mostly composed by mature, well-sorted, fine to medium grained sands which downlap onto underlying mudstones (Fyfe et al., 2003). They are characterized by quartz with subordinate feldspar, rich in bioclastic debris and glauconite which are indicative of marine deposition. The Utsira Sand is clearly identified in well logs with a block low-gamma ray response and presents interbedded clays separating thick sand units. The deposition of the Utsira Formation ranges from late Middle Miocene (c. 11 Ma) to earliest Late Pliocene (c. 3 Ma) as determined based on biostratigraphic data from an exploration well to the south of the Sleipner field (Eidvin et al, 1999).

Regional mapping of the Utsira Formation shows an elongated north-south trending deposit that extends more than 450 km north-south and between 50 and 100 km east-west, which gives an approximate formation area of 26000 km^2 (Chadwick et al., 2004a). Its eastern and western limits are defined by stratigraphic onlap onto the Middle Miocene Unconformity and the northern and southern limits are defined by a facies transition into more shaly sediments (Gregersen & Johannessen, 2007). The top of the Utsira Sand surface generally varies smoothly within the depth range of 55-1500m, around 800-900m near Sleipner. Formation thickness maps define two main depocentres (Figure 7), one in the south around Sleipner with thickness reaching 300 m, and one about 200 km to the north, with thickness approaching 200m (Chadwick et al., 2004a). It is interpreted that the deposition of the Utsira Sand was largely sourced from the uplifted East Shetland Platform to the west, with a significant component of Scandinavian-derived material in its northern part (Rundberg and Eidvin, 2002 *In* Head et al., 2004).

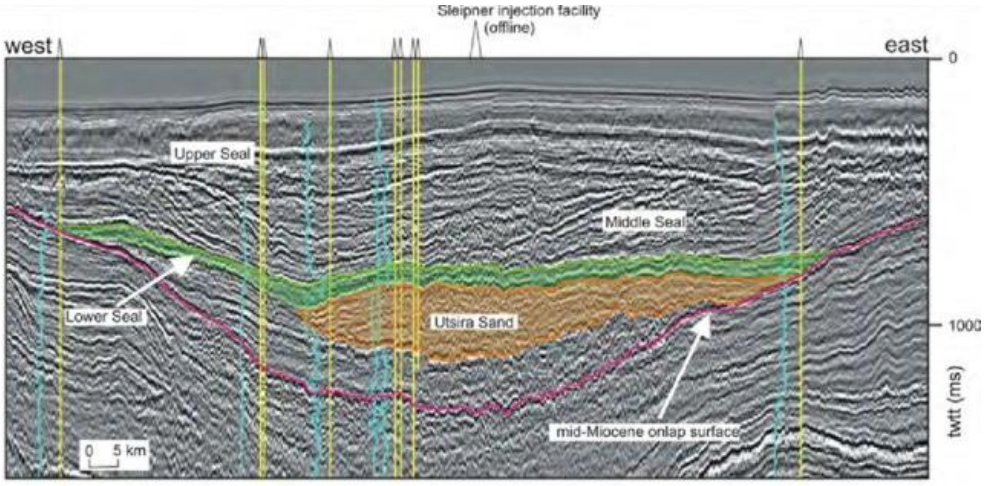

Figure 6– Regional 2D seismic line across the North Sea basin showing the Utsira Sand and the caprock succession. Vertical yellow lines represent well-bore profiles, and the vertical blue lines represent gamma-ray well-log traces (Hermanrud et al., 2010).

The Utsira Sand sediments are defined as basin-restricted marine lowstand deposits but there are a range of interpretations regarding their depositional environment. Some of the work carried out to date have suggested: tidal sand-ridge complexes (Rundberg, 1989); a linked strandplain and sandy shelf shoal deposits (Galloway, 2002); or an amalgamated submarine fan complex (Gregersen et al., 1997). Biostratigraphic data analysed by Eidvin et al. (1999) determined lower rates of sedimentation for the Utsira Sand than of

the overlying shales and considerably lower than the shaly deposits in the Central North Sea which are correlative to the Utsira Sand. Therefore, it has been interpreted by Zweigel et al. (2004) that favourable depositional models should include intensive sediment reworking in a broad channel connecting the Central North Sea and the North Atlantic as well as simultaneous deposition of finer grained or mixed material in the Central North Sea.

The predominant shale sediments of the Hordaland Formation underlain the Utsira Formation. They exhibit severe deformation by soft sediment mobilization and polygonal faulting (Zweigel et al., 2004) which have altered the seismic character of the Hordaland sediments and deformed its top surface (i.e. the Middle Miocene Unconformity - MMU). Hence, mud diapirs and mud volcanoes are present at the base of the Utsira Formation resulting in significant local thickness variations.

The overburden of the Utsira Sand is about 250m thick in the Sleipner area and consists of clay-rich sediments of the Nordland Group (Zweigel et al., 2004). This caprock succession can be divided in three main units (Figure 6): Lower Seal, a shaly basin-restricted unit about 50-100m thick; Middle Seal, prograding sediment wedges of Pliocene age shale-rich in the basin centre but coarsening both upwards and towards the basin margins; Upper Seal, Quaternary sediments mostly glacio-marine clays and glacial tills (Chadwick et al., 2004a).

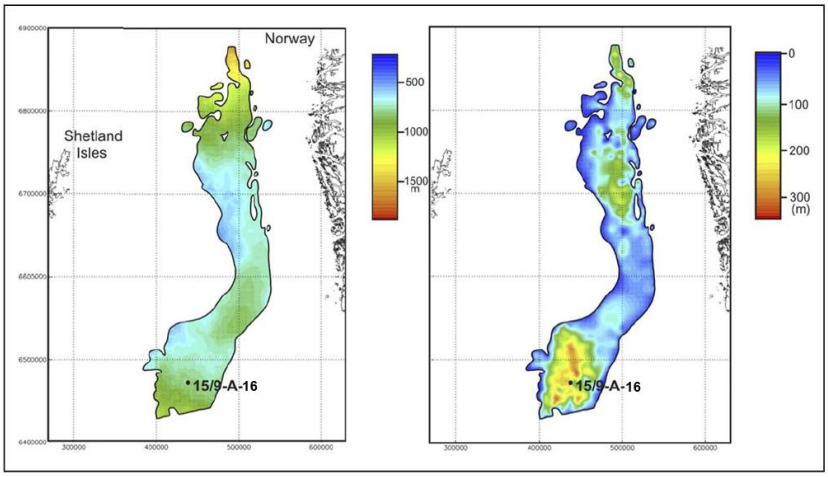

Figure 7 – Left: Two-way travel time structure map to Top Utsira Sand. Right: Utsira Sand isopach map, showing the two main depocentres. CO_2 injection well 15/9-A-16 displayed on both maps (Kirby et al., 2001 In Kennett, 2008).

2. Sleipner CO_2 Storage

2.1. Storage Reservoir

In Sleipner, the Utsira Formation is at a depth of 800-1100m below sea level. The CO_2 is injected via the deviated well 15/9-A-16 over a 38m perforation interval at about 1012m depth. The high-quality reservoir presents an average porosity of 36%, a permeability range of 1 to 5 Darcy and a net to gross of 98% (Singh et al., 2010).

The Utsira Formation is identified on wireline logs from its low gamma-ray, sonic velocity and neutron density response. The reservoir consists of two units: a lower Utsira Sand unit and an upper Sand Wedge unit which are separated by a 6.5m thick shale unit (Figure 8). The Sand Wedge unit thickens to the east and pinches out to the west. A number of thin spikes of higher gamma-ray, velocity and density log values

are present within the Utsira Sand unit, similar in values to those of the overlying Nordaland shale, corresponding to thin intra-formational shale beds (typically about 1m thick). These thin shale layers constitute important permeability barriers within the reservoir and have proven to have a significant effect on the CO_2 plume entrapment and migration.

There is no evidence for faults in the interior of the Utsira Sand (Zweigel et al., 2004). Exceptions are reverse faults at the margins of some mud edifices and more rarely faults from the polygonal faulting pattern of the underlying Hordaland Formation which can be present at the lowermost part of the Utsira Sand, close to its base and below the injection point.

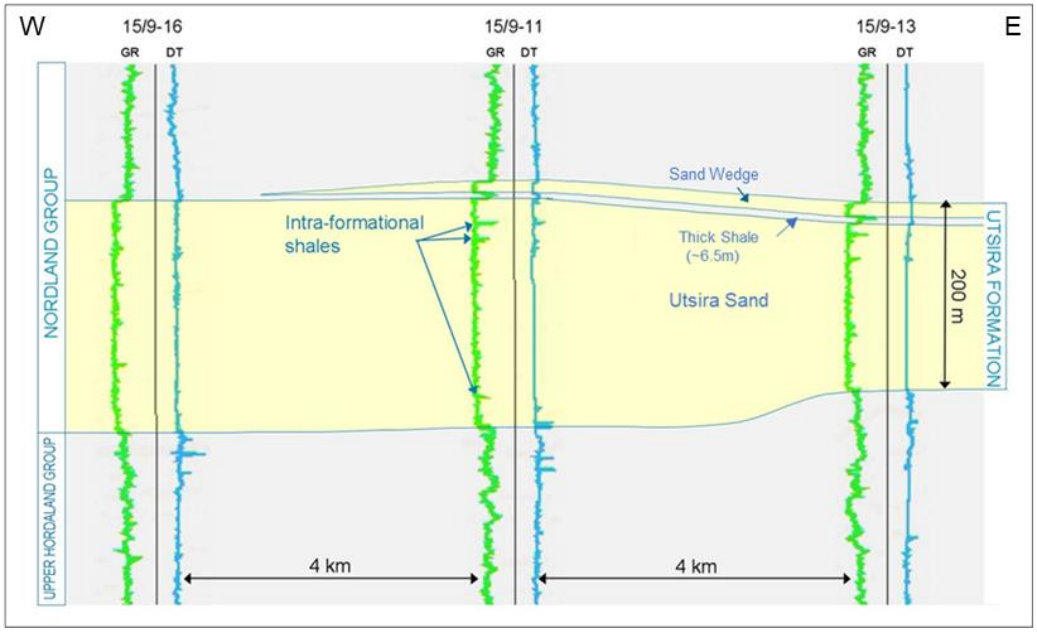

Figure 8 – Gamma ray and sonic wireline log response through the Utsira Formation and the caprock shale. Reservoir characterized by the Sand Wedge, the Thick Shale and the main Utsira Sand units (modified from Kennett, 2008).

Rock samples from the Utsira Sand are almost exclusively ditch cuttings. Limited core data of the Utsira Sand is available from nearby exploration well which consist of weakly consolidated sand that disintegrate when shaken in unfrozen conditions (Zweigel et al., 2004). Thin sections show a homogeneous, fine to medium grained, moderately to well sorted sand with high content of quartz and only minor amounts of cement. Microscopy reveal scarce grain contacts and almost no deformation of the grains confirming the unconsolidated state of the sediment.

The top of the Utsira Sand has been mapped based on wireline logs and 3D seismic surveys corresponding to depths of 750-900m in the injection area. It has a general southward dip on local scale and in detail is gently undulatory with small domes and valleys. The base of the Utsira Sand constitutes an unconformity at depths of 900-1100 m in the Sleipner area. It is structurally more complex with presence of numerous mounds, interpreted as mud edifices (mud diapirs and mud volcanoes) caused by localized mobilization of the underlying Hordaland Shale (Zweigel et al., 2000). Local depressions in the top Utsira level are observed in 3D seismic surveys above mounds at the base Utsira level which can be attributed to preferential compaction of the mud edifices during burial (Zweigel et al., 2004). Therefore, the presence of mud edifices at the base of the Utsira Formation has resulted in significant local thickness variations across the reservoir.

The clay-rich sediments of the Nordland Group Lower Seal are about 250 m thick in the Sleipner area and extend more than 50 km west and 40km east beyond the injection area, corresponding to the primary sealing unit (the caprock). Cutting samples of the caprock from wells in the vicinity of Sleipner indicated grey clay silts or silty clays, generally dominated by illite with minor kaolinite and traces of chlorite and smectite. Caprock core was acquired in 2002 around 20-25 m above the Utsira Sand reservoir and subjected to a detailed testing programme. The core material is typically grey to dark grey silty mudstone, uncemented and plastic, generally homogeneous with weak indications of bedding (Arts et al., 2008). Gas transport testing on core material (Harrington et al., 2008) indicated that the Sleipner caprock has favourable sealing capacities with the ability to hold supercritical CO_2 columns in excess of 100 m even up to 400 m depending on the CO_2 density, which in turn is sensitive to pressure and temperature at the reservoir top. This is much higher than the buoyancy pressures likely to occur in the Utsira reservoir, where maximum confined column heights are usually less than 10m (Arts et al., 2008).

2.2. Observed CO_2 Plume Distribution

An extensive monitoring programme has been carried out over the CO_2 injection area. A total of ten 3D seismic surveys and four gravity surveys have been acquired in Sleipner to date to monitor the CO_2 behaviour in the storage unit (Furre et al., 2017). A Controlled Source Electromagnetic (CSEM) test line was conducted in 2006 but the resolution was inferior at the time making it challenging to detect the CO_2 plume, consequently this study was not repeated. Sea bottom imaging surveys and sampling of sediments and water column have been conducted to investigate possible escape release structures and increased CO_2 levels, respectively. None of the monitoring techniques have showed any signs of leakage into the overburden (Arts et al., 2008; Eiken et al., 2011; Furre et al., 2017).

Prior to injection, a baseline 3D seismic survey acquired in 1994 was used to delineate the reservoir geometry. Repeated seismic acquisition to monitor the plume was performed in 1999, 2001, 2002, 2004, 2006, 2008, 2010, 2013 and 2016, respectively. These initial and repeated seismic surveys provide a detailed image of the CO_2 plume distribution and dynamics within the storage site.

CO_2 is injected into the reservoir in dense (supercritical) state which results in a large contrast in acoustic properties between the brine and the CO_2 and favourable conditions for seismic monitoring (Furre et al., 2017). The seismic response from this large acoustic impedance contrast can be observed on the vertical sections of time-lapse seismic surveys as shown in Figure 9. Nine bright reflections were already identified in the first time-lapse repeat survey in 1999, only 3 years after the injection started, indicating that the CO_2 ascended more than 200m vertically from the injection point to the caprock. The CO_2 plume is evidently layered and asymmetric with a vertical stack distribution indicating that it encountered and breached a series of thin shale barriers (about 1m thick) within the storage site. The thin shale layers acting as baffles to the CO_2 migration were identified on well data but, with the exception of the Thick Shale unit that separates the Utsira Sand and Sand Wedge units, it was not possible to correlate them between wells, due to the wide spread of the wellbores (>1km), nor to identify them in the baseline seismic considering its limited vertical resolution (given dominant frequency bandwidth of 20-50 Hz).

A distinct stack of broken reflectors with reduced amplitude strength has become apparent on the time-lapse seismic near the injection point, as can be observed on Figure 9. This vertical feature has been interpreted as a possible main vertical conduct of CO_2 in the plume and denoted CO_2 chimney (Chadwick et al., 2004b; Bickle et al., 2007). Since it was not possible to identify it on the baseline seismic, its origin, whether it's a pre-existing feature associated with sand injections from the underlying Hordaland Group

Skade Formation soft-sedimentary deformation (Kennett, 2008; Watsend, 2012) or related to the injection process (Hermanrud et al., 2009), is still debatable. The analysis and incorporation of high permeability chimney features through the intrashales of the Utsira Formation is outside the scope of this thesis.

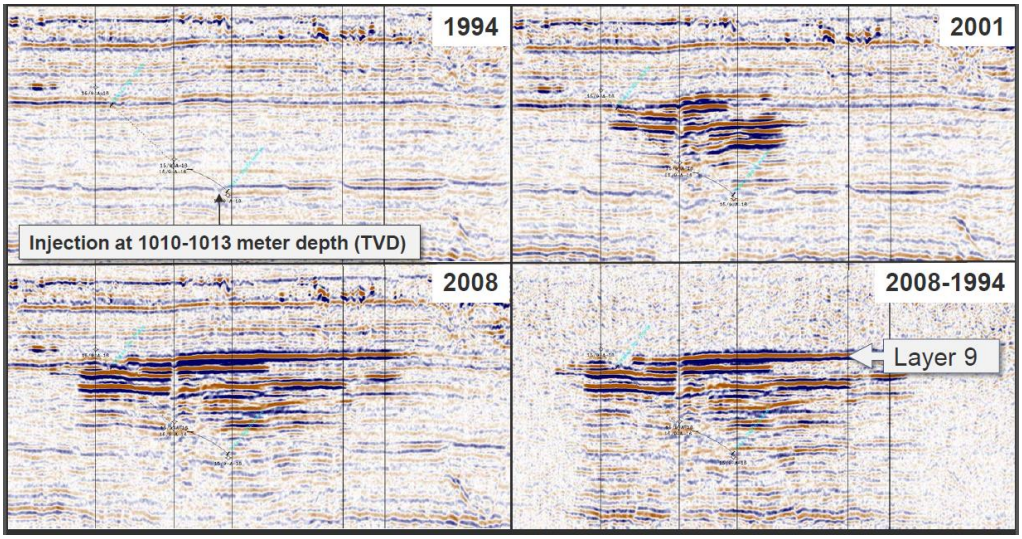

Figure 9 – Vertical seismic sections across the reservoir representing the 1994 baseline and the CO_2 plume growth differences in 2001 and 2008, respectively (courtesy of Equinor).

The mapped plume area has reached about 3 km^2 by 2008 and time-lapse seismic surveys have shown it has been growing steadily since 1999 (Figure 10) (Eiken et al., 2011). Each of the nine vertically stacked CO_2 layers have a pronounced north-south elongation and are estimated about 10-20m thick and a lateral extent of 1-3 km. The nine CO_2 accumulations have been interpreted and mapped on the seismic time-lapse datasets, with the lowest observable CO_2 layer referred to as layer 1 (L1) and the uppermost CO_2 layer as layer 9 (L9). The CO_2 layers 1 to 8 are accumulated within the Utsira Sand unit beneath the intraformational thin shales except for L8 which is trapped beneath the Thick Shale unit, and the CO_2 L9 is accumulated beneath the caprock within the Sand Wedge unit. The growth and areal distribution of each CO_2 layer from 1999 to 2008 can be seen on Figure 11, which is based on amplitude maps through time-lapse seismic data interpreted by Boait et al. (2012). The time-lapse seismic data also indicate that the uppermost CO_2 layers tend to follow topographic highs, closely conforming to the mapped topography of the caprock and underlying Thick Shale (Cavanagh et al., 2015).

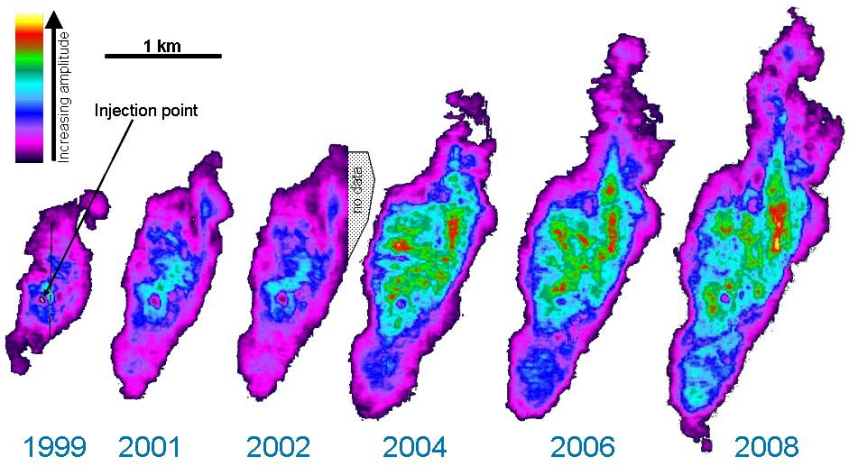

Figure 10 – CO_2 plume in map view based on time-lapse seismic difference reflection amplitude maps, cumulative for all layers. Expansion of the plume in all directions is observed, as well as intensified reflections in the central part of the plume (Eiken et al., 2011).

The CO_2 signatures in the early years of the shallower layers were spatially small and deeper reflectors were easier to interpret. With plume growth throughout the years, shallower layers have become larger, brighter and easier to interpret, impacting the definition of the deeper reflectors. Furre et al. (2017) has attributed the degradation of the deeper signals to a combination of inelastic attenuation, transmission loss of signal through the CO_2 layers and CO_2 migration and/or dissemination, which reduce the impedance contrast between sandstone and mudstone layers.

Identification of small CO_2 saturations in the reservoir as well as potential leakages is very successful in repeated seismic data but quantification of CO_2 saturation is difficult. This is because velocities change significantly as the fluid changes from pure brine to a brine with low CO_2 saturation, but much less as CO_2 saturation increases further (Furre et al., 2017; Boait et al., 2012). Gravity monitoring provide measurements of density changes and consequently of saturation, as density is linearly related to saturation. A baseline for gravity monitoring was acquired in 2002 over the CO_2 plume at Sleipner and subsequent surveys were performed in 2005, 2009 and 2013. Based on the gravimetric measurements and the plume geometry from seismic data, a mean *in situ* CO_2 density of 720±55 kg/m^3 is estimated, neglecting the effects of dissolution of CO_2 into brine (Furre et al., 2017). The amount of supercritical CO_2 in the Utsira Formation detected from gravity monitoring is the same as the injected amount of CO_2. It is possible to combine the free CO_2 mass change and the plume geometry, acquired from gravimetric and seismic data respectively, to make an estimate of CO_2 dissolution in water. Considering the temperature estimates for the reservoir, the CO_2 brine dissolution rate was estimated between 0% and 2.7% per year, in accordance with measurement uncertainty. This is an important process as it reduces the long-term risk of leakage since the brine with dissolved CO_2 is heavier than pure brine and will sink to the bottom of the formation (Eiken et al., 2011).

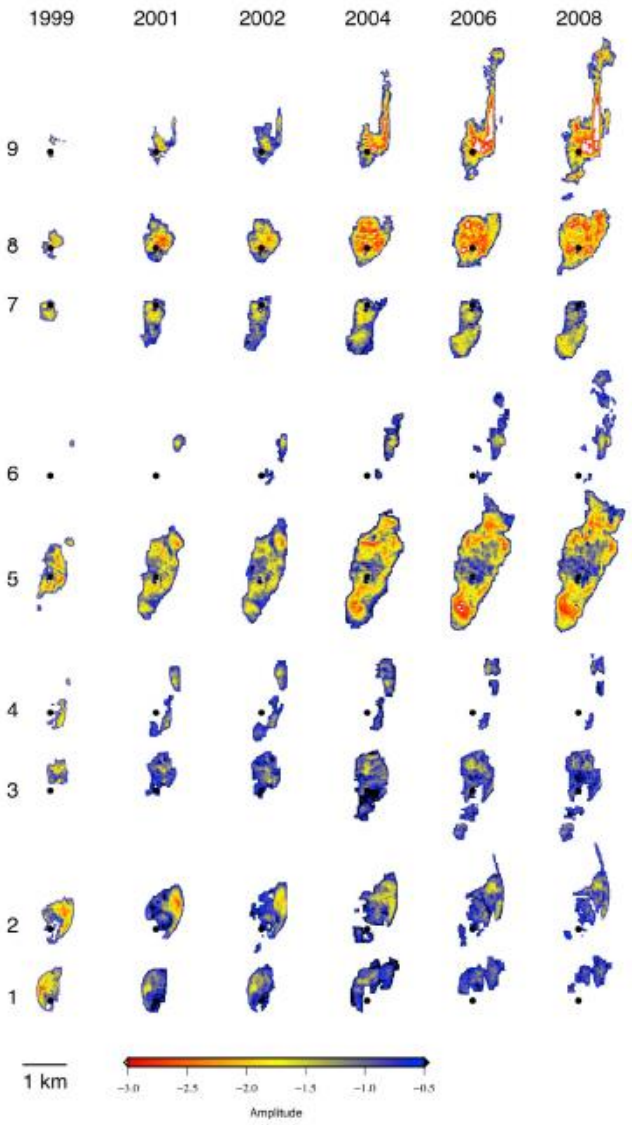

Figure 11 – CO_2 layers lateral expansion as a function of time up to 2008, layers 1 to 9 from base to top of the reservoir. Warmer and colder colour show stronger and weaker amplitudes, respectively; solid black dot shows injection point (Boait et al., 2012).

3. CO_2 Flow Dynamics

3.1. CO2 Storage Flow Dynamics

Carbon dioxide is a gas with density slightly higher than air at surface under atmospheric conditions. At pressure and temperature conditions reached at depths of 800m or deeper, CO_2 takes the form of a dense (supercritical) phase in which much larger amounts of mass can be stored per given volume and its density remain much smaller than the resident brine (Andersen, 2017). A storage formation should therefore be at least 800m deep in order to avoid the storage of CO_2 in the gas phase which would be very inefficient. This is also the depth at which it is known that geological storage seals are generally effective as gas fields have been contained for millions of years at similar depths.

The injection of CO_2 increases the pressure near the well which forces the CO_2 to enter the pore spaces initially occupied by *in situ* formation fluids. The CO_2 behaviour in the reservoir is determined by the pressure gradients created by the injection well(s), original hydraulic gradients, and the buoyancy force relative to the original formation fluids (Valberg, 2014). The pressure build-up caused by injection will depend on the rate of injection, permeability and thickness of the reservoir as well as the presence of permeability barriers within it (IPCC, 2005).

In a supercritical state, the CO_2 has the density of a fluid but the compressibility of a gas (Arts et al., 2004). This liquid or liquid-like supercritical dense phase of CO_2 injected in deep saline formations is immiscible in water (IPCC, 2005). Therefore, it forms a separate mobile dense phase (the CO_2 plume) which invades the medium and displaces the formation water that is present in the pore space. Since CO_2 is much less viscous than water (by an order of magnitude or more), its mobility is much higher than the brine and this contrast can result in viscous fingering, i.e. CO_2 bypassing much of the pore space with only some of the water formation being displaced, depending on the heterogeneity and anisotropy of rock permeability (Flett et al., 2005; IPCC, 2005).

In saline formations, the large difference in density between CO_2 and brine (30-50%) creates strong buoyancy forces which drives CO_2 upwards until it reaches a baffle or barrier. A lower permeability layer will act as a barrier making the CO_2 migrate laterally filling any stratigraphic or structural trap it encounters. Thus, the CO_2 plume distribution is strongly affected by formation heterogeneities.

As CO_2 migrates through a formation, and their volume fraction reduces below a certain level, they can be retained in the pore space of the formation by capillary forces which may immobilize (store permanently) significant amounts of CO_2 and is referred to as residual trapping (Figure 12). Over time, much of the trapped CO_2 dissolves into the formation water through a process called solubility trapping. This is a relatively fast process if the brine and CO_2 share the same pore space, but once the formation fluid is saturated with CO_2, the rate of dissolution slows and is controlled by diffusion and convection rates, which happen as the water saturated with CO_2 becomes slightly denser than the original formation water. These processes may take several thousand years to immobilize the CO_2 as a dissolved phase in brine. The solubility of CO_2 in brine decreases with increasing pressure, decreasing temperature and increasing salinity (IPCC, 2005). The most permanent form of geological storage is mineral trapping, when dissolved CO_2 may be converted to stable carbonate minerals, which is a comparatively slow process taking thousands of years or longer. The migration process of CO_2 will cease when all the injected CO_2 has been permanently immobilized by trapping mechanisms or otherwise leaked back out (Hermanrud et al., 2009). A simple sketch illustrating the dynamics of CO storage can be seen on Figure 13.

Three forces are commonly assumed to determine hydrocarbon flow in the subsurface (Hubbert, 1953 *In* Hantschel and Kauerauf, 2009). These forces are buoyancy, originated from gravity and density contrast between the hydrocarbon and water; capillary pressure, due to the interfacial tension between the hydrocarbon and water; and friction of the moving fluid, described by viscosity and mobility (Hantschel and Kauerauf, 2009). The reservoir conditions and dynamics between oil and gas production and injection of CO_2 for storage are fundamentally different.CO_2 storage represents the injection of a non-wetting fluid that displaces the *in situ* brine which is a drainage process, as opposed to imbibition in hydrocarbon production by aquifer driver or waterflood. This drainage displacement is more typical of regional basin modelling and percolating oil and gas migration (Cavanagh et al., 2015). Therefore, near the CO_2 injection well the migration of the non-wetting fluid into the pore space of the rock formation will be due to the pressure gradient under a viscous dominated regime but as the CO_2 moves away from the well, gravity and capillary forces will tend to dominate the migration of the buoyant fluid.

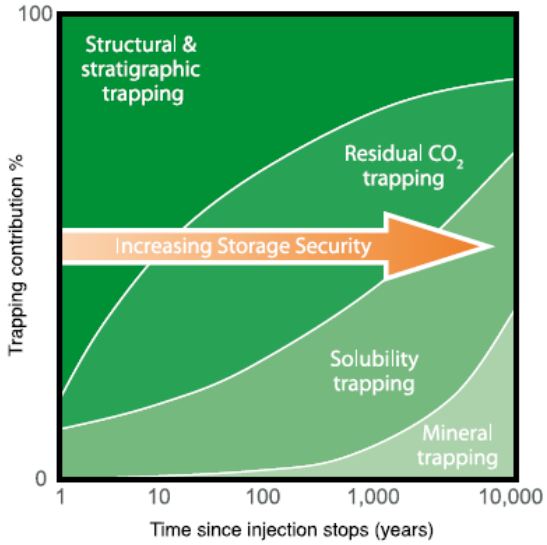

Figure 12 – Effectiveness of geological storage in a saline formation increase with time as the physically trapped CO_2 plume reacts with to brine becoming more immobile until it gets converted to solid minerals (IPCC, 2005).

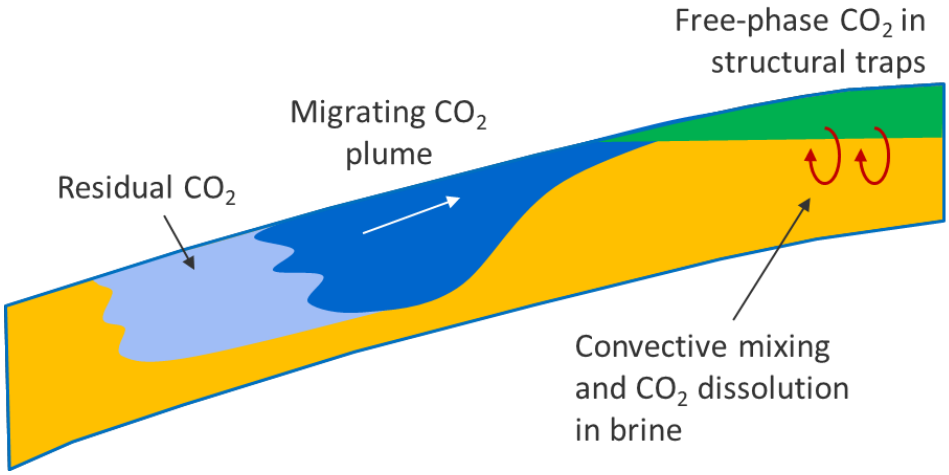

Figure 13 – Illustration of the dynamics of CO_2 storage. The injected CO_2 will migrate upwards due to buoyancy and eventually fill a structural trap. Some residual trapping of CO_2 may be left behind the migrating plume. There will be some convective mixing of CO_2 with brine resulting in dissolved phase trapping of CO_2 (Ringrose, 2018).

3.2. Sleipner CO_2 Flow Behaviour

CO_2 is just at the phase transition between gas and fluid (two-phase flow) at the Sleipner well head. During the 22 years of injection, the well head temperature has been controlled to be stable at 25 degrees Celsius, with pressure consequently also stable at the phase transition around 62-65 bar (Eiken et al., 2011). There are no down-hole pressure gauges as this technology was not readily available when CO_2 injection started in Sleipner in 1996 (Furre et al., 2017). However, based on the stable injection rate and 4D seismic imaging showing vertical flow and topography control, it is possible to assume that any pressure build-up is small, implying pressures would only be marginally above hydrostatic. The lack of down-hole data has raised uncertainty in the initial temperature of the Utsira Formation but temperature measurements from a

water producing well at the Volve field, about 10 km north of Sleipner, has narrowed down this uncertainty (Alnes et al., 2011).

The injected CO_2 in Sleipner will have temperatures and pressures close to critical point but still in the dense phase in the subsurface (Figure 14). The Sleipner reservoir temperature at the injection point (about 1012m below sea level), based on the nearby well data and on regional knowledge of the temperature gradient, is estimated to be 41 degrees Celsius (Arts et al., 2008). In the North Sea, for geological formations down to about 1500 m below sea level, the pressure is typically hydrostatic.

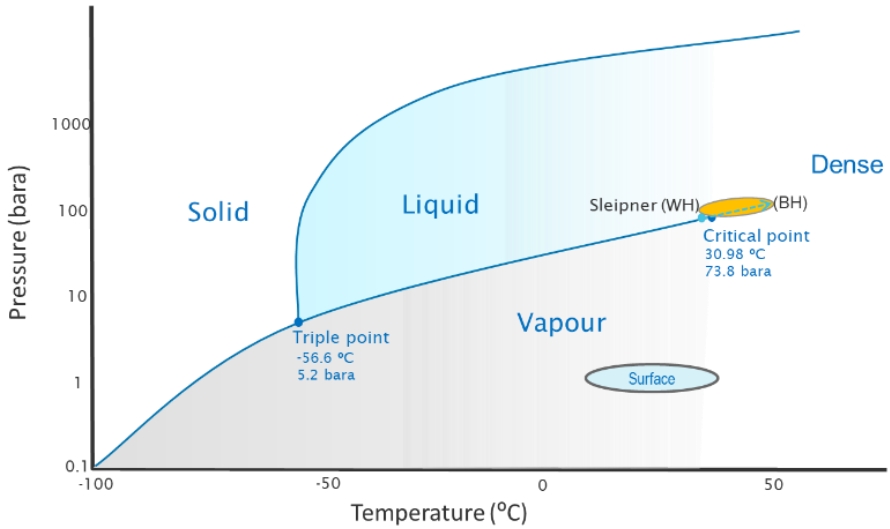

Figure 14 – CO_2 phase behavior for the Sleipner storage reservoir (WH=Well Head, BH= Bottom-hole) and at surface (vapour around 20 degrees and 1 bar). The injected CO_2 is very close to the critical point but still in the dense phase (modified from Eiken et al., 2011).

The CO_2 plume in Sleipner is likely to have ascended due to gravity segregation, given the strong density contrast between CO_2 and brine, the high permeability of the Utsira Formation sandstones and the elongated shape of the CO_2 plume layers conforming to the caprock and shale topography as observed on time-lapse seismic (Singh et al., 2010; Cavanagh and Haszeldine, 2014; Cavanagh et al., 2015).

III. Dataset

All the data analysed in this master's thesis is from latest public release from the Sleipner CO_2 storage reservoir provided by Equinor. Many research institutes worldwide have worked on Sleipner CO_2 monitoring data in the past and a large number of publications exist. Equinor and the Sleipner partners are favourable to the public awareness of the project and its positive effect on the development of CCS in general.

The latest release data package of 4D seismic data covers the CO_2 plume in a 3.4 km by 6.1 km area (Figure 15) for the vintages 1994, 1999, 2001, 2002, 2004, 2006, 2008 and 2010. It includes the amount of CO_2 injected up to 2010 and coordinates of the injection well perforation (15/9-A-16), as described in more details below.

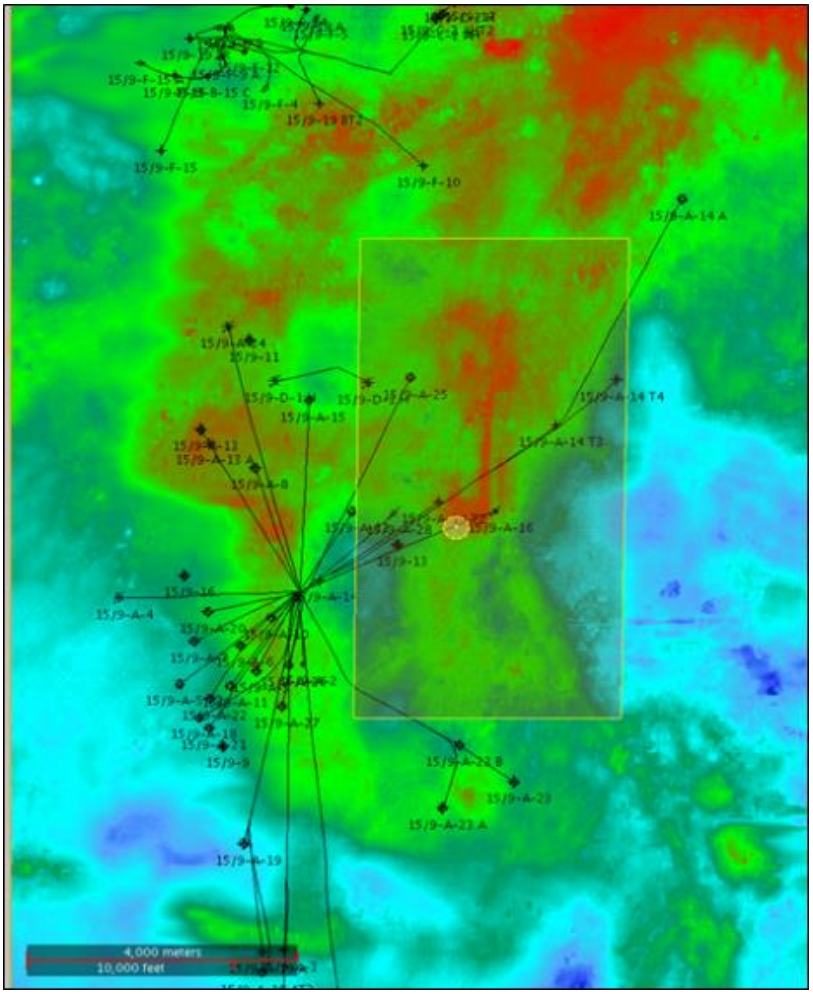

Figure 15 – Top Utsira TWT and wells in the area. Yellow rectangle shows the coverage of the released seismic data and yellow circle is the location of the injection point (well 15/9-A-16) (courtesy of Equinor).

1. Seismic Data

The 1994 baseline seismic and time-lapse surveys up to 2010 are included in the latest release of the Sleipner CO_2 storage data available to the scientific community. The large contrast in acoustic properties between the CO_2 and formation brine gives a strong time-lapse response (Figure 16).

The depth converted seismic horizons provided by Equinor for this master's thesis are Top Sand Wedge, Top Utsira Formation ad Base Utsira Formation (Figure 17). They were interpreted on the 2007 processing of the 1994 baseline seismic data tied to Top Utsira Formation picks in wells 15/9-13 (exploration) and 15/9-A-16 (injector).

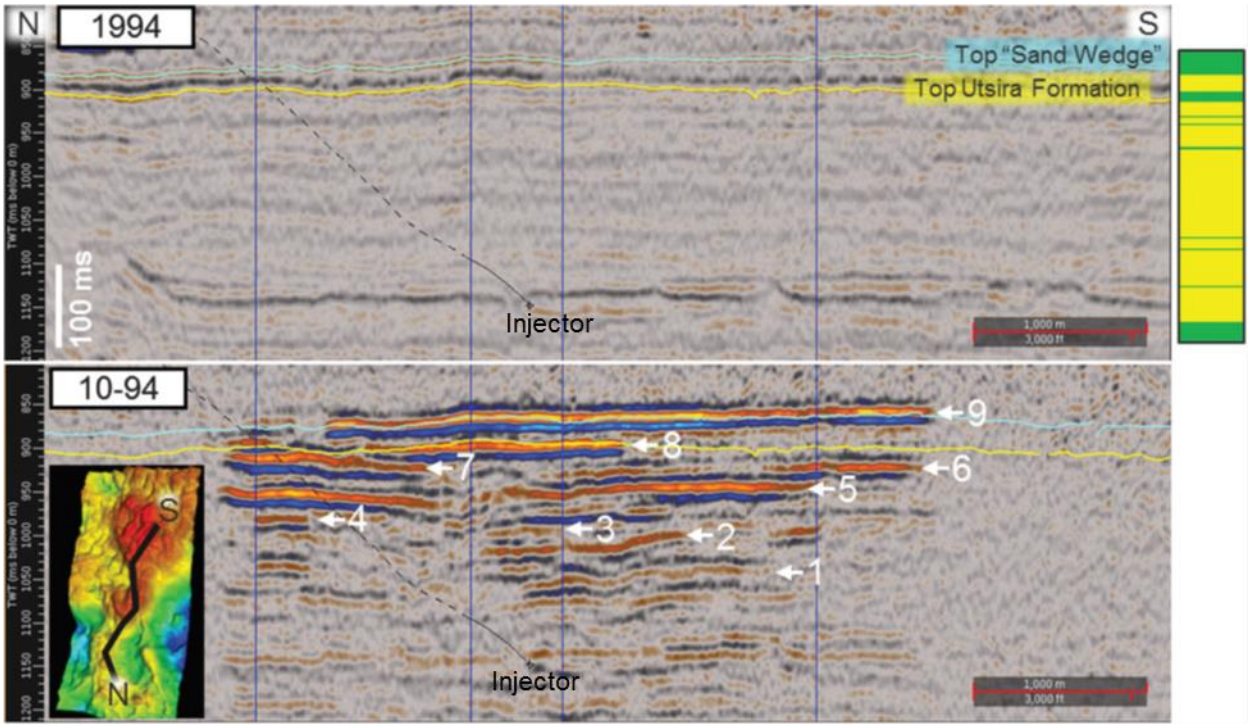

Figure 16 - Top: Baseline seismic survey N-S section (1994) - blue reflector corresponds to an increase in acoustic impedance, and a red reflector corresponds to a decrease. Projection of the injection well path 15/9-A-16 (black line). Top right: Stratigraphic column (green is shale and yellow sandstone). Bottom: Difference N-S seismic section from 2010 with the 9 interpreted CO2-filled layers. Inset: Top Sand Wedge with the location of the N-S seismic section as a black line (Furre et al., 2015).

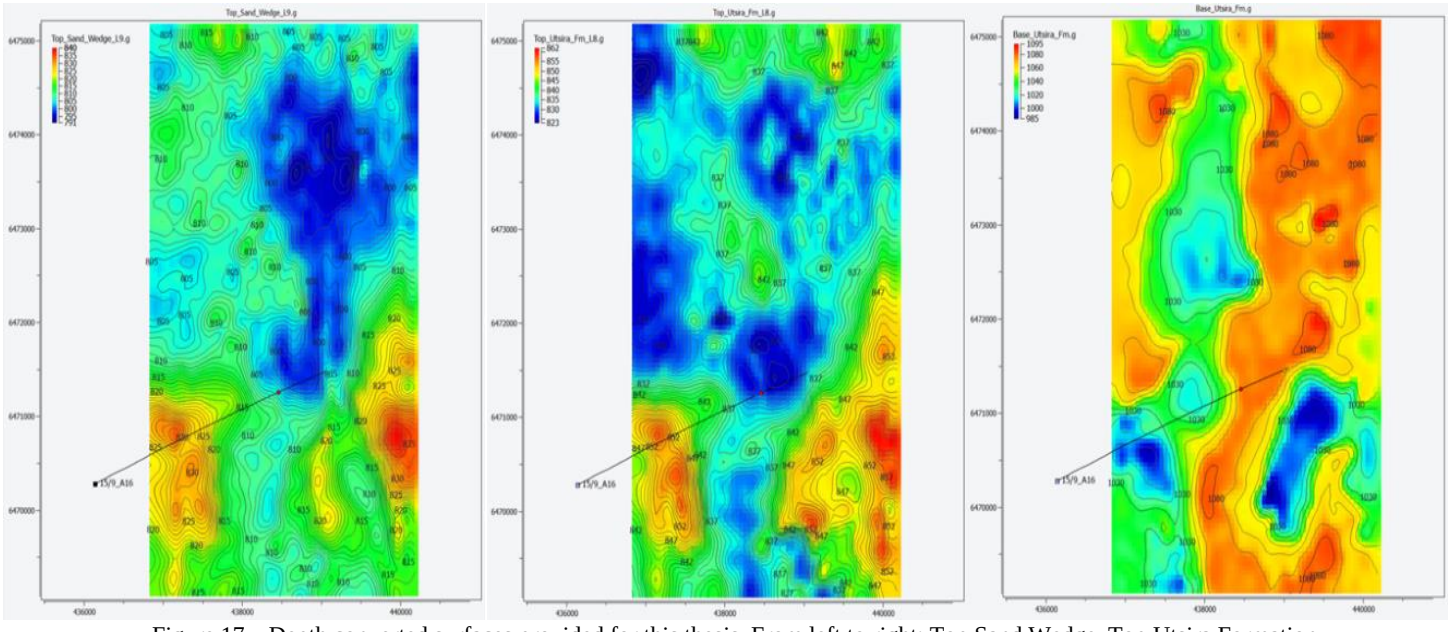

Figure 17 – Depth converted surfaces provided for this thesis. From left to right: Top Sand Wedge, Top Utsira Formation, Base Utsira Formation. Colors scale get warmer with increase in depth. Injector well 15/9-A-16 is displayed and injection point (red circle).

2. Well Data

Injector well 15/9- A-16 trajectory and coordinates of the perforation were provided by Equinor for this project (Table 2). Reservoir and fluid properties are summarized on Appendix 1 – Input Parameters (SPE 134891) from Singh et al. (2010) which were provided by Equinor as a reference for this thesis. These are based on well data penetrating the Utsira Formation regionally in the Norwegian sector and from the Sleipner field exploration and production wells, with around 30 wells within 20 km of the injection site. The well data included wireline logs, core material (reservoir and caprock), drill cuttings (reservoir and caprock), and three reservoir pressure measurements (two from Sleipner and one from the Brage field, some 250 km to the north).

Table 2 - Coordinates of the injection well 15/9-A-16 perforation.

	Min (m)	Max (m)
UTM X	438450.59	438486.18
UTM Y	6471255.52	6471258.58
Z	1010.5	1013.3

2.1. Reservoir Properties

The reservoir properties estimated based on wireline logs, core and cutting samples for the sandstones and shales of the Sleipner storage reservoir are summarized on Table 3. Porosity values have been determined from density logs, liquid invasion methods on core samples and modal analysis of thin sections.

The Utsira Sand permeability was estimated from core analysis, giving an average value of 2 D. There is no well test data for the Utsira Sand in the Sleipner area. Well tests in the Grane area (which lies around 90 km to the northeast of Sleipner) yielded 5.8 D and for the Oseberg area (located about 250 km to the northeast of Sleipner) they have resulted in permeabilities ranging from 1.1 to 8.14 D (Zweigel et al., 2004). The Sand Wedge unit above the Thick Shale has a cleaner gamma ray signature than the Utsira Sand unit below and the core samples analysed for the porosity and permeability estimates lie within the Utsira Sand, therefore recent studies have suggested assumption of higher properties distributions for this unit is reasonable (Williams and Chadwick, 2017; Eidvin et al., 2013).

Table 3– Summary of reservoir properties input parameters for the sandstones and caprock/shales (Appendix 1 – Input Parameters (SPE 134891)).

	Porosity (%)			Permeability (mD)			Threshold Pressures (kPa)		
	Mean	Min	Max	Mean	Min	Max	Mean	Min	Max
Sandstones	36	32	40	2000	1100	5000	1	0.7	1.3
Caprock/Shales	30	28	32	0.001	0.0075	0.0015	1700	1600	1900

Capillary entry pressures (threshold pressures) were estimated based on core studies. Laboratory measurements for the caprock threshold pressure from a cored production well close to the storage site suggest a range of 1.6 to 1.9 MPa, i.e. the CO_2 fluid pressure needed to break through a low permeability rock (Cavanagh and Haszeldine, 2014).

Permeability-Threshold Pressure Transforms in mercury-air system based on the work developed by Sorkhabi and Tsuji (2005) and Harper and Lundin (1997) were provided by Equinor (Table 4 and Figure

18), as they were considered in previous modelling studies developed by Cavanagh et al. (2015). Harper and Lundin (1997) have proposed a theoretical equation relating capillary pressure to permeability. Sorkhabi and Tsuji (2005) have compiled datasets from multiple studies with 244 pairs of gas permeability and capillary pressure from mercury injection tests for fault rocks and sandstone rocks. Their results have shown very similar regression lines implying that both sedimentary and faulting processes in sandstones produce rock materials with hydraulic properties that follow the same percolation laws of porous media.

As can be seen on Figure 18, the theoretical transform from Harper and Lundin (1997) in comparison to the others tend to over represent the end-member values of threshold pressures, overestimate for low permeability values and underestimate for high values. Sorkhabi and Tsuji (2005) is a robust study and the average transform was selected for the analysis in this master's thesis, since it represents the middle values between the two proposed transforms, for faulted rocks and sandstones.

Table 4 – Permeability-Threshold Pressure Transforms based on Sorkhabi and Tsuji (2005) and Harper and Lundin (1997).

Permeability-Threshold Pressure Transforms (Hg-Air)	
Conversion factor	Psi to kPa: 6.89475729316836
Co-variables:	Intrinsic permeability (mD): x Threshold pressure, Pth (kPa): f(x)
Sandstone, Sorkhabi and Tsuji (2005)	f(x) = 6.894757293168361*55.402*x^-0.4273
Faults, Sorkhabi and Tsuji (2005)	f(x) = 6.894757293168361*55.560*x^-0.4014
Average,Sorkhabi and Tsuji (2005)	f(x) = 6.894757293168361*55.703*x^-0.4147
Theoretical, Harper and Lundin (1997)	f(x) = 6.894757293168361*65.453*x^-0.5056

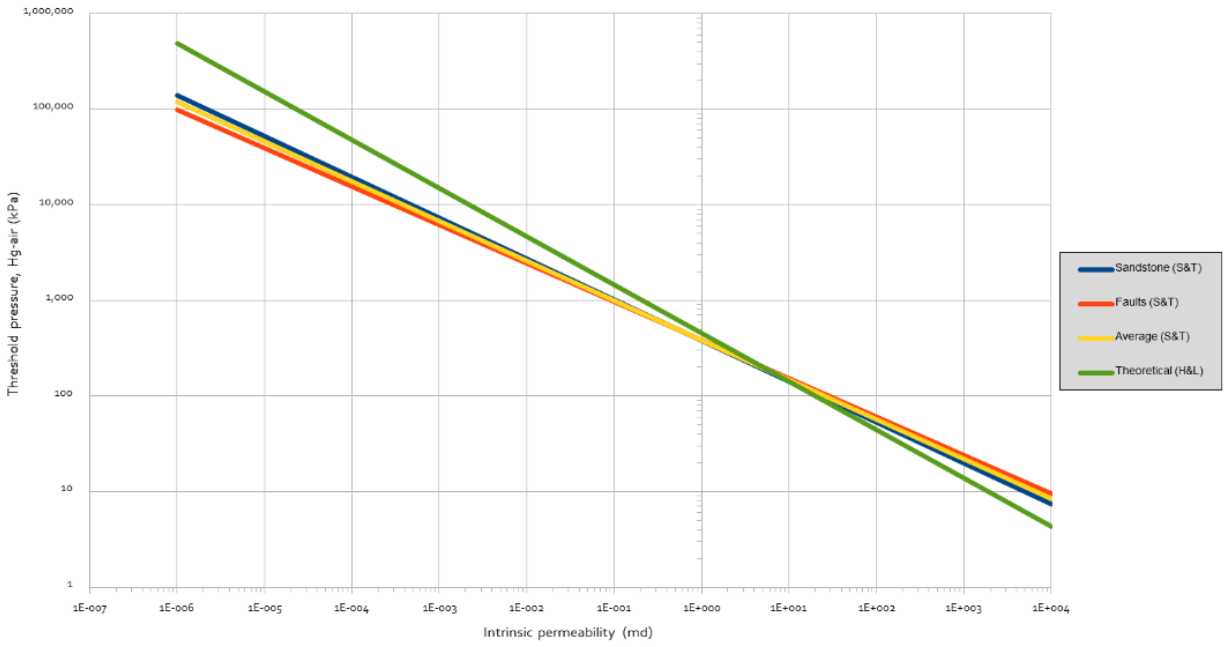

Figure 18 – Permeability-Threshold Pressure Transforms (Hg-Air system) based on Sorkhabi and Tsuji (2005) and Harper and Lundin (1997).

2.2. Fluid Properties

A seabed temperature of 7 degrees Celsius at 80m water depth and a geothermal gradient of 35.6 degrees Celsius/km are estimated as references for the Sleipner storage reservoir (Singh et al., 2010). The ambient temperature at the injection depth is constrained at 41ºC ±1ºC (Bickle et al., 2007).

There are no indications for overpressure in the Sleipner storage reservoir (Zweigel et al., 2004). The formation is water filled and pressure is hydrostatic, varying from about 8 MPa at the top of the reservoir to about 11 MPa at the bottom (Baklid et al., 1996). The brine at the reservoir depths have a salinity and composition that can be compared to sea water (3.5% salt) (Singh et al., 2010).

The density of CO_2 depends on temperature, pressure and amount of impurities. In Sleipner, impurities are mainly methane and butenes, toluenes, and xylenes (BTX). Since methane tends to reduce the density of the CO_2 mixture and BTX increases it, their effects cancel each other out in the Sleipner case (Zweigel et al., 2004). Therefore, the thermodynamics properties of pure CO_2 are considered for density calculations, with an overall reference estimate of 760 kg/m^3 (Alnes et al., 2008; Singh et al., 2010).

Considering that the temperature at the top of the reservoir is poorly understood with estimates of 34ºC ± 3ºC, which would result in a potential density range for CO_2 in the uppermost layer (layer 9) of 300-700 kg/m^3 (Cavanagh and Haszeldine, 2014), a mid-range scenario is assumed as a reference in this master's thesis, with a temperature of 35 ºC at the caprock (same assumption as in Cavanagh and Haszeldine, 2014; and Cavanagh et al., 2015).

Reference maximum CO_2 saturation is defined as 89%, remaining 11% corresponds to irreducible water (Swc), and residual gas saturation is 2%, as provided by Appendix 1 – Input Parameters (SPE 134891). A summary of key input parameters is listed on Table 5.

Table 5 – Summary of fluid properties input parameters (Appendix 1 – Input Parameters (SPE 134891)).

Property	Input Value (SPE)
Geothermal Gradient (C/km)	35.6
Hydrostatic Gradient (mPa/km)	10
Connate water saturation Swc	0.11
Critical gas saturation Socr	0.02
Brine density (kg/m3)	1020
Brine salinity (ppm)	33500

2.3. Injected volumes

The Sleipner injected CO_2 volumes per year were provided by Equinor from 1996 to 2010 (Table 6 and Figure 19). The total cumulative amount of CO_2 injected into the Utsira Formation by the end of 2010 is 12.08 Mt.

Table 6 – Sleipner CO_2 injected volumes per year and cumulative in million tonnes (Mt) (courtesy of Equinor).

CO2 Annual (Mt)	1996	1997	1998	1999	2000	2001	2002	2003	2004	2005	2006	2007	2008	2009	2010
Sleipner (per year)	0.07	0.66	0.84	0.93	0.93	1.01	0.96	0.91	0.75	0.86	0.82	0.92	0.81	0.86	0.74
Sleipner (total)	0.07	0.73	1.58	2.50	3.44	4.44	5.40	6.31	7.06	7.92	8.74	9.66	10.48	11.34	12.08

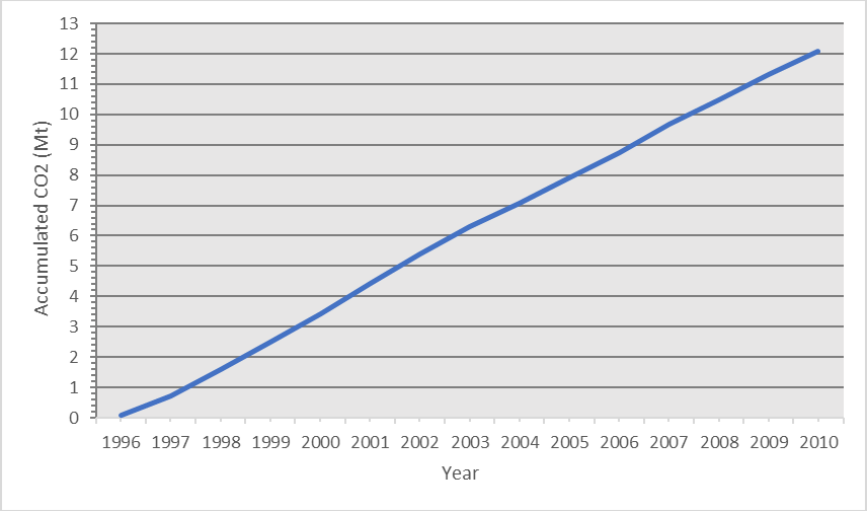

Figure 19 – Cumulative distribution of injected CO_2 into Sleipner from 1996 to 2010.

2.4. Previous Sleipner Benchmark Models

A single 3D geological model was built from the Sleipner dataset of the period of 1999-2008 and made available to the scientific community. The Sleipner benchmark originally released by Equinor in 2011 consisted of a numerical mesh and related data of the uppermost layer only (layer 9 within the Sand Wedge unit), whereas the updated release in 2015 was extended to include layer 8 as well (uppermost part of the Utsira Sand unit, just below the Thick Shale unit). The aim of the benchmark is to improve modelling tools and further our understanding of CO_2 flow dynamics (Cavanagh et al., 2013). The reason the benchmark models have been focused so far on the upper two layers is because only these layers were possible to interpret on the baseline seismic survey which thereby defined the structural surfaces for the reservoir model (Furre et al., 2017).

Despite the high quality time-lapse seismic surveys imaging of the areal distribution of the CO_2 plume in Sleipner, to date no published dynamic model has accurately replicated the layered morphology or flow behaviour of the plume (Bickle et al., 2007; Singh et al., 2010; Boait et al., 2012; Cavanagh, 2013; Cavanagh and Nazarian, 2014; Furre et al., 2017). This is due to challenges around the underlying flow physics of CO_2 and uncertainties in geological assumptions.

It is still debatable whether the upscaled flow process is dominated by viscous or gravity forces, but increasingly a gravity-dominated interpretation is being proposed (Furre et al., 2017). Early attempts with conventional Darcy flow simulators have failed to match the CO_2 plume distribution due to its underlying flow physics requiring viscous flow via a series of aligned holes within the shale barriers, related to conceptual models with discrete vertical pathways such as chimneys, sand injectites and sub-seismic faults (Cavanagh et al., 2015). Viscous dominated models in general are not able to replicate the north-south elongation trend observed especially in the uppermost layer 9 (Singh et al., 2010). Gravity dominated models using invasion percolation simulation tend to overestimate the plume extension to the north as it strongly follows topographic highs. Gravity-dominant flow is considered the most important flow process operating at the Sleipner CO_2 storage site but pure gravity does not provide a match to the plume distribution as it fails to represent viscous effects close to the injection point (Singh et al., 2010). The interplay between viscous and gravity forces may be important in order to get a match to the plume distribution. It is not within the scope of this thesis to conclude on the way forward for flow simulations.

The input data provided for this project will correspond to the latest Sleipner benchmark release with a data package up to 2010. It has been used to define the full multi-layer plume distribution of CO_2 in Sleipner (from the Base Utsira Formation to Caprock, layer 1 to layer 9), based on assumptions from the Cavanagh et al. (2015) paper.

IV. Modelling Methodology

A three-dimensional geological model is built to capture the full multi-layer plume distribution of the Sleipner CO_2 storage reservoir in order to understand the key factors impacting the CO_2 plume migration. The framework consists of nine alternating zones of sandstone and shale from the base of the Utsira Formation, below the injection point, to the caprock (primary seal) above the reservoir. Published modelling and simulation of the Sleipner storage site including the CO_2 layers below the uppermost two layers (Cavanagh et al., 2015) was used to constrain their vertical distribution. An invasion percolation approach was selected to simulate the CO_2 migration using the Permedia software (version 5000.12), which assumes a flow domain dominated by capillary and gravity forces. Scenarios were tested to try to capture the CO_2 plume morphology considering geological constraints. A sensitivity assessment of the range in the input parameters was performed to verify their control on the plume flow dynamics.

1. Geological Controls on CO_2 Migration

Fluid migration and entrapment in a reservoir is controlled by two competing forces, buoyancy and capillary pressures. Buoyancy acts to displace lesser dense fluid upwards (CO_2) and capillary pressure acts to displace denser fluids (brine) downwards (Slatt, 2006). In a reservoir, if buoyancy pressure is smaller than capillary pressure, hydrocarbons cannot migrate upward to displace brine so the pore spaces remain filled with water (S_w is 100%). When buoyancy pressure exceeds the capillary pressure, the brine will be displaced and the pore spaces will contain hydrocarbons (S_w<100%). Buoyancy forces increase with the density difference between pore water and hydrocarbon and with increasing height of the hydrocarbon column (Figure 20). This can be expressed as:

$$P_c = \Delta\rho g h$$

where P_c is the capillary pressure of the invading phase at the interface, $\Delta\rho$ is the density different between the two fluid phases (such as CO_2 and brine), g is the standard gravity, h is the column height of the invading phase.

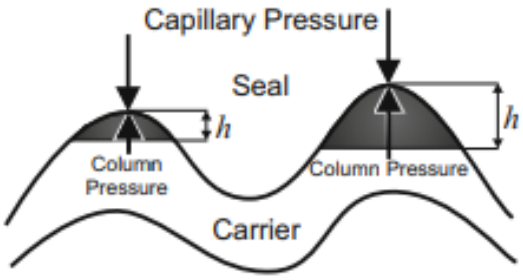

Figure 20 – Pressure acting on top of an accumulation against a seal (h =column height). The column pressure (buoyancy pressure or capillary pressure of the invading phase) must exceed the capillary pressure of the seal in order for breakthrough to occur (Hantschel and Kauerauf, 2009).

Interfacial tension (IFT) occurs at the interface between reservoir fluids and between the fluids and the rock matrix. It rises because of the differently sized attraction forces between molecules within one phase and across a boundary to molecules within another phase (Hantschel and Kauerauf, 2009). Interfacial tension is a function of density difference with a higher density contrast between two fluids increasing the interfacial tension. Therefore, it is also dependent on pressure, temperature and brine salinity as they impact the densities of the reservoir fluids. The interfacial forces give rise to the capillary pressure. Capillary entry pressure (Pth), also known as threshold or displacement pressure, is the amount of pressure required in order to force the non-wetting phase (oil, gas, CO_2) to displace the wetting phase (brine) in a capillary (pore) (Slatt, 2006). Mathematically it is defined as:

$$Pth = \frac{2\sigma(cos\theta)}{r_c}$$

where, Pth is the capillary threshold pressure of the rock at which breakthrough occurs, σ is the interfacial tension, θ is the contact angle, r_c is the pore (capillary) radius. The different entry level pressures are therefore inversely related to the sizes of the pore throats (radius or r_c). The larger the pore throat size, the smaller the Pth required for the non-wetting phase fluid to displace the wetting phase fluid (Figure 21).

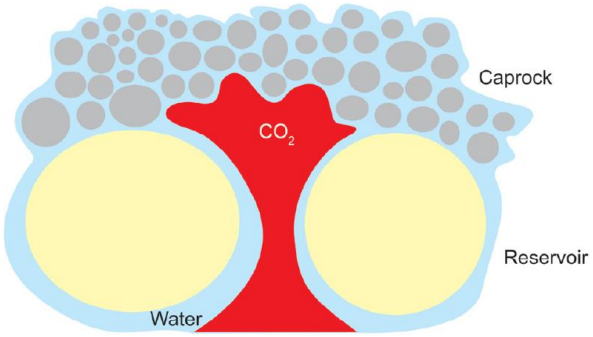

Figure 21 – Pore scale capillary trapping. The density contrast between CO_2 and brine drives CO_2 upwards through the reservoir (large pore throats) and it accumulates underneath rocks with small pore throats (high capillary entry pressures) (Hermanrud et al., 2009).

Capillary pressure is usually measured for mercury-air systems in laboratory experiments. In order to apply mercury injection data to the reservoir, the data must be converted from the laboratory mercury-air

system to the subsurface hydrocarbon-brine system of the reservoir (Vavra et al., 1992). It can be transformed to water-petroleum systems by:

$$Pc_{res} = Pc_{Hg-Air} \frac{\sigma_{res} \cos \theta_{res}}{\sigma_{Hg-Air} \cos \theta_{Hg-Air}}$$

where Pc_{res} is the capillary pressure of the hydrocarbon-brine reservoir system, Pc_{Hg-Air} is the capillary pressure of mercury-air system, σ_{res} is the interfacial tension of the reservoir system, σ_{Hg-Air} is the interfacial tension of the mercury-air system, θ_{res} is the contact angle of reservoir system, θ_{Hg-Air} is the contact angle of mercury-air system.

A mercury-air system has an interfacial tension of 0.484 N/m and a contact angle of 141 degrees. Considering a CO_2-pore water contact angle of 140 degrees and given a CO_2-brine interfacial tension of 0.027 N/m, the multiplier conversion factor would be 0.055. In the Permedia CO_2 toolkit software, all input values for capillary threshold pressures are in mercury-air system (Hg-Air) and a multiplier conversion factor (named the IFT multiplier) is estimated as a property based on pressure, temperature, salinity and density contrast and applied in the background to convert them to the CO_2-brine system before running migration simulation (confirmed via email communication with Permedia support).

Capillary pressure controls the original static distribution of reservoir fluids and the possible movement of hydrocarbon through the reservoir (Vavra et al., 1992). Movement of fluids within a rock depends more on the size of the pore throats than on the size of the pores, hence there is a direct relationship between permeability and capillary threshold pressure (Slatt, 2006). Considering the estimated multiplier conversion factor, the provided Permeability-Threshold Pressure Transforms, based on the work developed by Sorkhabi and Tsuji (2005) and Harper and Lundin (1997) (Figure 18), which are in mercury-air system can be converted to the CO-brine system of the Sleipner reservoir as shown in Figure 22.

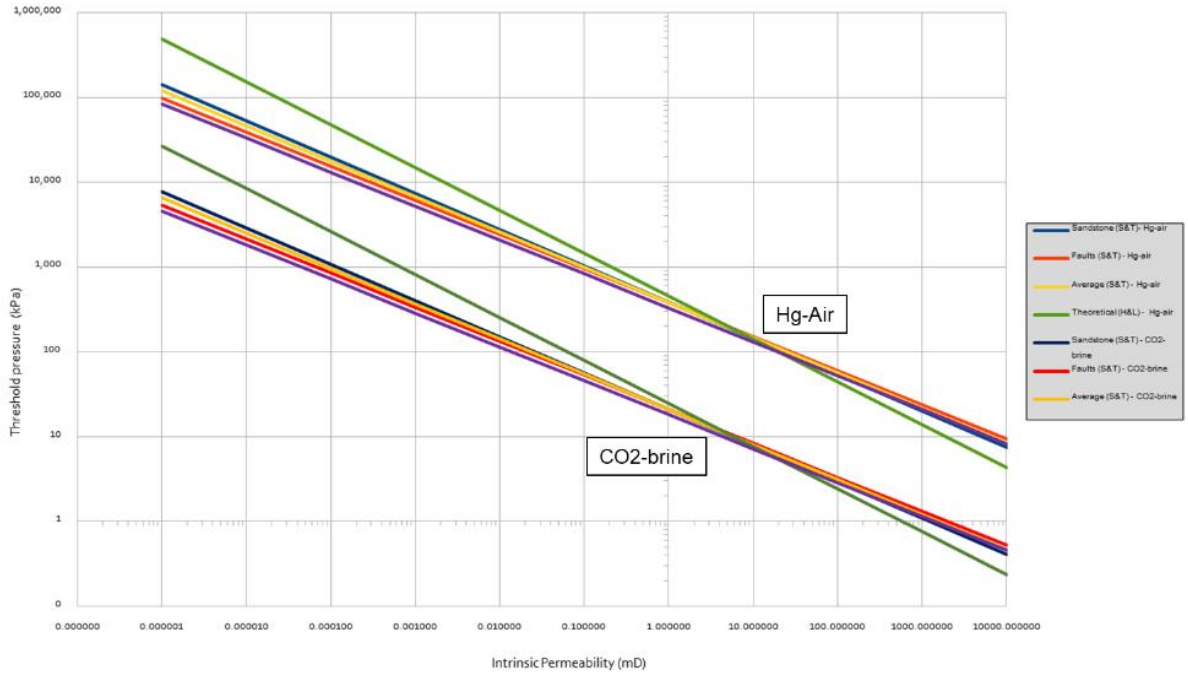

Figure 22 – Permeability-Threshold Pressure Transforms in Hg-Air system based on Sorkhabi and Tsuji (2005) and Harper and Lundin (1997) converted to the CO_2-brine system of the Sleipner reservoir.

2. Conceptual Model

The Sleipner reservoir consists of weakly consolidated shallow marine sandstones with high porosities around 36% and permeabilities in the Darcy range. It can be divided into two sandstone units, Utsira Sand and Sand Wedge, which are separated by a Thick Shale unit about 6.5m thick above the Utsira Sand and capped by the Nordland shales which act as the primary seal (caprock). A number of thin (about 1m thick) shale barriers within the Utsira Sand unit act as baffles to flow by trapping and dividing the CO_2 plume vertically into distinct layers as observed on seismic (Figure 16).

The supercritical CO_2 ascends upwards due to the strong density contrast between brine and CO_2 as well as the high permeabilities of the reservoir sandstones, characteristic of a gravity-controlled migration. As the CO_2 encounters a low permeability shale barrier, it accumulates beneath the barrier, under near hydrostatic pressure conditions, by back-filling small trap structures conforming to the barrier topography (Cavanagh et al., 2015). These CO_2 layers accumulate within the sandstone intervals as thin but highly saturated layers. The CO_2 breaks through when the buoyancy force of the CO_2 overcomes the capillary threshold pressures of the shale barrier. This results in the vertical stack of CO_2 layers distribution that conform to the caprock and shale topography which defines the Sleipner CO_2 plume distribution.

Invasion percolation simulation assumes a flow domain dominated by gravity and capillary forces over viscous forces, similar to the expected in Sleipner. This approach describes the behaviour of an immiscible fluid (CO_2) that is migrating, or percolating into, a porous medium (sandstone and shales). This displacement of the original pore fluid (brine) is commonly known in petroleum systems modelling as drainage, and is opposed to imbibition which characterizes oil and gas production. It has been successfully applied in regional hydrocarbon migration and local hydrocarbon field charge processes (Carruthers and Ringrose, 1998).

The invasion percolation approach is valid at low flux rates as the viscosity contribution to flow is negligible, hence the viscous dominated Darcy flow approximation breaks down (Cavanagh and Haszeldine, 2014). The boundary condition between viscous and capillary flow is defined by the capillary number, which is a dimensionless ratio of the viscous force to the interfacial tension that controls percolation (Cavanagh et al., 2015). The capillary number is estimated as follows:

$$Ca = \frac{\mu q}{\gamma}$$

where, Ca is the capillary number for a given flow regime, μ is the viscosity of the most viscous fluid in a two-phase system, q is the volumetric flux, γ is the interfacial tension between the invading and resident phases. A capillary number of less than 10^{-4} is the limiting condition for buoyant fluids such as oil, gas and CO_2 to percolate through the sedimentary strata as gravity-driven ganglia (England et al., 1987). Hydrocarbon migration typically has a capillary number of $10^{-10} – 10^{-14}$. The capillary number estimated for Sleipner CO_2 plume by Cavanagh and Haszeldine (2014) is about 10^{-7} which is inconsistent with viscous flow and closer approximates to invasion percolation.

The modelling approach of this master's project applied the Permedia CO_2 Migration simulator, which is a multi-phase invasion percolation simulator based on the capillary threshold pressures and fluid density descriptions. The intra-formational thin shales are treated as laterally continuous barriers that trap the percolating CO_2 which accumulate within the sandstone intervals backfilling against each barrier and breaking through when the CO_2 capillary forces exceed the threshold pressures of the shales. This migration simulation approach has been applied by Cavanagh and Haszeldine (2014) and Cavanagh et al. (2015) with a similar result to the layered distribution in Sleipner and definition of the threshold pressures required in the intraformational shales to allow for CO_2 to migrate upwards and reach the caprock.

Caprock threshold pressures from core laboratory measurements suggest a range of 1.6 to 1.9 MPa, i.e. the CO_2 fluid pressure needed to break through a low permeability rock (Singh et al., 2010). However, if this range is applicable to the shale barriers within the Utsira Formation, the CO_2 layers column heights would result in hundreds of meters and they would have acted as seals rather than baffles to flow, preventing the vertical stack of layers observed. In this case, the plume would have taken much longer to breakthrough, if at all, and the behaviour would have been more of a zig-zag pattern distribution with lateral spilling migration.

In order to match the "pancake style" stack of CO_2 layers in Sleipner, Cavanagh and Haszedine (2014) defined much lower threshold pressures for the intraformational shale barriers with values around 50kPa, which is about 35-fold less than the measured on the caprock sample. This result was reached by iterative experimentation with gradual reduction of the shales threshold pressures, from the starting point of the cored caprock, until the simulation exhibited a CO_2 plume distribution similar to the observed in seismic. They have interpreted this significant low threshold pressures to be due to microfracturing of the shale barriers which would have resulted from pore pressure fluctuations associated with rapid deglaciation in the region over the last million years. The caprock is much thicker than the shale barriers within the reservoir and have shown no evidence of CO_2 leakage indicating a different response to CO_2 retention. Therefore, the authors have inferred that similar fracture networks within the primary seal are potentially only proximal to the formation with limited percolation connectivity which would prevent vertical migration through the overburden. In this master's thesis, iterative experimentation of the threshold pressures of the shales was

also performed in order to define a distribution range that allowed for migration simulation of a vertical stack of CO_2 layers, and the results compared to Cavanagh and Haszeldine (2014).

3. Geomodel Grid Design

A 3D reservoir model was built from the input high resolution seismic maps of the Top Sand Wedge (L9), Top Utsira Formation (L8) and Base Utsira Formation (Figure 23), the remained surfaces were then mapped using isochores. Within the Utsira Fm, the intrashales defining L1 to L7 are 1m thick laterally continuous barriers/baffles conforming with the Top L8 structure. A sensitivity analysis was performed on the thickness of the intrashales laterally continuous zones, with 0.5 to 2 m instead of 1 m and up to 4 m only for layer 5 (since it presents the larger CO_2 plume as observed on seismic) and all other inputs kept the same. There was no impact on the CO_2 migration simulation based sole on the thickness of the intrashales which indicates that the percolation simulator is much more sensitive to the threshold pressure value of each cell than the number of cells to break through vertically. Therefore, the mean thickness of 1m was applied to all intrashales zones (L1 to L7).

The intrashales depths within the Utsira Formation were estimated based on Cavanagh et al. (2015) paper and calculated from the Top L8 structure depth (Figure 24). Thick Shale is defined as a 6.5 m thick laterally continuous barrier/baffle following the Top L8 structure (Appendix 1 – Input Parameters (SPE 134891)). Caprock is represented with 10m thickness in the model conforming with Top L9 structure.

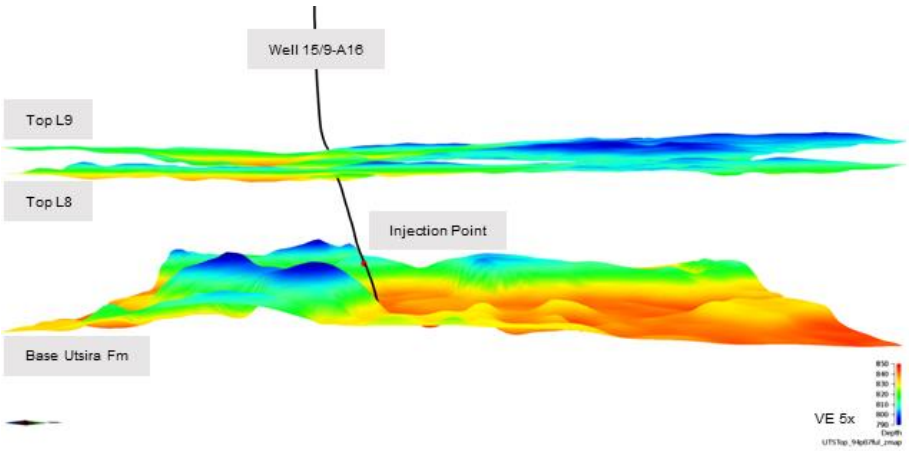

Figure 23 – Input data observed in 3D view in the Permedia software (VE= vertical exaggeration). High resolution input seismic surfaces Top Sand Wedge L9, Top Utsira Formation L8 and Base Utsira Formation, injector well 15/9-A16 and injection point.

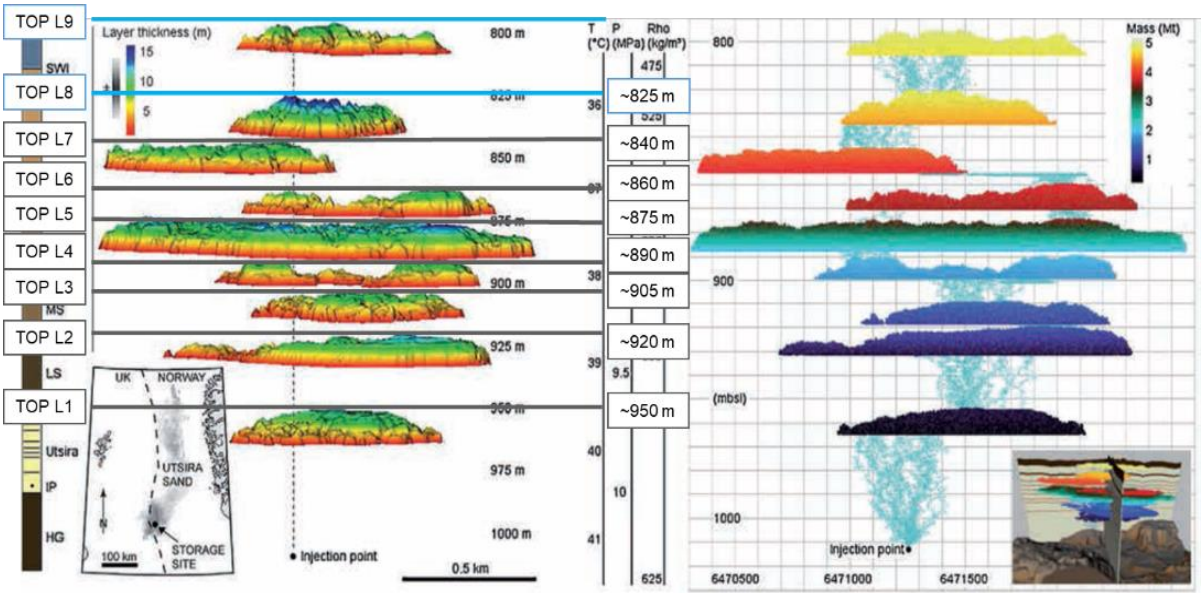

Figure 24 - The intrashales depths within the Utsira Formation were estimated based on the cross-section provided by Cavanagh et al. (2015) and calculated conforming to the Top L8 structure depth.

The lateral resolution of the grid is 50m x 50m, following the input seismic depth surfaces, with 0.5m thick layers in order to represent each thin intra-formational shale barrier by 2 cells vertically. The layering scheme is a limitation on the Permedia software for a large grid with multiple zones. The only available option is Follow Base which truncates the layers towards the top horizon for each zone. Software packages developed for reservoir modelling such as Petrel allow for more options of layering to capture the geological interpretation, such as Follow Top or Follow Base (truncated towards the base or the top horizon, respectively), Proportional (considers the thickness of the entire zone), Fraction (the number of layers and their thickness can be specified) and Combination (a depositional surface can be added as a guide). Considering the discussions regarding the depositional environment for the Utsira Formation and the master's thesis goal, ideally the layering scheme for the Sleipner reservoir model would have been Proportional as the impact on flow is the least significant.

The grid boundary is the same as the input seismic surfaces with a lateral extension of 3.4 km x 6.1 km. The three-dimensional model has a total of approximate 5.2 million cells (68x122x626) and is represented by 9 reservoir layers separated by laterally extensive shale barriers/baffles (Figure 25).

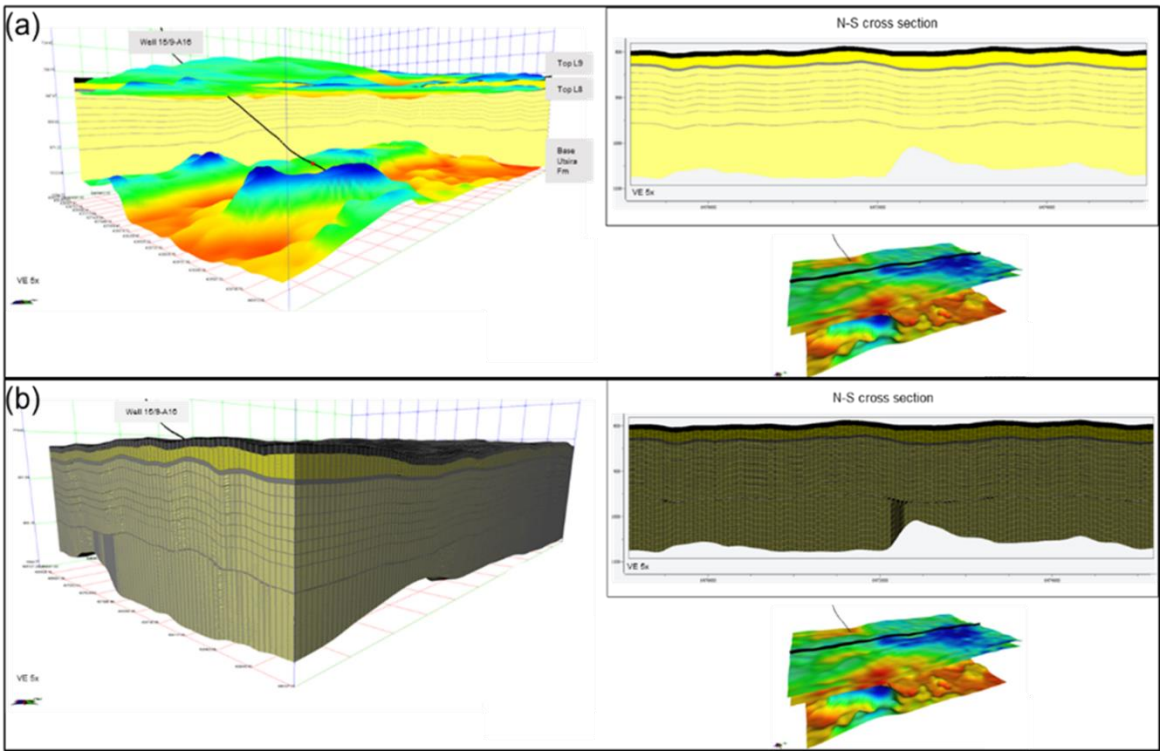

Figure 25 – Geomodel grid design 3D view (left) and cross-section (right). (a) Nine reservoir zones divided by laterally continuous shale barriers. (b) Three-dimensional grid with cell dimensions 50mx50mx0.5m.

4. Property Modelling

Permedia is primarily a petroleum systems software which reflects basin scale modelling. It presents a customized CO_2 toolkit module for CO_2 storage exploration, monitoring and prediction. However, the reservoir scale modelling functionalities available to date are limited and simplistic in comparison to other Exploration and Production software packages such as RMS and Petrel.

Considering the input data available for Sleipner, two reservoir property modelling methods are possible in Permedia. A lithology-controlled method which is based on the porosity variation with depth per lithology with their subsequent properties (ie. permeability, threshold pressures) related to porosity. And a map-based interpolation method which presents a lateral control of the property distribution. The map can also be created pixel based from a property distribution, but the only type of distribution available is uniform.

Porosity reduction due to compaction should be negligible in the Sleipner model due to its shallow depth and almost unconsolidated sands with minor shape changes of grains as evidenced by core samples from well 15/9-A23 (Zweigel et al., 2004). Therefore, a simple approach for property modelling was applied considering constant values for each lithology (Table 7). The threshold pressures for the intrashales were defined by iterative experimentation to capture the vertical stack of CO_2 plume layers as observed in the Sleipner CO_2 plume distribution. This was a manual process with the systematic reduction of the input threshold pressure from the cored caprock of 1.7 MPa in the intrashales until a value that allowed for the breakthrough of each shale barrier was reached. The CO_2 plume L5 is the largest observed layer on seismic and its estimated threshold pressure was consequently slightly higher than the other layers. The caprock threshold pressure was defined applying the average permeability-threshold pressure transform to the core

input of 0.001 mD for consistency. The threshold pressure input value of 1700 kPa provides an equivalent permeability value of 0.0005 mD (Figure 26).

Table 7– Simple Approach – constant values for each property per lithology. Threshold pressures in Hg-Air system.

Simple Approach - Inputs					
Layers	Porosity	Pth X Hg-Air (kPa)	Pth Z Hg-Air (kPa)	Perm X (mD)	Perm Z (mD)
SW	0.36	14	56	3000	300
US	0.34	16	64	2000	200
Caprock	0.30	6737	11972	0.001	0.0003
L5	0.30	687	2750	0.246	0.0087
Intrashales	0.30	562	2250	0.399	0.0141

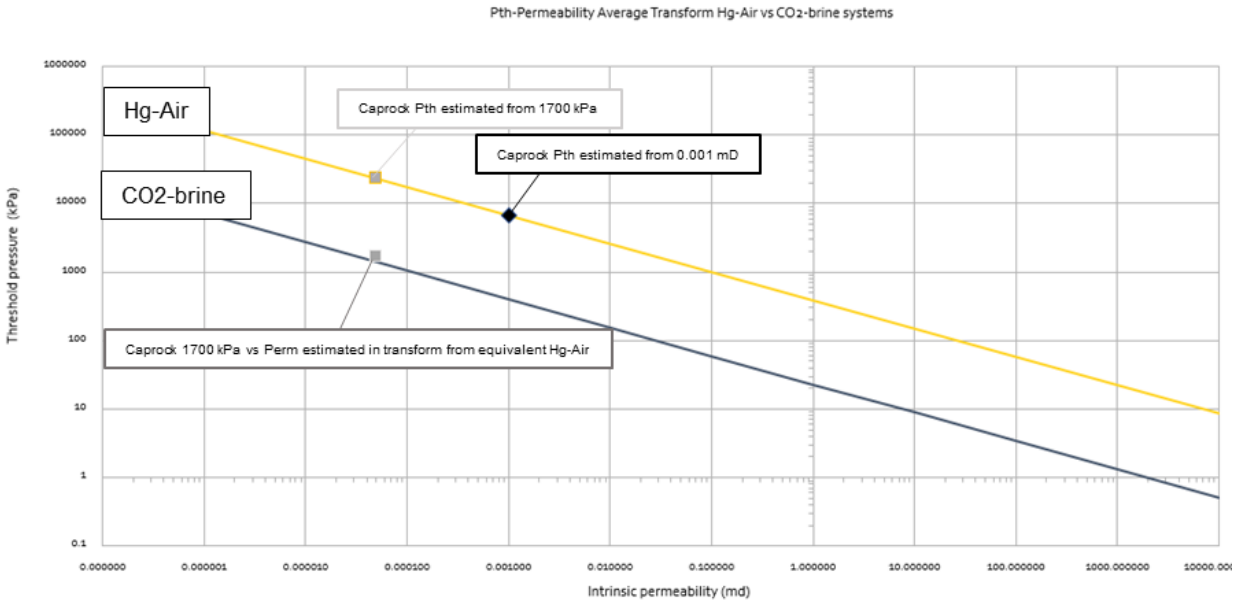

Figure 26 – Permeability-Threshold Pressure Average Transform in Hg-Air (yellow) and CO_2-brine system (blue) for caprock input values.

The map-based approach was then applied in an attempt to capture the lateral distribution of the CO_2 plume layers with a general NNE-SSW elongation trend. It is noted that Permedia does not provide soft conditioning options for lateral direction/azimuth control or vertical proportion curves. Different maps were defined and applied for the reservoir units Sand Wedge, Utsira Formation, intrashales and caprock.

Williams and Chadwick (2017) published an improved black oil simulation history match of the topmost CO_2 layer with north-south oriented channel features with high permeabilities within the Sand Wedge interval. They have based this interpretation on seismic observations and the associated deposition in a marine high energy environment, possibly by gravity flow in turbidity currents. The definition of the high permeability channel feature was computed from the isochore map for the Sand Wedge interval, by assigning a permeability of 8 Darcy to any area where the thickness exceeded 20 m (which followed the channel) and a permeability of 3 Darcy for the area outside the channel (Figure 27, I). This variation in

permeability N-S and E-W based on thickness provided the best fit to the observed CO_2 distribution with ECLIPSE 100 flow simulation in Williams and Chadwick (2017).

A similar workflow was performed here for the Sand Wedge L9 interval. An isochore between the provided input seismic depth surfaces Top Sand Wedge and Top Thick shale was created (Figure 27, II) and 8 Darcy permeabilities were assigned to the channeling north-south elongated feature (thickness > 24 m) with 3 Darcy for the rest of the map (Figure 27, III). A trend map was defined with the application of a smoothing factor onto it. This general trend from the isochore was applied following the same workflow to the porosity and threshold pressure maps, in an attempt to capture their minimum and maximum ranges (Figure 28). Porosity values were defined from the input 0.36±0.04 (Cavanagh and Haszeldine, 2014). Permeability is not a direct input into CO_2 invasion percolation migration in Permedia, the threshold pressures were estimated from the average permeability-threshold pressure transform based on the input permeability map.

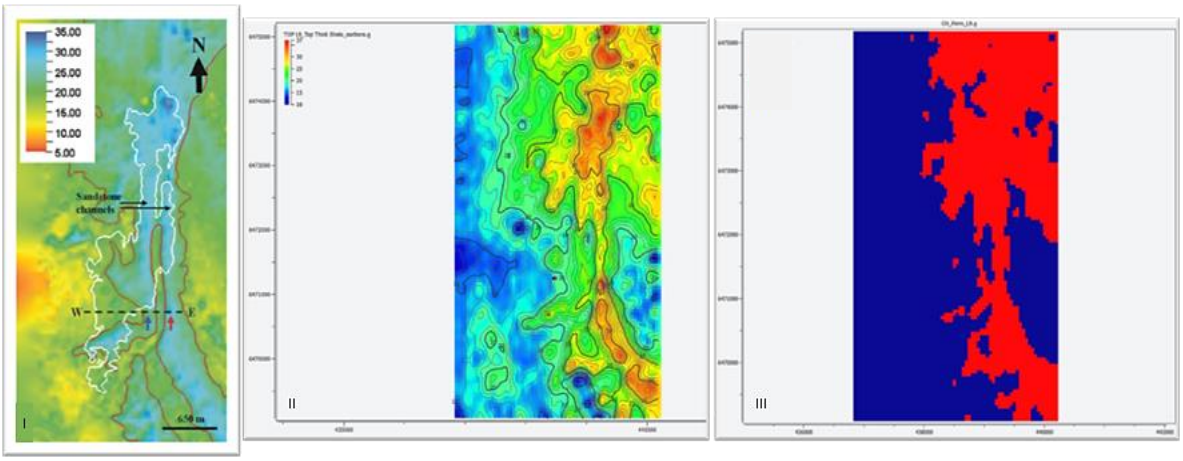

Figure 27 – Map-based approach for Sand Wedge (L9). I. Isochore map from Williams and Chadwick (2017) with red polygon outlining the 20m isochore. II. Isochore map for the Sand Wedge L9 interval based on current input seismic depth surfaces. III. Permeability map with 8 D within thickness > 24m (red) and 3 D outside (blue).

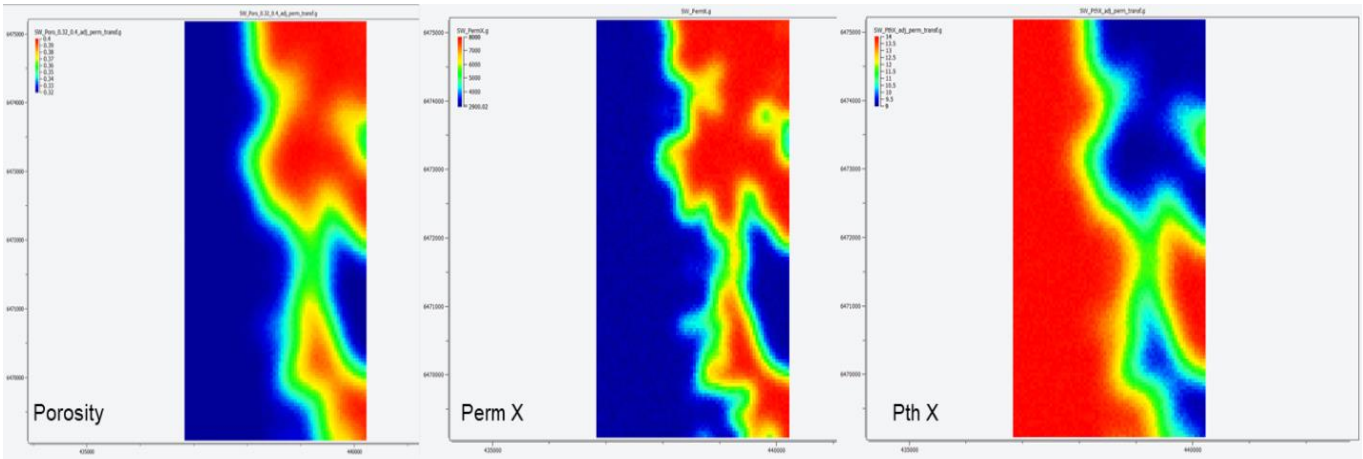

Figure 28 – Map-based approach for the Sand Wedge (L9) unit – property maps created from the isochore (porosity, horizontal permeability and threshold pressure).

The map-based approach for the Utsira Formation reservoir interval (L8-L1) was defined to capture the general NNE-SSW plume distribution observed in these layers (Figure 11). A polygon was created from the Top Utsira Formation seismic structure based on closure and fetch analysis (Figure 29). Porosity values were defined from the input 0.34±0.04 (Cavanagh and Haszeldine, 2014). The permeability range of 1 to 5 Darcy was based on the Appendix 1 – Input Parameters (SPE 134891) input table and the average permeability-threshold pressure transform was applied to these values to define the threshold pressures range (Figure 30).

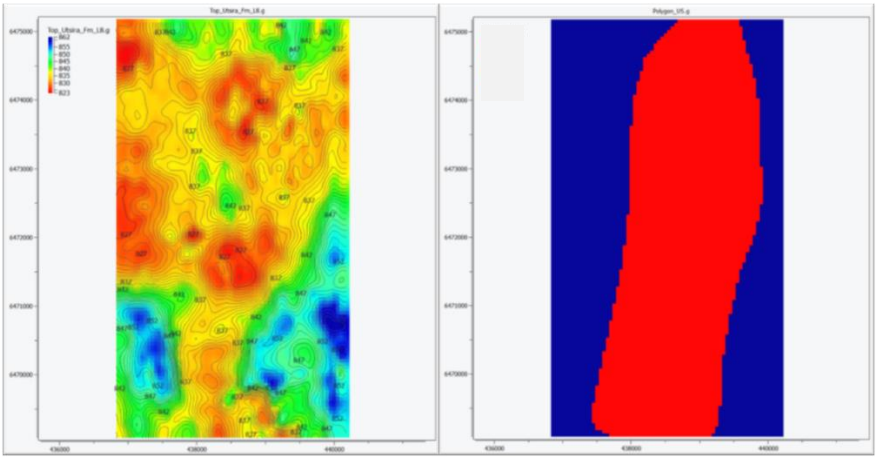

Figure 29 – Map-based approach for the Utsira Formation unit. Left: Top Utsira Formation seismic structure used to define a polygon trend. Right: Map created from polygon with high porosity and permeability zone (red) and lower outside (blue).

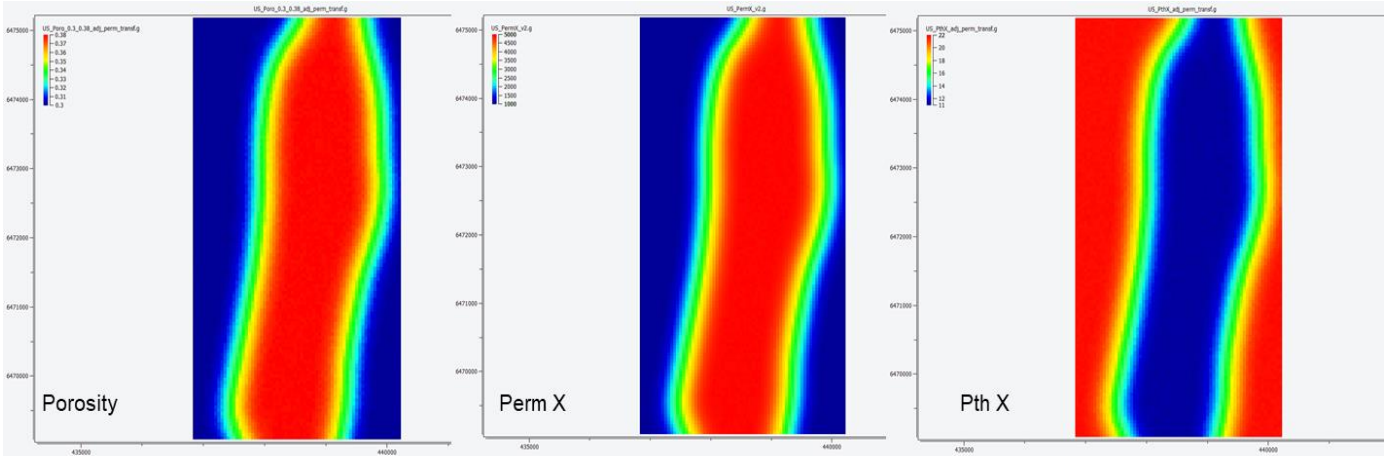

Figure 30 – Map-based approach for the Utsira Formation unit – property maps created from the isochore (porosity, horizontal permeability and threshold pressure).

In order to add variability from a distribution to the intrashales and caprock properties in Permedia, it is possible to apply an uncertainty tool based on minimum and maximum values as the only distribution type available is uniform. Porosity values for the intrashales and caprock were defined from the input 0.30±0.02 (Cavanagh and Haszeldine, 2014). From iterative experimentation, it was possible to define a mean value for Pth_z in Hg-Air system that would allow for breakthrough for the intrashales layers of 2500 kPa and for L5 of 3000 kPa. If these values are applied as constants for all layers, they are generally too

high. However, by adding a variability of about 10% to these values with the pixel-based distribution within a map, the CO_2 migrates into the vertical stack of 9 plumes (Table 8). Threshold pressures anisotropy ratio of 4 was applied (Figure 31). Caprock ranges for threshold pressures were estimated from the input minimum and maximum permeability ranges from the Appendix 1 – Input Parameters (SPE 134891) with the average permeability-threshold pressure transform (Table 9), and a permeability anisotropy of 1/4 (shales with low permeability). As the uncertainty tool available to generate the pixel-based maps only follow a uniform distribution, one value deviation was applied which allowed to capture the maximum values but not fully the minimum (Figure 32).

Table 8 - Threshold pressures input minimum and maximum values with a uniform distribution from the pixel-based maps.

Layer	Pth X (kPa - Hg-Air)		Pth Z (kPa - Hg-Air)	
	Min	Max	Min	Max
Intrashales	562	687	2250	2750
Layer 5	687	812	2750	3250
Caprock	5883	7591	10455	13489

Table 9 - Threshold pressures for the caprock estimated from the permeability ranges input (Appendix 1 – Input Parameters (SPE 134891)) with the application of the Permeability-Threshold Pressure Average Transform.

Caprock - Threshold Pressures estimated from Permeability ranges (SPE)											
Perm X (mD)			Perm Z (mD)			PthX Hg-Air (kPa)			PthZ Hg-Air (kPa)		
Mean	Min	Max	Mean	Min	Max	Mean	Min	Max	Mean	Min	Max
0.001	0.00075	0.0015	0.00025	0.000188	0.00038	6737	7591	5695	11972	13489	10119

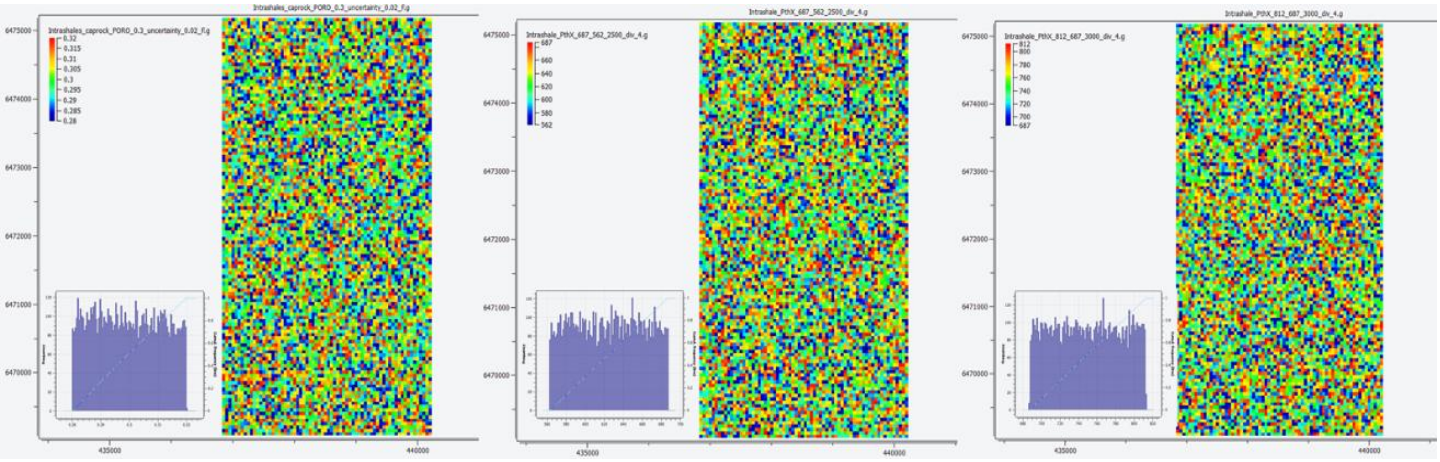

Figure 31 - Map-based approach for the intrashales and caprock. Left: Porosity distribution map and histogram for the intrashales and caprock. Middle: Threshold pressures distribution map and histogram for the intrashales L1-L4 and L6-L8. Right: Threshold pressures distribution map and histogram for the intrashale L5.

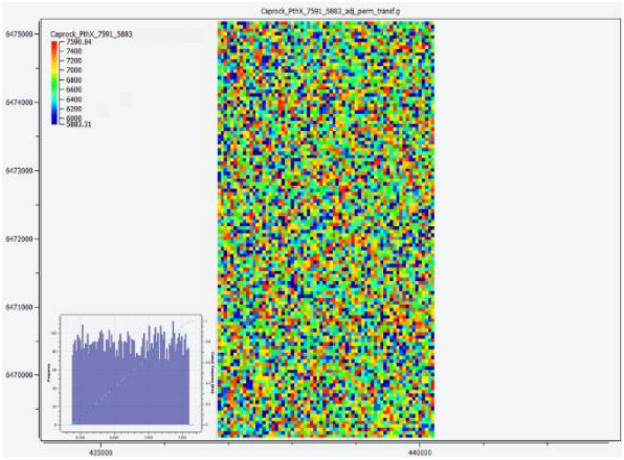

Figure 32 - Map-based approach for the caprock. Threshold pressures distribution map and histogram for the caprock.

5. CO_2 Migration Simulation

The Permedia CO_2 migration is a CO_2-adapted invasion percolation simulator for free-phase plume modelling. It provides high resolution models of gravity-segregated plume distributions in heterogeneous reservoir settings (Cavanagh and Ringrose, 2011).

The annual injection rates for the Sleipner reservoir from 1996 to 2010 were defined from Table 6, with a cumulative amount of CO_2 injected by 2010 of 12.08 Mt. The coordinates for the injection perforation on well 15/9-A-16 (Table 2) defined a length of 2.8m, which considering a model grid resolution of 0.5 m, corresponded to 4 cells along the deviated well path. A comparison between the simulation results inputting the 4 cells perforation interval, 2 injection points (Min and Max) and a single injection point (Max) into CO_2 migration showed no difference in the final CO_2 accumulations (final injected vs accumulated CO_2 mass in model of 99.99%) so a single injection point was selected for simplicity.

The rock properties considered in the CO_2 migration simulator from the reservoir model or defined as constants are the critical CO_2 saturation (Socr), connate water saturation (Swc), porosity and threshold pressure, also known as breakthrough or displacement pressure, in the horizontal and vertical directions (Pth_x and Pth_z, in Hg-Air kPa). It is also possible to make threshold pressure isotropic by setting the scalar to 1 between Pth_x and Pth_z. Permeability is not a direct rock property input into CO_2 migration. There is an option to estimate the threshold pressure (Pth_x) from the permeability grid property based on a permeability-threshold pressure curve but the final input into migration is the estimated Pth_x. In CO_2 Migration, when a grid cell in a model is invaded by CO_2, the saturation of this grid cell is first marked as being critical (Socr, ie. saturation required for the CO_2 to start to invade) and if the invasion front reaches a baffle or seal, then the invading fluid starts to backfill. Backfilled cells (accumulations) are assigned a saturation corresponding to the connate water saturation (Swc), or irreducible water, which represents the maximum CO_2 saturation that is possible.

Critical CO_2 saturation (Socr) and connate water saturation (Swc) were defined as constants based on Table 5 for the simple and map-based approaches. Porosity and threshold pressures (Pth_x and Pth_z) were selected from the reservoir model properties for each approach.

In order to initialize the CO_2 multi-phase migration simulation, the initial storage formation conditions, such as gas and brine phase density, compressibility, viscosity, solubility and interfacial tension, need to be set in the Permedia CO_2 dashboard. The CO_2 dashboard consists on a CO_2 specific equation of state and

PVT wizard that has been validated against several published works containing both theoretical and experimental data. The input storage environment parameters (datum depth, pressure and temperature, pressure and temperature gradients) and PVT parameters (salinity, temperature, brine density) were defined as shown on Table 5. Based on these inputs, the CO_2 dashboard calculates key PVT-related variables, such as CO_2 density and IFT factor, and generates a set of plots describing their relationships as shown on Figure 33. As can be observed, IFT values generally increase with decreasing pressure which in turn corresponds to increasing resistance on upward CO_2 migration due to increasing IFT.

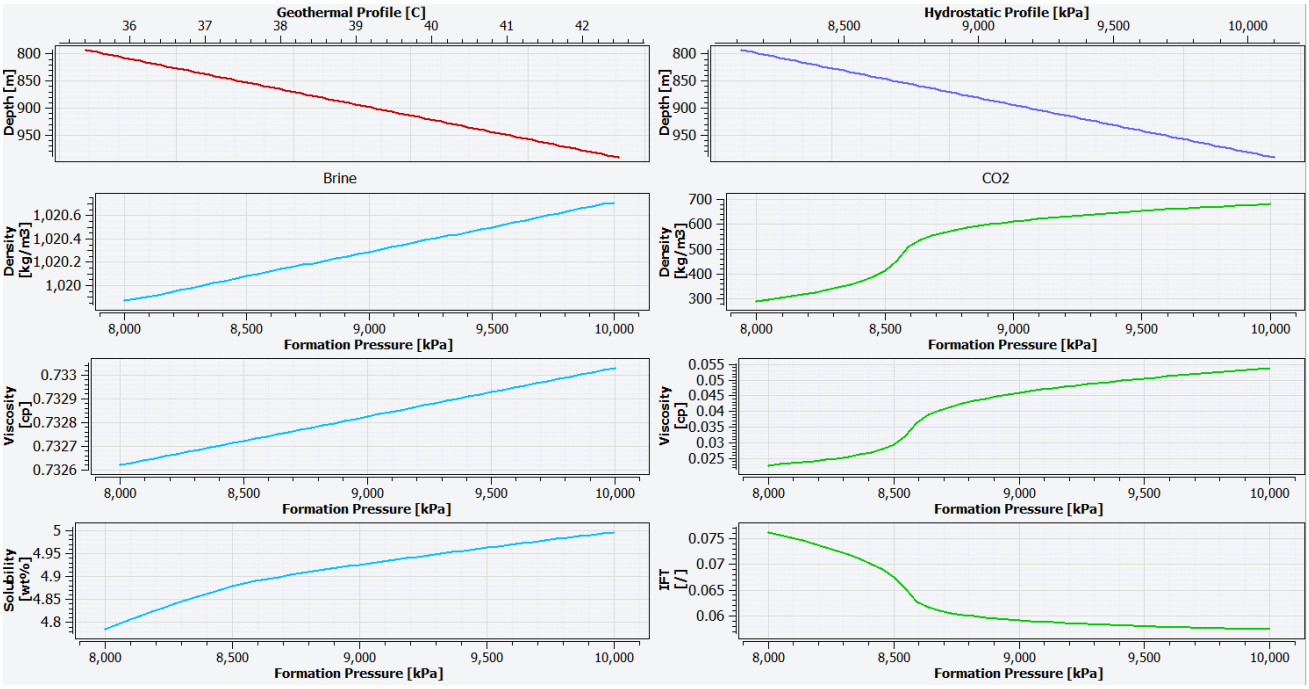

Figure 33 – CO_2 dashboard generated graphs considering the Sleipner storage environment inputs.

Considering the poorly understood aspects of the plume discussed in sections II.2.2 and III.2.2, temperature profiles with related CO_2 density and saturations for the plume layers, a sensitivity analysis of these factors was performed in the simple approach model (used as a reference) in order to investigate their impact on the CO_2 plume. The temperature uncertainty at the reservoir top is poorly constrained with an estimated range of 34ºC ± 3ºC according to Cavanagh and Haszeldine (2014). Therefore, two scenarios were tested, cold and warm plume scenarios, with a temperature of 31˚C and 37˚C respectively at the reservoir top, and corresponding variations in the density values (Figure 34 and Figure *35*).

Saturation profiling, ie. pores filled with brine vs pores filled with CO_2, is an uncertain parameter since it is difficult to distinguish in seismic between moderate and high gas saturations. The 89% gas saturation assumed for Sleipner from the Appendix 1 – Input Parameters (SPE 134891) represents a reasonable upper limit to the mean saturation of the plume, but the lower limit could be as low as 40% (Cavanagh and Haszeldine, 2014). Therefore, the gas saturations applied in the reference model which are based on the SPE reference input values of Table 5 (Swc and Socr) correspond to a high gas saturation scenario, with maximum CO_2 saturation of 89% and critical gas saturation of 2%. Three scenarios were tested to analyse the migration simulation sensitivity to these parameters (ie. variation of each input with all other inputs kept the same) as shown on Table 10.

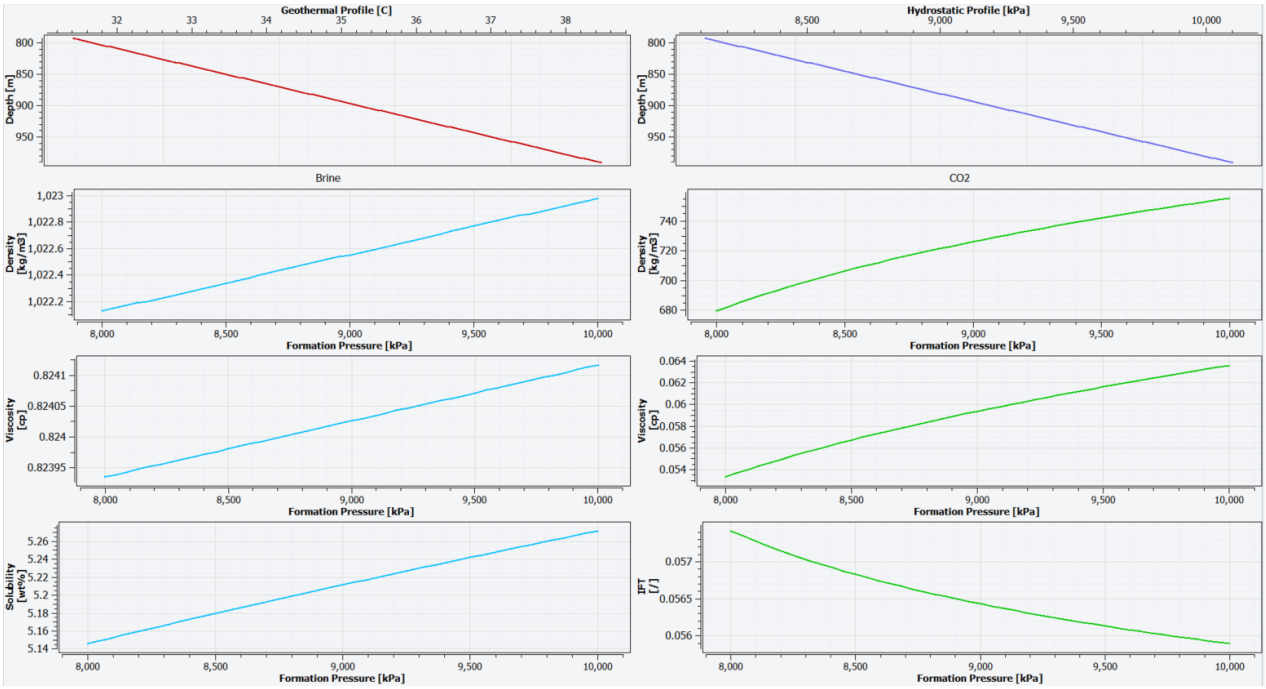

Figure 34 - CO_2 dashboard generated graphs considering the Sleipner storage environment inputs for the cold plume scenario (31˚C at the reservoir top as observed on the Geothermal Profile graph on the top left).

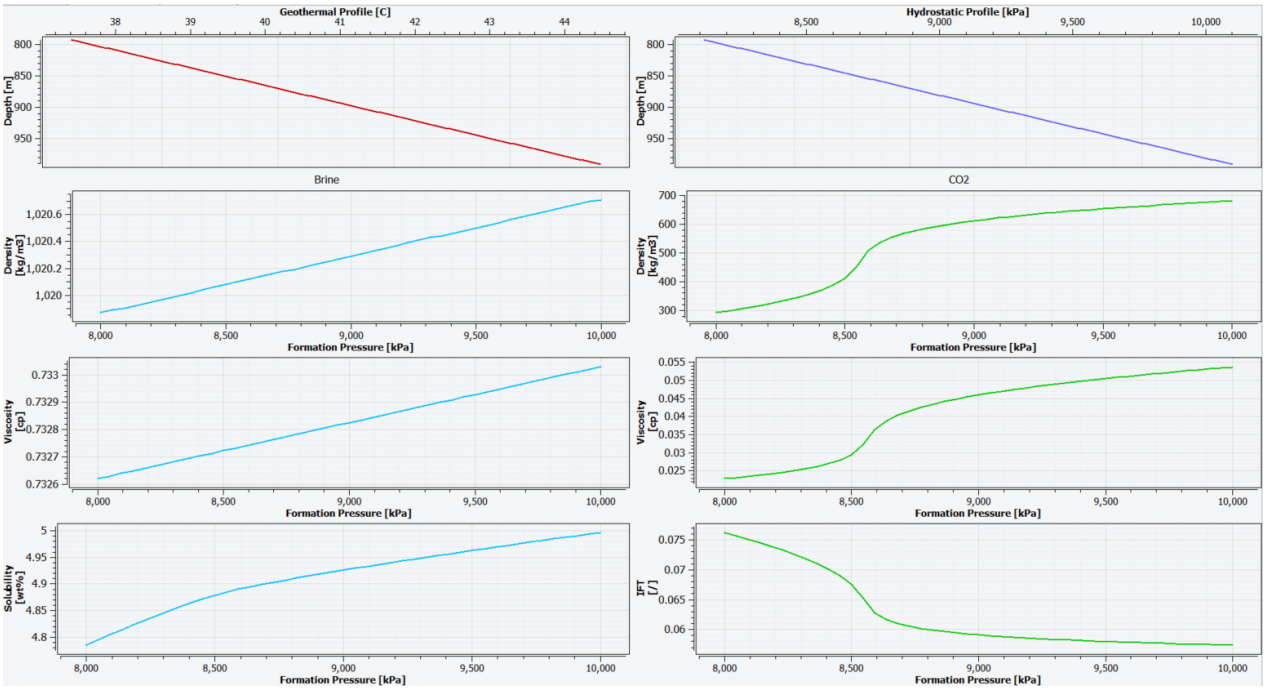

Figure 35 - CO_2 dashboard generated graphs considering the Sleipner storage environment inputs for the warm plume scenario (37˚C at the reservoir top as observed on the Geothermal Profile graph on the top left).

Table 10 - CO_2 saturations sensitivity analysis scenarios. RF: reference case (simple approach). SC1: scenario 1. SC2: scenario 2. SC3: scenario 3. Varying input parameter from the reference case in each scenario in bold.

	RF	SC1	SC2	SC3
CO2 saturation (%)	89	**40**	89	**40**
Critical CO2 saturation (%)	2	2	**20**	**20**

V. Modelling and Migration Simulation Results

The results for the key variables temperature, pressure, density and IFT multiplier from the CO_2 dashboard per reservoir zone are summarized on Table 11. These consider the mid-range scenario of 35˚C at the reservoir top and 41˚C at the injection point (same assumption as in Cavanagh and Haszeldine, 2014; and Cavanagh et al., 2015). The corresponding estimated density range is 565 kg/m3 at deepest L1 and 350 kg/m3 at the uppermost L9. All approaches resulted in ~100% of the injected CO_2 mass accumulated in the model (12.08 Mt in total in 2010).

The CO_2 migration simulation results in Permedia are reported per accumulation body/plume layer (above the CO_2-brine contact). Each accumulation state is output through time as either leaking, filling, spilling or leaking and spilling. Filling shows that the structure is currently underfilled; spilling is when the CO_2 has filled the structural closure and spills laterally to another structure since it has not exceeded the barrier threshold pressure; leaking is when the CO2 breaks through the top of the accumulation against a barrier (as illustrated on Figure 20); leaking and spilling shows both lateral migration through a spill point and breakthrough at the top of the accumulation at a particular time (spilling state precedes leaking as the CO2 migrates laterally until its accumulation buoyancy pressure overcomes the lower permeability rock threshold pressure).

Table 11 – Key PVT variables modelled in the CO_2 dashboard for Sleipner.

	Modelled in CO2 Dashboard			
	Temperature (°C)	Pressure (kPa)	Density(kg/m3)	IFT Multiplier
Caprock	35.0	8013	333	0.0729
L9	35.4	8123	350	0.0716
L8	36.6	8431	469	0.0645
L7	37.1	8578	495	0.0633
L6	37.8	8775	480	0.0640
L5	38.3	8922	507	0.0628
L4	38.9	9069	542	0.0614
L3	39.4	9216	541	0.0615
L2	39.9	9363	542	0.0614
L1	41.0	9659	565	0.0606

1. Reservoir Modelling Approaches

The simple approach shows a vertical stack of 9 CO_2 plume layers with a lateral distribution strongly conforming to topography and a larger areal extension for L5 as observed on seismic (Figure 36). The threshold pressures for the intrashales per layer (L1 to L8 as L9 accumulates underneath the caprock) considering their IFT multiplier are shown on Table 12. The accumulated CO_2 mass per layer by 2010 can be observed on Figure 36 (c). The accumulations summary is displayed on Table 13, which shows that with a total of 12.08 Mt injected CO_2, L1 to L8 are leaking (have breached through the intrashales) and L9 is filling.

Table 12 - Modelled threshold pressures per intrashale layer in the horizontal and vertical directions for the simple approach.

Simple Approach -Intrashales Layers		
Layer	Pth X CO2-brine (kPa)	Pth Z CO2-brine (kPa)
L8	36	145
L7	36	142
L6	36	144
L5	43	173
L4	35	138
L3	35	138
L2	35	138
L1	34	136

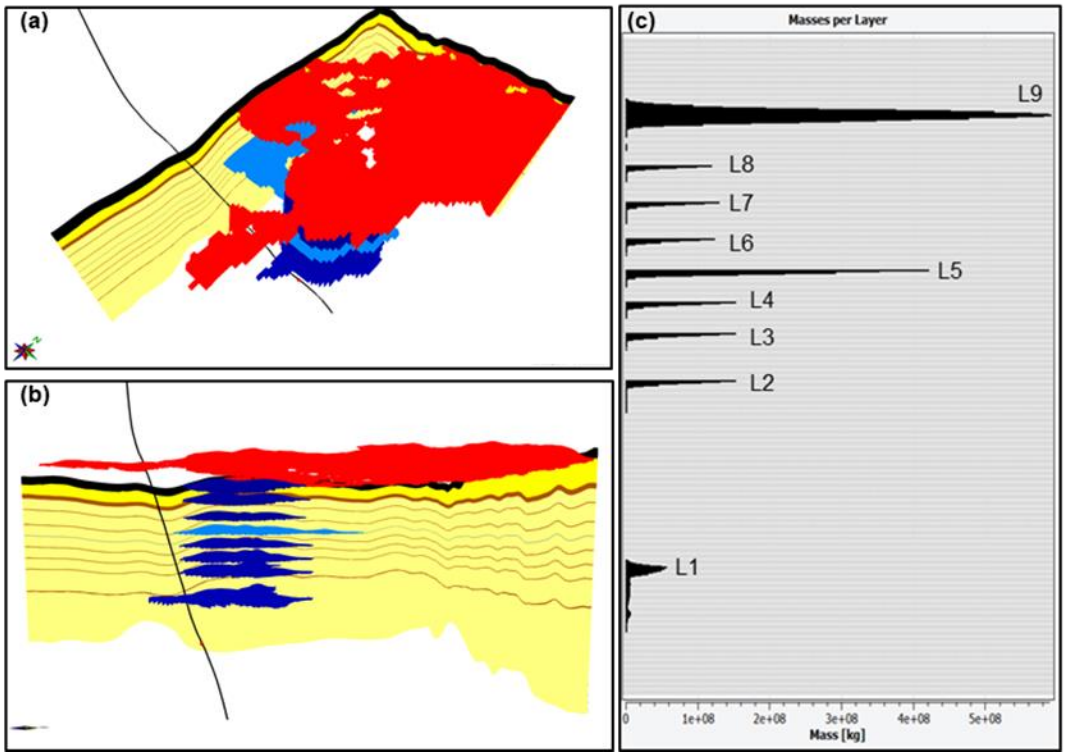

Figure 36 - Simple approach migration simulation results in 2010 (12.08 Mt). (a) and (b) CO_2 plume distribution in 3D view (vertical exaggeration 10x). (c) CO_2 mass accumulated per layer (X axis from 0 to 5.8 x 10^8 kg).

Table 13 - Accumulations summary for the simple approach. Liquid heavy mass (kg) corresponds to CO_2 mass (total 12.08 Mt by 2010).

Simple Approach - Accumulations Summary						
Layers	Accumulation State	Bulk Rock Volume [m3]	Pore Volume [m3]	Total HC Volume [m3]	Liquid Heavy Mass [kg]	Total Column Height [m]
L9	Filling	6.34E+07	2.28E+07	2.03E+07	7.10E+09	18
L8	Leaking	2.55E+06	866192	770911	3.62E+08	7
L7	Leaking	2.74E+06	932999	830368	4.11E+08	7
L6	Leaking	2.62E+06	892171	794032	3.81E+08	7
L5	Leaking	1.02E+07	3.47E+06	3.09E+06	1.57E+09	9
L4	Leaking	3.20E+06	1.09E+06	969281	5.25E+08	7
L3	Leaking	3.19E+06	1.09E+06	966786	5.23E+08	7
L2	Leaking	3.21E+06	1.09E+06	970779	5.26E+08	7
L1	Leaking	3.52E+06	1.20E+06	1.06E+06	6.01E+08	8

The map-based approach property models followed laterally the input property distribution maps per lithology as illustrated for the property Pth_z on Figure 37. As there is no vertical control of the property distribution in Permedia, each layer of each lithology zone equally distributes the input property maps in the vertical direction. The resulting plume distribution shows a vertical stack of 9 CO_2 layers but their lateral distribution does not follow closely the input maps as expected (Figure 38), with very little variation from the simple approach. This shows that the topography plays a key role on the migration of CO_2 within the reservoir. The modelled threshold pressures distribution per intrashales layers in CO_2-brine system is displayed on Table 14. The accumulations summary for the map-based approach is on Table 15.

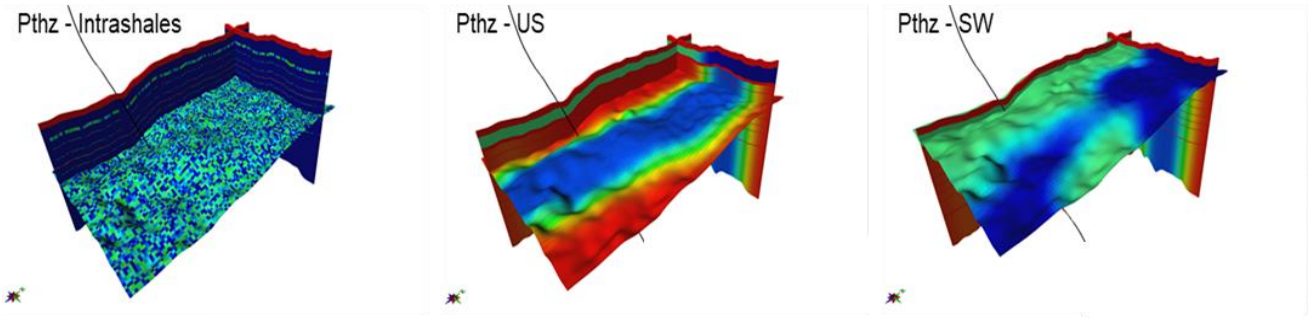

Figure 37 - Map-based approach Pth_z property for the intrashales, Utsira Sand (US) and Sand Wedge (SW). Distributions as discussed in section IV.4 (vertical exaggeration 10x).

Table 14 - Modelled threshold pressures minimum and maximum values per intrashale layer in the horizontal and vertical directions for the map-based approach.

Map-based Approach - Intrashales Layers				
Layer	Pth X CO2- brine (kPa)		Pth Z CO2- brine (kPa)	
	Min	Max	Min	Max
L8	36	44	145	177
L7	36	43	142	174
L6	36	44	144	176
L5	43	51	173	204
L4	35	42	138	169
L3	35	42	138	169
L2	35	42	138	169
L1	34	42	136	167

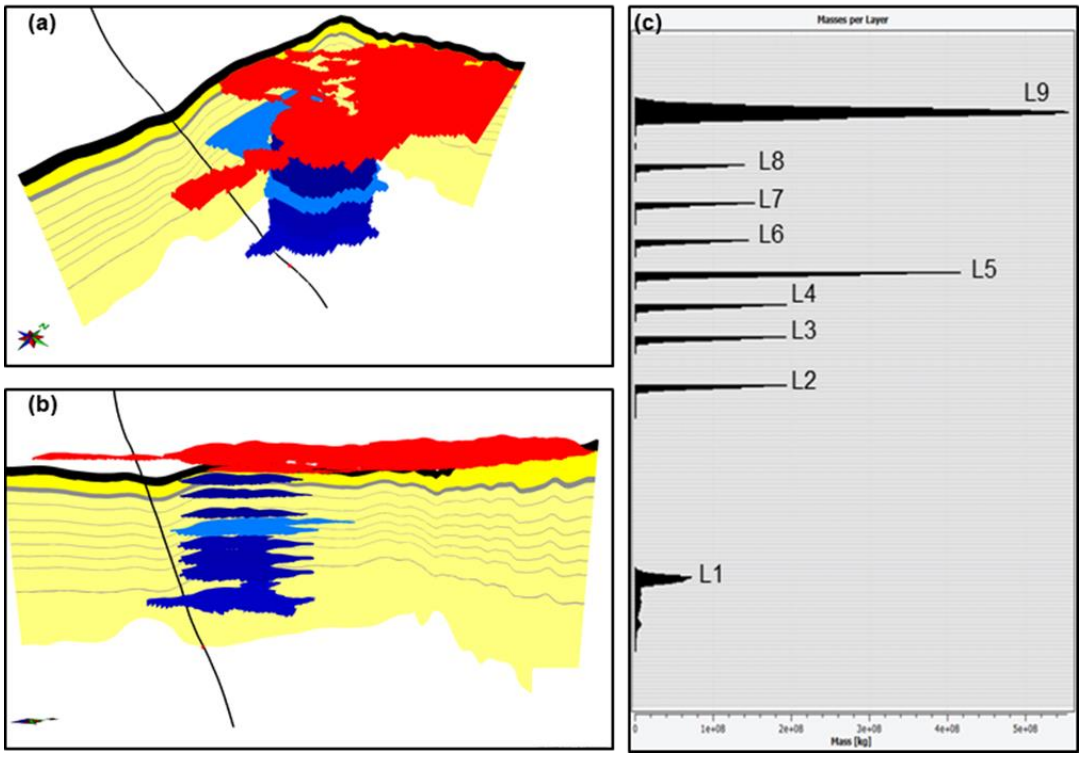

Figure 38 - Map-based approach migration simulation results in 2010 (12.08 Mt). (a) and (b) CO_2 plume distribution in 3D view (vertical exaggeration 10x). (c) CO_2 mass accumulated per layer (X axis from 0 to 5.4 x 10^8 kg).

Table 15 - Accumulations summary for the map-based approach. Liquid heavy mass (kg) corresponds to CO_2 mass (total 12.08 Mt by 2010).

Map-based Approach - Accumulations Summary						
Layers	Accumulation State	Bulk Rock Volume [m3]	Pore Volume [m3]	Total HC Volume [m3]	Liquid Heavy Mass [kg]	Total Column Height [m]
L9	Filling	5.19E+07	1.94E+07	1.73E+07	6.03E+09	18
L8	Leaking	2.89E+06	1097060	976384	4.58E+08	7
L7	Leaking	3.11E+06	1179950	1050150	5.20E+08	7
L6	Leaking	2.98E+06	1129260	1005040	4.82E+08	7
L5	Leaking	1.03E+07	3.47E+06	3.09E+06	1.57E+09	9
L4	Leaking	3.85E+06	1.45E+06	1292040	7.00E+08	8
L3	Leaking	3.84E+06	1.45E+06	1288530	6.97E+08	8
L2	Leaking	3.86E+06	1.45E+06	1294110	7.01E+08	8
L1	Leaking	4.43E+06	1.67E+06	1.48E+06	8.37E+08	9

2. Plume Temperature Scenarios

The cold plume scenario with 31˚C at the uppermost L9, shows a density range of 677 kg/m3 at the L9 and 663 kg/m3 at the deepest L1 as summarized on Table 16. This increase in CO_2 densities reduces the density contrast between CO_2 and brine which in turn reduces the corresponding IFT values, making CO_2 less buoyant. The resulting plume distribution by 2010 can be seen on Figure 39 and the accumulations summary on Table 16.

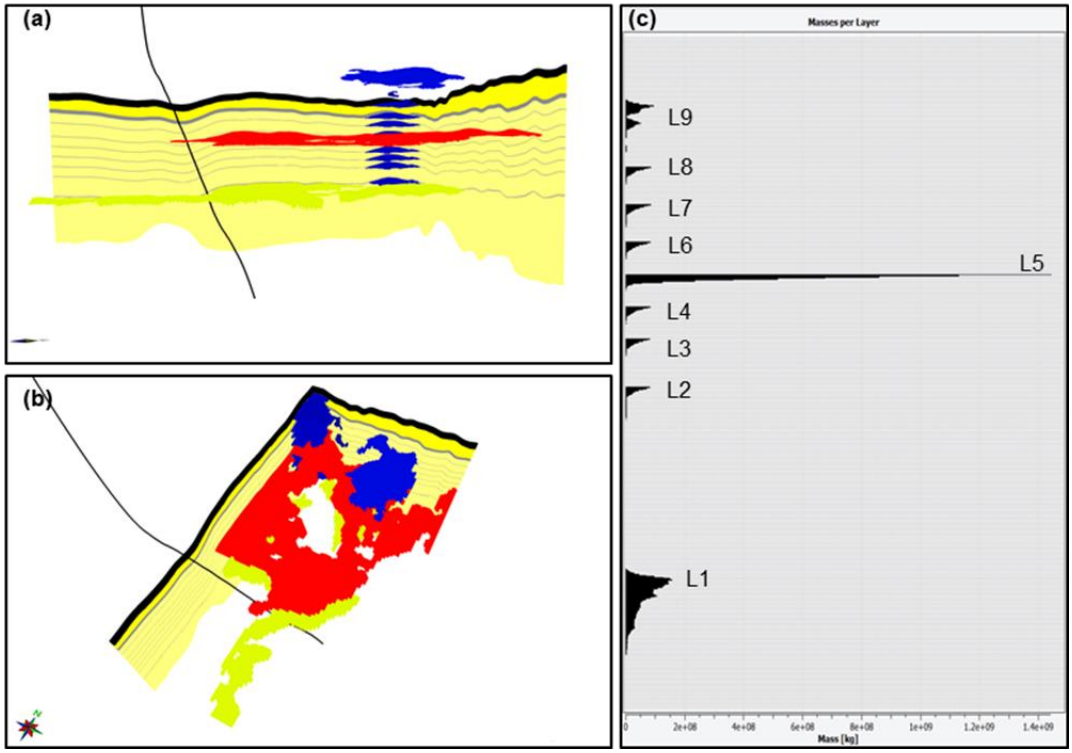

Figure 39 - Cold plume scenario migration simulation results in 2010 (12.08 Mt). (a) and (b) CO_2 plume distribution in 3D view (vertical exaggeration 10x). (c) CO_2 mass accumulated per layer (X axis from 0 to 1.4 x 10^9 kg).

Table 16 - Accumulations summary for the cold plume scenario. Liquid heavy mass (kg) corresponds to CO_2 mass (total 12.08 Mt by 2010).

Cold Plume Scenario - Accumulations Summary									
Layers	Accumulation State	Bulk Rock Volume [m3]	Pore Volume [m3]	Total HC Volume [m3]	Temperature (°C)	Density(kg/m3)	Liquid Heavy Mass [kg]	Total Column Height [m]	IFT Multiplier
L9	Filling	3.96E+06	1.43E+06	1.27E+06	31	677	8.59E+08	7	0.0574
L8	Leaking	1.74E+06	590386	525444	33	672	3.53E+08	10	0.0575
L7	Leaking	1.74E+06	591218	526176	33	672	3.54E+08	10	0.0575
L6	Leaking	1.71E+06	580764	516879	34	670	3.46E+08	10	0.0576
L5	Leaking	2.66E+07	9.04E+06	8.04E+06	34	668	5.37E+09	12	0.0576
L4	Leaking	1.69E+06	5.73E+05	510119	35	667	3.40E+08	10	0.0577
L3	Leaking	1.67E+06	5.68E+05	505207	35	666	3.36E+08	10	0.0577
L2	Leaking	1.65E+06	5.62E+05	499939	36	664	3.32E+08	10	0.0577
L1	Leaking and Spilling	1.83E+07	6.23E+06	5.53E+06	37	663	3.66E+09	10	0.0578

The warm plume scenario with 37˚C at the uppermost L9, resulted in a density range of 307 kg/m3 at the L9 and 483 kg/m3 at the deepest L1 as summarized on Table 17. The smaller density values resulted in an increase of IFT with an increase on the density contrast between CO_2 and brine. The plume distribution is shown in Figure 40 and the accumulations in Table 17.

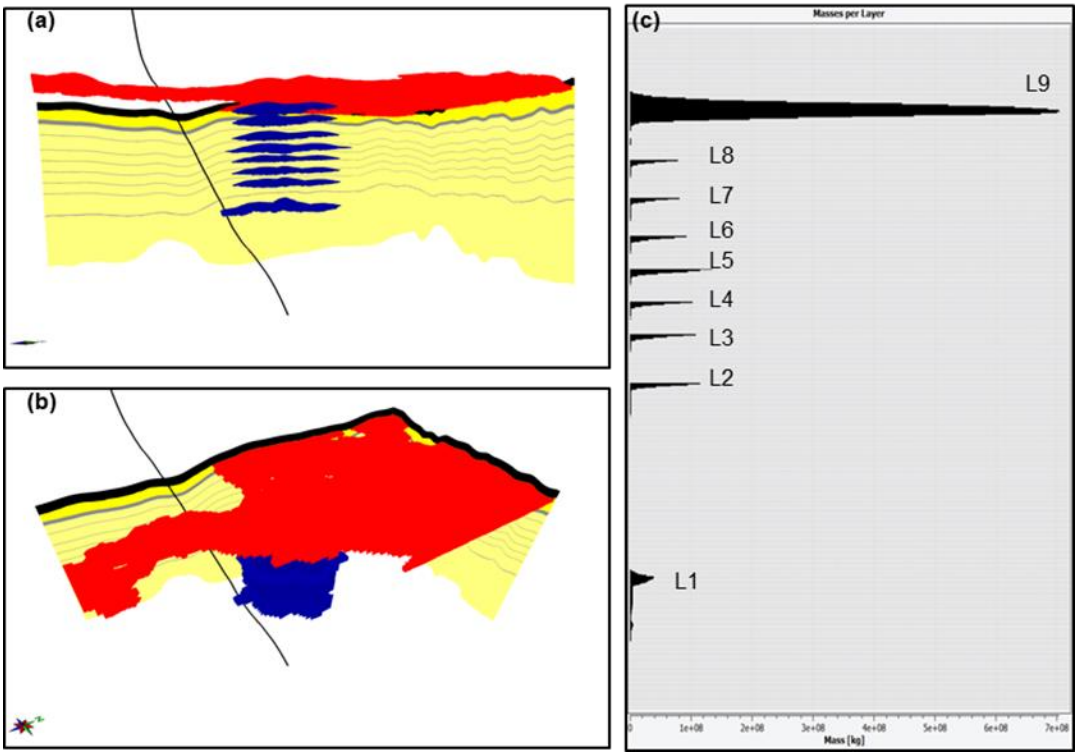

Figure 40 - Warm plume scenario migration simulation results in 2010 (12.08 Mt). (a) and (b) CO_2 plume distribution in 3D view (vertical exaggeration 10x). (c) CO_2 mass accumulated per layer (X axis from 0 to 7 x 10^8 kg).

Table 17- Accumulations summary for the warm plume scenario. Liquid heavy mass (kg) corresponds to CO_2 mass (total 12.08 Mt by 2010).

Warm Plume Scenario - Accumulations Summary									
Layers	Accumulation State	Bulk Rock Volume [m3]	Pore Volume [m3]	Total HC Volume [m3]	Temperature (°C)	Density(kg/m3)	Liquid Heavy Mass [kg]	Total Column Height [m]	IFT Multiplier
L9	Filling	9.67E+07	3.49E+07	3.10E+07	37	307	9.53E+09	21	0.0749
L8	Leaking	1.99E+06	678109	603518	39	344	2.08E+08	6	0.0720
L7	Leaking and Spilling	2.02E+06	685174	609804	39	352	2.15E+08	6	0.0714
L6	Leaking	2.15E+06	731122	650697	40	394	2.56E+08	6	0.0686
L5	Leaking	3.86E+06	1.31E+06	1.17E+06	40	414	4.84E+08	8	0.0674
L4	Leaking and Spilling	2.27E+06	7.72E+05	687514	41	422	2.90E+08	6	0.0670
L3	Leaking	2.35E+06	8.01E+05	712575	41	438	3.12E+08	7	0.0661
L2	Leaking	2.47E+06	8.40E+05	747196	42	457	3.42E+08	7	0.0651
L1	Leaking	2.57E+06	8.74E+05	7.78E+05	43	483	3.76E+08	7	0.0639

3. CO_2 Saturations Scenarios

The saturations scenario 1 with the low-end CO_2 saturation of 40% resulted in the accumulation of larger volumes since each cell maximum saturation is reduced but the total mass injected is the same, 12.08 Mt by 2010 (Figure 41 and Table 18). The scenario 2, with an increase on the critical gas saturation to 20%, reduced the accumulations CO_2 volumes due to the increase of CO_2 saturation in the migration pathway cells below the accumulations (Figure 42 and Table 19). Scenario 3 which reduced the accumulations CO_2 saturation to 40% and increased the critical CO_2 saturations to 20% showed an increase in the accumulations' volumes and a slight reduction in the total CO_2 mass accumulated within the plume layers (Figure 43 and Table 20).

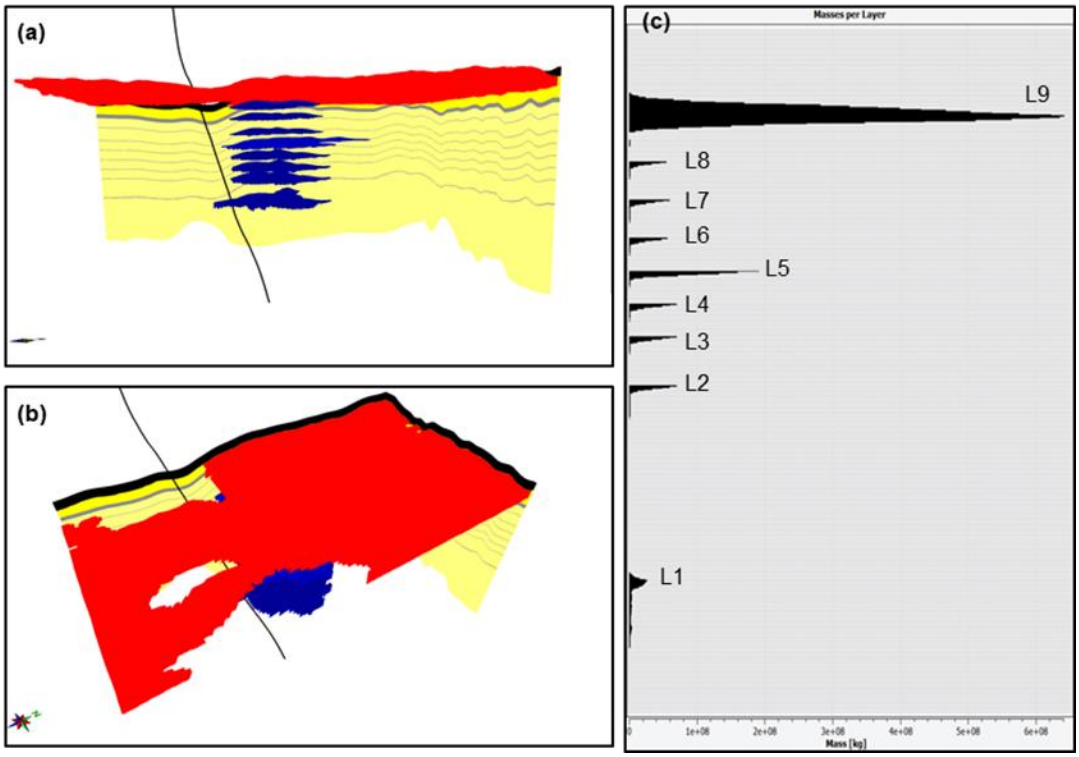

Figure 41 - Saturations sensitivity scenario 1 (SC1) migration simulation results in 2010 (12.08 Mt). (a) and (b) CO_2 plume distribution in 3D view (vertical exaggeration 10x). (c) CO_2 mass accumulated per layer (X axis from 0 to 6.4 x 10^8 kg).

Table 18 - Accumulations summary for the saturations sensitivity scenario 1 (SC1). Liquid heavy mass (kg) corresponds to CO_2 mass (total 12.08 Mt by 2010).

SC1 - Accumulations Summary						
Layers	Accumulation State	Bulk Rock Volume [m3]	Pore Volume [m3]	Total HC Volume [m3]	Liquid Heavy Mass [kg]	Total Column Height [m]
L9	Filling	1.94E+08	7.01E+07	2.80E+07	9.78E+09	27
L8	Leaking and Spilling	2.55E+06	866192	346477	1.63E+08	7
L7	Leaking	2.74E+06	932999	373199	1.85E+08	7
L6	Leaking	2.62E+06	892171	356868	1.71E+08	7
L5	Leaking	1.02E+07	3.47E+06	1.39E+06	7.04E+08	9
L4	Leaking	3.20E+06	1.09E+06	435632	2.36E+08	7
L3	Leaking	3.19E+06	1.09E+06	434510	2.35E+08	7
L2	Leaking and Spilling	3.21E+06	1.09E+06	436305	2.36E+08	7
L1	Leaking	3.52E+06	1.20E+06	4.79E+05	2.70E+08	8

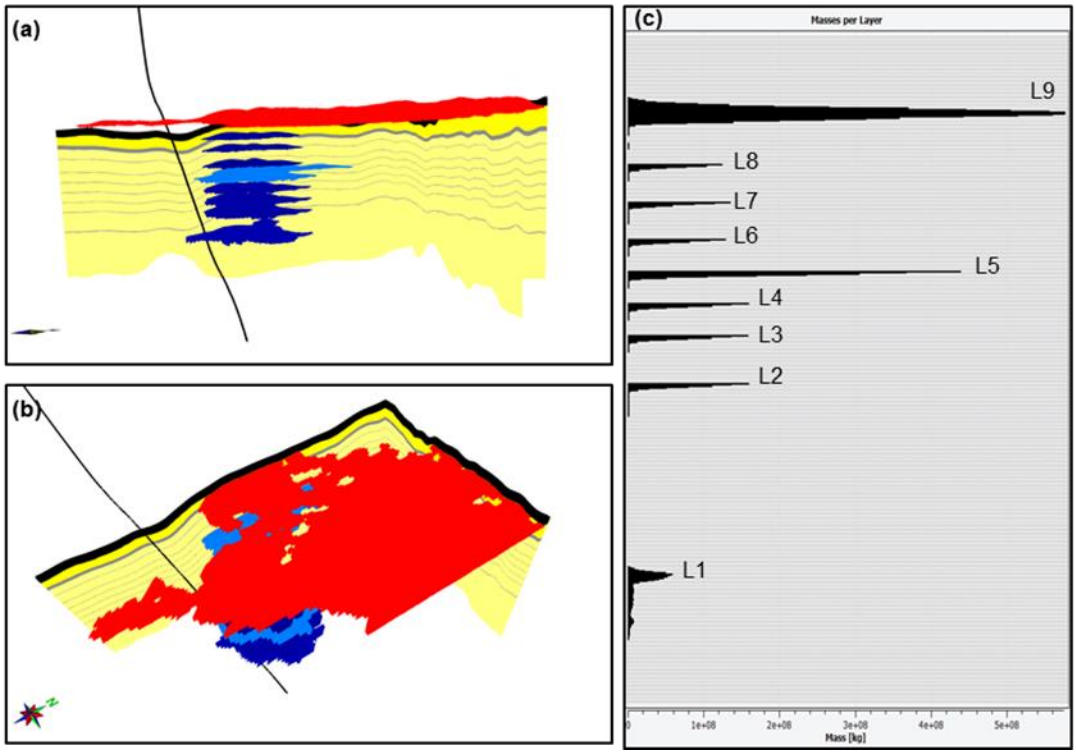

Figure 42 - Saturations sensitivity scenario 2 (SC2) migration simulation results in 2010 (12.08 Mt). (a) and (b) CO_2 plume distribution in 3D view (vertical exaggeration 10x). (c) CO_2 mass accumulated per layer (X axis from 0 to 5.6 x 10^8 kg).

Table 19 - Accumulations summary for the saturations sensitivity scenario 2 (SC2). Liquid heavy mass (kg) corresponds to CO_2 mass (total 12.08 Mt by 2010).

SC2 - Accumulations Summary						
Layers	Accumulation State	Bulk Rock Volume [m3]	Pore Volume [m3]	Total HC Volume [m3]	Liquid Heavy Mass [kg]	Total Column Height [m]
L9	Filling	5.74E+07	2.07E+07	1.84E+07	6.43E+09	18
L8	Leaking	2.55E+06	866192	770911	3.62E+08	7
L7	Leaking	2.74E+06	932999	830368	4.11E+08	7
L6	Leaking	2.62E+06	892171	794032	3.81E+08	7
L5	Leaking	1.02E+07	3.47E+06	3.09E+06	1.57E+09	9
L4	Leaking	3.20E+06	1.09E+06	969281	5.25E+08	7
L3	Leaking	3.19E+06	1.09E+06	966786	5.23E+08	7
L2	Leaking	3.21E+06	1.09E+06	970779	5.26E+08	7
L1	Leaking	3.52E+06	1.20E+06	1.06E+06	6.01E+08	8

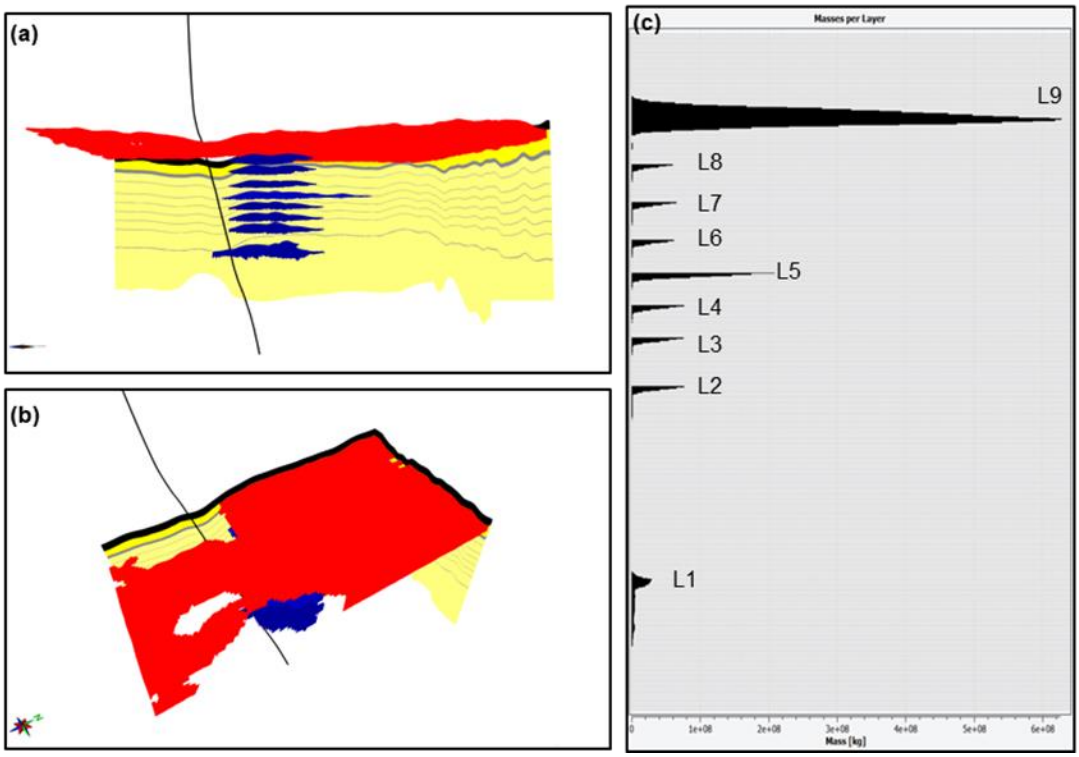

Figure 43 - Saturations sensitivity scenario 3 (SC3) migration simulation results in 2010 (12.08 Mt). (a) and (b) CO_2 plume distribution in 3D view (vertical exaggeration 10x). (c) CO_2 mass accumulated per layer (X axis from 0 to 6.2 x10^8 kg).

Table 20 - Accumulations summary for the saturations sensitivity scenario 3 (SC3). Liquid heavy mass (kg) corresponds to CO_2 mass (total 12.08 Mt by 2010).

SC3 - Accumulations Summary						
Layers	Accumulation State	Bulk Rock Volume [m3]	Pore Volume [m3]	Total HC Volume [m3]	Liquid Heavy Mass [kg]	Total Column Height [m]
L9	Spilling	1.77E+08	6.40E+07	2.56E+07	8.93E+09	27
L8	Leaking	2.55E+06	866192	346477	1.63E+08	7
L7	Leaking	2.74E+06	932999	373199	1.85E+08	7
L6	Leaking and Spilling	2.62E+06	892171	356868	1.71E+08	7
L5	Leaking	1.02E+07	3.47E+06	1.39E+06	7.04E+08	9
L4	Leaking	3.20E+06	1.09E+06	435632	2.36E+08	7
L3	Leaking and Spilling	3.19E+06	1.09E+06	434510	2.35E+08	7
L2	Leaking	3.21E+06	1.09E+06	436305	2.36E+08	7
L1	Leaking	3.52E+06	1.20E+06	4.79E+05	2.70E+08	8

VI. Analysis and Discussion

1. Reservoir Modelling Approaches

The modelled PVT variables in the CO_2 dashboard were compared per layer to the values presented on the Cavanagh et al. (2015) paper as shown on Table 21. The results for temperature, pressure and density per layer are very similar considering these are different grids with different input surfaces, grid resolution and size. The IFT applied per layer by Cavanagh et al. (2015) is not provided on the paper.

The CO_2 migration results from the simple approach show column heights between 7 and 8 m for layers 1 to 4 and layers 6 to 8, 9 m for layer 5 and 18 m for layer 9 by 2010. These results show relatively thin layers up to layer 8 and an overestimate for layer 9 based on seismic observations. An improved distribution

range for the threshold pressures of the intrashales would refine this result as the migration is highly sensitive to small variations in the property with the intrashale behaviour easily interchanging between baffle (with break through) and barrier. The definition of distributions for the threshold pressures of the intrashales would require a probabilitistic analysis of the reservoir using an uncertainty tool to generate multiple realizations.

Table 21 – Comparison of temperature, pressure and density properties per layer from Cavanagh et al. (2015) and the modelled results with the Permedia CO_2 dashboard.

	Modelled in CO2 Dashboard			Cavanagh et al. (2015)		
	Temperature (°C)	Pressure (KPa)	Density(kg/m3)	Temperature (°C)	Pressure (KPa)	Density(kg/m3)
L9	35.4	8123	350	35.0	8120	355
L8	36.6	8431	469	35.9	8430	551
L7	37.1	8578	495	36.4	8600	571
L6	37.8	8775	480	36.9	8770	582
L5	38.3	8922	507	37.3	8910	589
L4	38.9	9069	542	37.7	9060	597
L3	39.4	9216	541	38.1	9200	602
L2	39.9	9363	542	38.6	9370	606
L1	41.0	9659	565	39.5	9710	616

In Permedia the sensitivity and uncertainty analysis functionality offers an indirect control of the variables distribution which means it does not allow for the input values to be directly defined per variable but their variation is based on scalar (multipliers) and coefficients of variation (Permedia derives the corresponding standard deviation from it based on: standard deviation=coefficient of variation *mean). In addition, no filtering tool is available per lithology so one input is applied to all zones. The CO_2 migration properties only are allowed for variation in the uncetainty analysis tool so permeability is not included. The simulated distributions (output) for properties such as threshold pressures and porosity are generated only for the accumulations (within the reservoir sandstones). Therefore, it is not possible to analyse the threshold pressures distributions within the shales/barriers. These were confirmed and discussed with Permedia support in Halliburton that explained a script would need to be developed in order to account for the distributions within the intrashales.Considering the timeframe and academic nature of this thesis this option was not feasible. Consequently, the threshold pressures for the intrashales were defined with iterative experimentation until the vertical stack of 9 CO_2 layers was achieved, as discussed in section 4.4. and shown on Table 7. The controls for this process were the reproduction of a vertical stack of 9 CO_2 layers with a larger accumulation at L5 as observed on seismic (Figure 11) by 2010 and a modelled mass balance of ~100% (total CO_2 mass accumulated in the model is the same as the total mass injected). The replication of the CO_2 plume migration reaching L9 by 1999 was not possible without an uncertainty tool for multiple realizations. Thus some differencies are observed for the CO_2 mass distribution per layer through time for the simple and map-based approaches but the CO_2 plume distribution in 2010 is very similar for both approaches.

The simple approach reaches L9 by 2002 after injection of 5.4 Mt of CO_2 (Table 6) as illustrated on Figure 44. Three years after injection, in 1999, the plume migrates up to L5 which could indicate that the threshold pressures for this layer are slightly high not allowing CO_2 to break through. The addition of heterogeneity in the map-based approach has allowed to increase the threshold pressures distributions and therefore has delayed the arrival of CO_2 into L9 until 2005 (7.92 Mt CO_2 injected), stopping at L4 by 1999

(Figure 45). These variations could have been fine tuned to history match the CO_2 plume with the application of a probability tool for the distribution of threshold pressures in the intrashales.

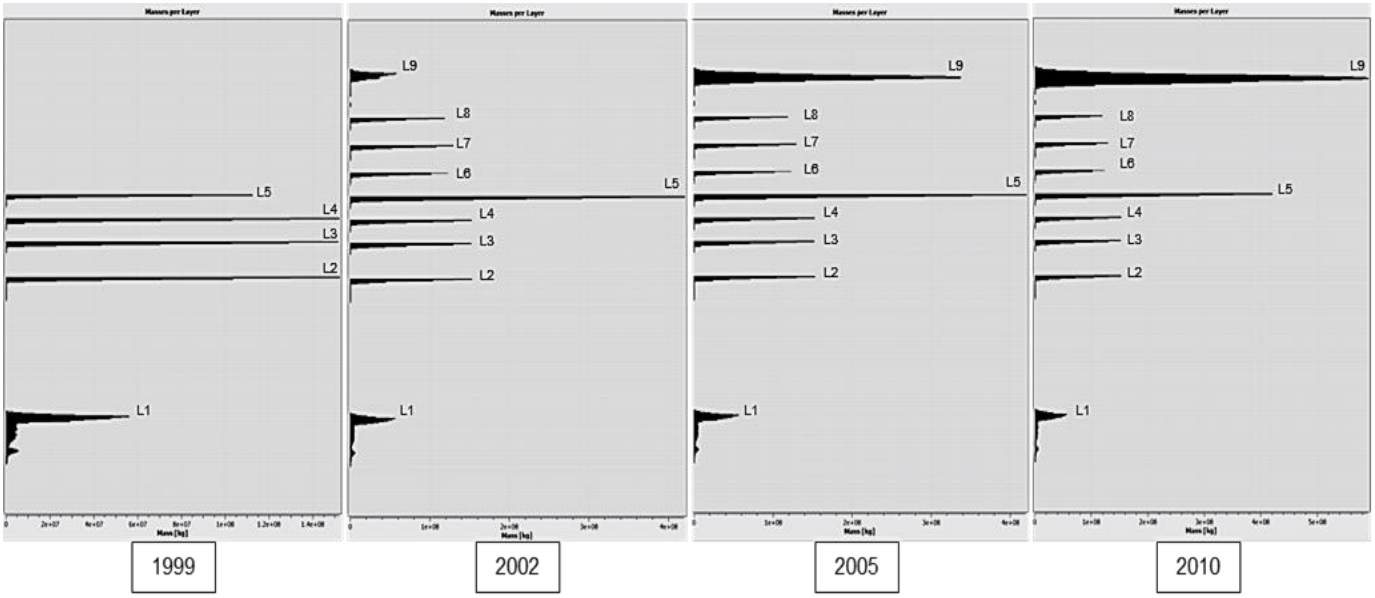

Figure 44 - CO_2 mass accumulated per layer (in kg) per year for the simple approach (1999 X axis from 0 to 1.44 x 10^8 kg; 2002 X axis from 0 to 4 x 10^8 kg; 2005 X axis from 0 to 4 x 10^8 kg; 2010 X axis from 0 to 5.8 x 10^8 kg).

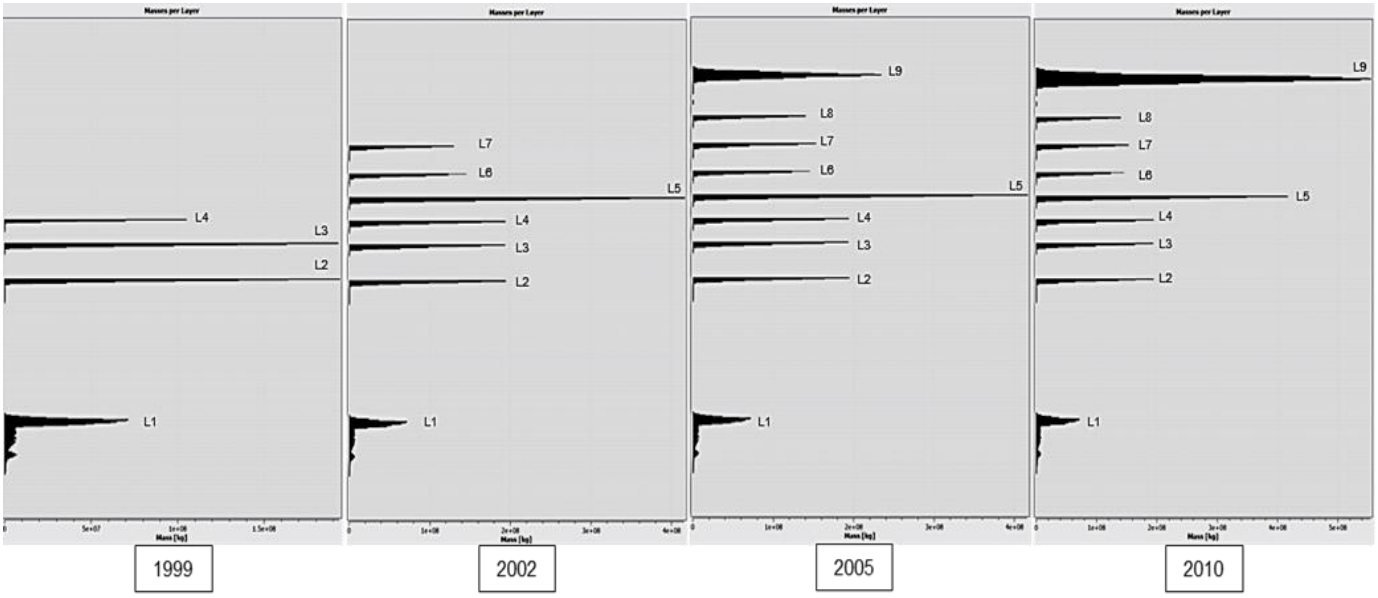

Figure 45- CO_2 mass accumulated per layer (in kg) per year for the map-based approach (1999 X axis from 0 to 2 x 10^8 kg; 2002 X axis from 0 to 4 x 10^8 kg; 2005 X axis from 0 to 4 x 10^8 kg; 2010 X axis from 0 to 5.4 x 10^8 kg).

The map-based approach (Figure 38) did not show a significant improvement on the lateral distribution of the plumes to account for the N-S trend on the sandstones with results very similar to the simple approach (Figure 36). This is a strong indication that the CO_2 plume distribution is highly sensitive to topography.

The heterogeneity added to the intrashales threshold pressures in the map-based approach has increased the CO_2 mass accumulations (kg) in each shale baffle before reaching L9, with the exception of L5, as shown on Figure 46. Both cases have accumulated 100% of the total CO_2 mass of 12.08 Mt injected by 2010 in the model. This is evidence that a heterogeneous model with a range of distribution for the intrashales would significantly improve the match to the observed plume distribution.

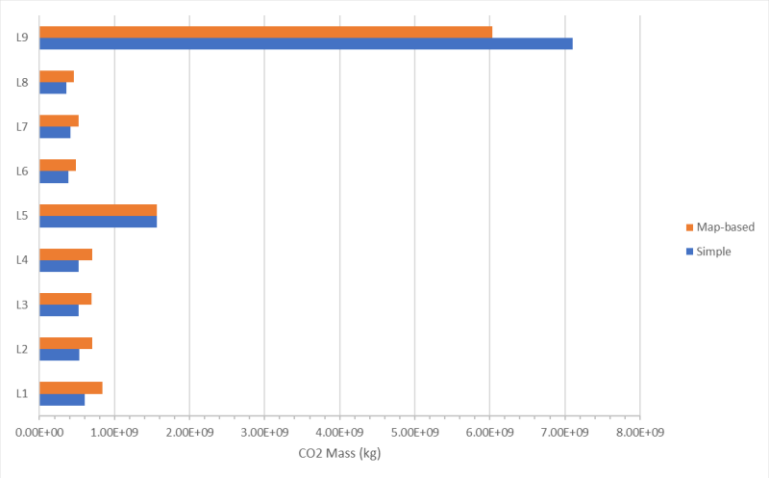

Figure 46 - CO_2 Mass accumulation (kg) per layer for the Simple (blue) and the Map-based (orange) approaches (2010, 12.08 Mt).

The modelled effective horizontal threshold pressures in CO_2-brine system vary between 34 to 51 kPa depending on the layer (IFT values increase upwards) and the effective vertical threshold pressures in CO_2-brine system from 136 to 204 kPa (Table 14), resulting in threshold pressures anisotropy of 4 (ratio Pth_z/Pth_x). The intrashales threshold pressures modelled in the Cavanagh et al. (2015) paper range from 38 to 68 kPa in CO_2-brine system. This is a similar range regarding the effective horizontal threshold pressures of the intrashales. There is no information on the the effective vertical threshold pressures applied by Cavanagh et al. (2015) which could allow for an isotropic assumption.

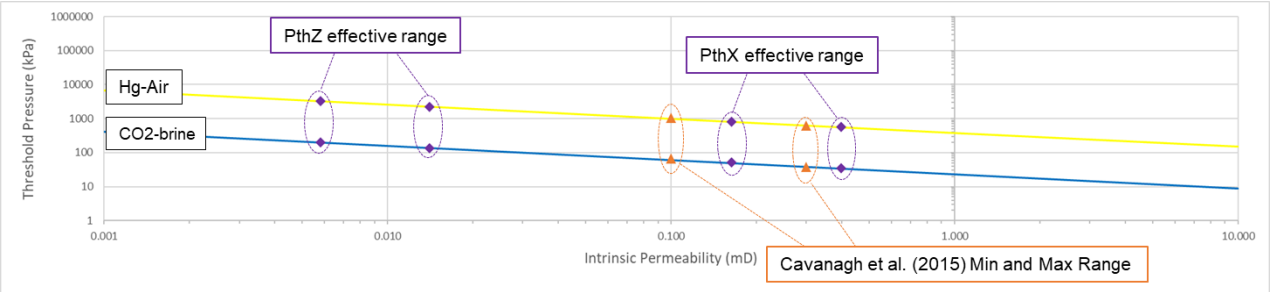

Figure 47 – Effective ranges for intrashales threshold pressures and their corresponding permeabilities based on the Pth-K Average Transform for the modelled results and Cavanagh et al. (2015) in Hg-Air and CO_2-brine systems.

Cavanagh et al. (2015) have explained the estimated threshold pressures for the intrashales of about 50 kPa (CO_2-brine system) to be due to fracturing of the shale barriers associated to pressure fluctuation from rapid deglaciation in the region (~24 ka), as exposed in section 4.2. The consideration of threshold pressures anisotropy has allowed for this effective range to increase to about 200 kPa (CO_2-brine) in the vertical

direction for L5 and 170 kPa (CO_2-brine) on average for the other intrashales layers (L1 to L4 and L6 to L8). Considering the corresponding values for permeabilities with the application of the K-Pth Average Transform as demonstrated on Figure 47, the equivalent permeability kv/kh is about 1/28 (Table 7). This permeability anisotropy (ratio of horizontal to vertical permability) closely approximates to the anisotropy observed in siltstones with some degree of sands (Figure 48). Bioturbation and/or erosion can lead to mixing of silt-mud grade material with sand (Armitage et al., 2011). Zweigel et al. (2000) have suggested that the thin intrashale layers observed in Sleipner may have been partly eroded during deposition of overlying sands.

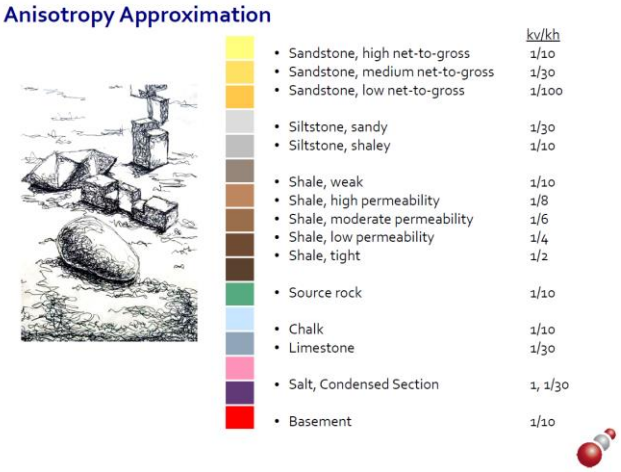

Figure 48 – Permeability anisotropy approximation for different lithologies (from Permedia).

Permeability anisotropy represents the higher permeability of layer-parallel flow (Kh>Kv) and is generally interpreted in terms of the directional fluid flow path length or tortuosity. Armitage et al. (2011) have measured vertical and horizontal permeabilities from cores of caprocks with grain sizes from fine silt to muddy siltstone at 60 MPa effective stress pressures for each sample (total of 8 samples) with ratios varying from 2 to 100, except for one extreme case ~50,000 which is attributed to be due to layering (Figure 49). They have also concluded that increasing clay mineral contents typically reduce permeability logarithmically (by over 4 orders of magnitude), and consequently increase threshold pressures.

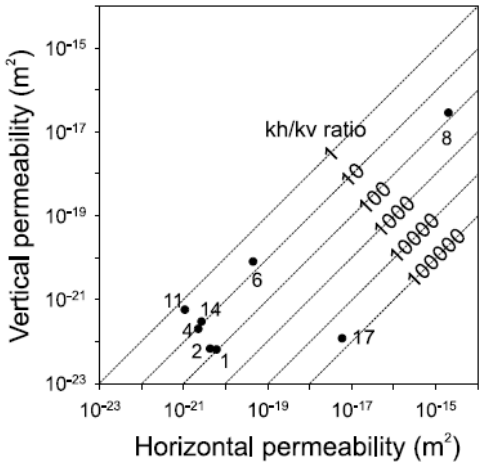

Figure 49 - Horizontal to vertical permeability ratios (kh/kv) at 60 MPa effective stress per sample with grain sizes from fine silt to muddy siltstone. Sample 17 shows an extreme ratio of ~50,000 which is attributed to greater mineralogical layering (Armitage et al., 2011).

The caprock core material sampled at Sleipner discussed in section 2.2 was analysed with X-ray diffraction (XRD) which suggested pore throat diamaters in the range of 2.2 to 21 nm (Kemp et al., 2001). Figure 50 illustrates the grain size distribution measured on the caprock core. According to Lindeberg (1997) it is possible to relate the displacement pore throat radius to the required pressure difference for CO_2 to enter a water wet shale pore as follows:

$$\Delta p = \frac{2\sigma}{r}$$

where, Δp is the required pressure difference (Pa), σ is the surface tension between water and CO_2 (Nm^{-1}) and r is pore throat radius (m). For a CO_2 interfacial tension of 27 mN/m (Cavanagh and Haszeldine, 2014), the capillary entry pressures for the measured caprock pore throat diameters can be estimated with a range of approximately 5 to 50 MPa.

Cavanagh and Haszeldine (2014) have suggested that the low threshold pressures for the intrashales in Sleipner estimated of about 50kPa can only occur in fractured rocks. Therefore they have inferred a network of micro-fractures in the shale barriers within the Utsira Formation with estimated fracture widths around 2µm. Considering the effective threshold pressure in the vertical direction herein estimated to reach about 200 kPa (CO_2-brine) in L5 and 170 kPa (CO_2-brine) for the other intrashales layers, the corresponding calculated pore throat radius would be 27µm and 32 µm, respectively. Hence with pore throat sizes of 54µm and 64µm. Shales generally present a pore throat size range of 0.1 to 0.005 µm (Nelson, 2009). Grain sizes attributed to silts vary between 2 to 63 µm, from fine to coarse silts respectivelly. Pore throats of siliciclastic rocks are typically smaller than their pores (Armitage et al., 2011).

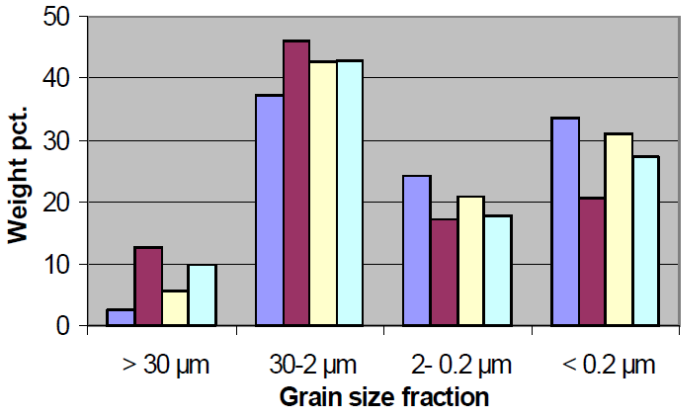

Figure 50- Grain size distribution measured on the caprock core samples (Springer and Lindgren, 2006).

The modelled effective threshold pressures for the intraformational barriers/baffles indicate pore throat sizes and permeability anisotropies relatively coarser and more heterogeneous than the sampled caprock. Therefore, a larger grain size fraction for the intrashales could correspond to the silt size class distribution characterizing silt-rich shales. A decrease in clay minerals results in larger pore throat sizes, higher permeabilities and lower threshold pressures which would allow the intraformational shales to behave as semi-permeable/baffles to the CO_2 migration. Springer and Lindgren (2006) have demonstrated that permeability and capillary entry pressure properties of shalow deposits are very sensitive to grain size distribution and compaction. The cores and cuttings sampled have shown a weakly consolidated state of the sediments deposited at depths of 750-900 m below sea level in the injection area as discussed in section 2.2. Thus the overall capillary entry pressures to supercritical CO_2 for the sampled caprock (~1.7 MPa) and for the intrashales (estimated with a maximum of 204 kPa) are also relatively low in comparison to deeper reservoir systems.

2. Plume Temperature Scenarios

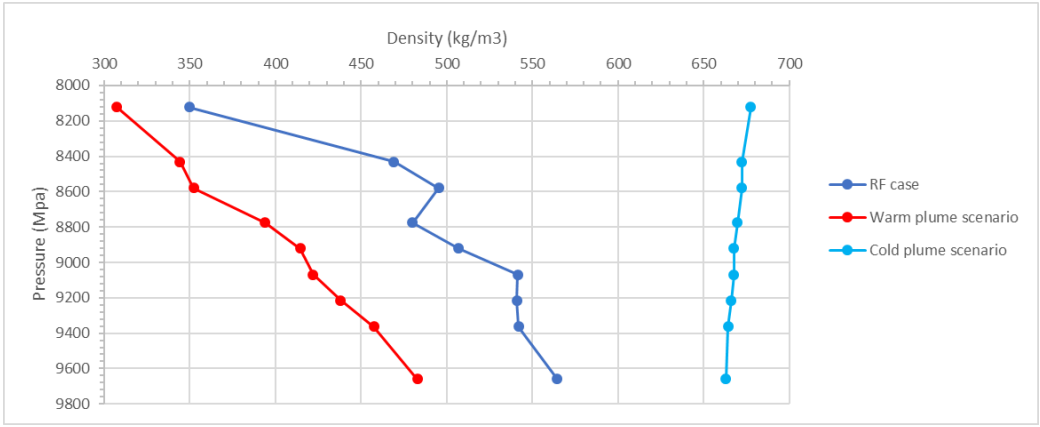

Figure 51 - Comparison of density variation per layer (L9 at the top – 8123 MPa) for the warm and cold scenarios and the reference case.

The warm and cold plume scenarios with their corresponding density variation are compared on Figure 51. The warm plume scenario (37 ºC at the reservoir top, Table 17) consistently presents lower density

values at every layer in comparison to the reference case, with densities decreasing with decreasing pressure (ie. from L1 to L9). The cold plume scenario (31 ºC at the reservoir top, Table 16) presents higher densities with a smaller variation between layers and an increasing density value with decreasing pressure. This is due to the IFT multiplier values decrease upwards in the cold plume scenario since the interfacial tension between CO_2 and brine decreases with decreasing density contrast (brine density 1020 kg/m3; CO_2 density for cold plume scenario of 663 kg/m3 for L1 and 677 kg/m3 for L9).

The less buoyant CO_2 in the cold plume scenario results in larger accumulations in the deepest layer L1 and smaller accumulations on the shallower layers (Figure 39). The large accumulation at L1 shows considerate lateral spilling with breakthrough (leaking) through a small structure towards the NW which impacted the plume upward migration to L9.

On the other hand, in the warm plume scenario the CO_2 is more buoyant (higher densities contrast with brine) requiring smaller accumulations volumes in order the breach the shales (Figure 40). This results in larger CO_2 mass accumulation at the uppermost CO_2 layer L9 (12.08 Mt injected by 2010) as illustrated on Figure 52.

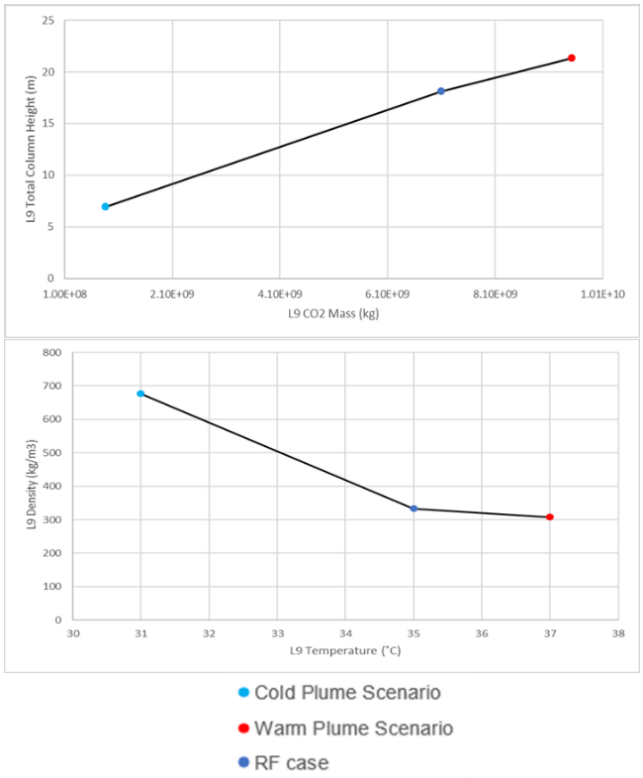

Figure 52 - Comparison between the total CO_2 mass accumulated and total column height for the uppermost layer L9 for the warm and cold scenarios and the reference case (top plot) with 12.08 Mt total CO_2 injected in the reservoir (2010). Uppermost CO_2 layer L9 density variation with temperature (bottom plot).

3. CO_2 Saturations Scenarios

The saturation scenario SC1 reduced the CO_2 saturation so each cell within the accumulations in the reservoir model has reduced its saturation from 89% in the reference case to 40% in SC1. This means that

for the same injected mass of CO_2 (12.08 Mt), SC1 resulted in larger volumes (8% increase) since each backfilled cell is saturated with less CO_2 as demonstrated on Figure 53.

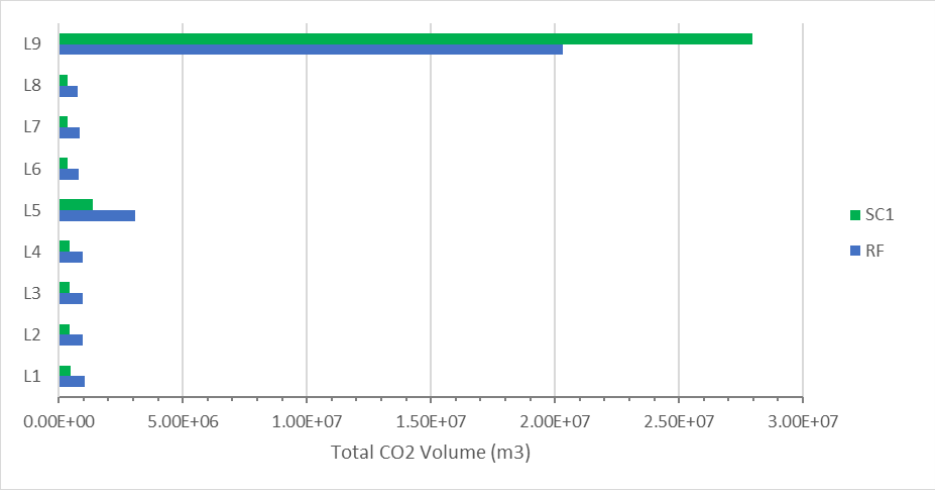

Figure 53 - Comparison between the reference case (CO_2 saturation 89%, blue) and SC1 (CO_2 saturation 40%, green) per layer for the same injected CO_2 mass of 12.08 Mt (2010).

For the saturation scenario SC2, the critical CO_2 saturation increased from 2% in the reference case to 20%. The implication of this change is that the saturation required for a cell to start to invade has increased, therefore increasing the saturations of the migration pathway cells (below the accumulations). This resulted in a 6.5% reduction in the total CO_2 volume accumulated in the SC2 scenario (Table 19). This difference in the accumulated CO_2 volume is evident in the uppermost layer 9 with about 10% reduction as shown on Figure 54.

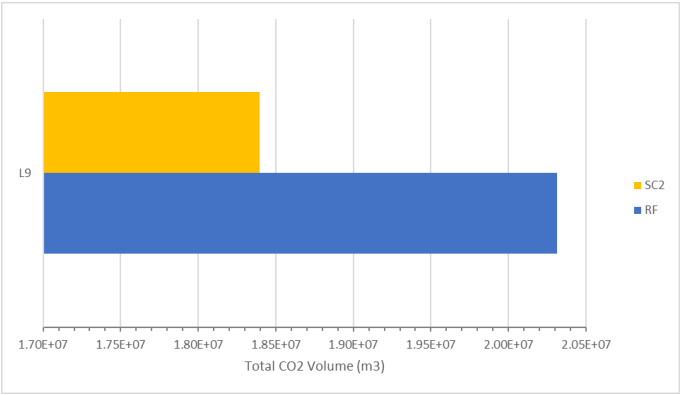

Figure 54 - Total CO_2 volume comparison between reference case (critical CO_2 saturation 2%, blue) and SC2 (critical CO_2 saturation 20%, yellow) for the uppermost CO_2 layer L9.

The saturation scenario SC3 (CO_2 saturation 40% and critical CO_2 saturation 20%) presents an overall total CO_2 mass acummulated very similar to the reference case (0.1% increase). The uppermost layer L9 in the SC3 case resulted in a 26% increase of the total CO_2 volume accumulated in comparison to the reference case, with the other layers with volumes very similar to the SC2 case (Figure 55). The results overal in the SC2 case are more similar to the reference case, whereas SC1 and SC3 are similar to each other. This shows

that the CO_2 saturation parameter had a larger impact on the results than the critical CO_2 saturation. A lithology based (heterogeneous) saturation model would potentially improve these results.

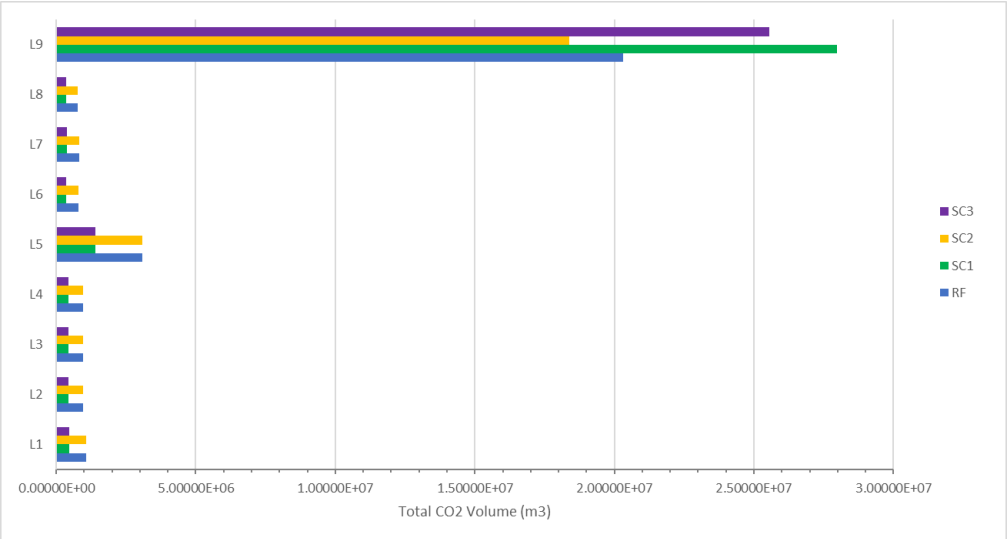

Figure 55 - Total CO_2 volume accumulated per layer for the 3 saturation scenarios and the reference case.

VII. Conclusions

The following points summarize the key factors impacting multi-layer plume distribution in CO_2 storage reservoirs based on the main findings derived from the Sleipner invasion percolation simulation work performed for this master's thesis, with reference simulation illustrated on Figure 36:

- Structure: the CO_2 plume distribution is highly sensitive to topography as it backfills trap structures. This factor was evidenced by the results from the map-based approach which did not follow the input N-S elongation trends;
- Threshold pressures of the intraformational shales: main control on the gravity-dominated CO_2 migration which is also intrinsically related to permeabilities and affects the accumulations' column heights. The modelled effective horizontal threshold pressures for the intrashales varied between 34 to 51 kPa depending on the layer and the effective vertical threshold pressures from 136 to 204 kPa (CO_2-brine system). Their corresponding permeability anisotropies and pore throat diameters can be interpreted as indicative of silt-rich shales which would allow the intraformational shales to behave as semi-permeable/baffles to the CO_2 migration. This result suggests another possible interpretation for the low threshold pressures estimated for the intrashales in the Sleipner reservoir which has been previously explained to be due to fractures (Cavanagh and Haszeldine, 2014);
- Plume temperature profile (and related CO_2 density ranges): the sensitivity analysis of a warm plume scenario with 37ºC at the top of the reservoir and a cold plume scenario with 31ºC, resulted in a CO_2 density range for the uppermost L9 of 307 to 677 kg/m3, respectively. This significant impact on the CO_2 density also indicates that a cold high-density plume results in less buoyant CO_2 with the uppermost layer L9 thickness reduced to about 7 m, whereas the warm low-density and highly buoyant plume increased the L9 thickness to 21 m (12.08 Mt injected, 2010);

- CO_2 saturations: the gas saturations sensitivity study showed that a decrease in the CO_2 saturation within the accumulations (backfilled cells) increases the overall CO_2 volumes, whereas the critical CO_2 saturation parameter reduced the CO_2 volumes overall but with a much smaller impact than expected (<10%), all other parameters kept the same. Therefore, the CO_2 saturation parameter had a larger impact on the accumulations results than the critical CO_2 saturation.

It is recommended for future work for the reservoir model to be built in a reservoir modelling package (like RMS or Petrel) in order to allow incorporation of geological heterogeneities with rock properties distributions per facies/lithology (porosity, permeability, threshold pressures and saturations). This heterogeneous model can be imported into the Permedia software for the CO_2 migration simulations. Different scenarios could be considered to capture the depositional environments interpretations.

The incorporation of interpreted CO_2 chimneys and feeders (leakage points) from seismic (Furre and Eiken, 2013) in the simulation of the Sleipner CO_2 reservoir could potentially provide a successful match to the observed vertical distribution and lateral spread of each CO_2 layer. Williams and Chadwick (2018) have achieved a satisfactory history match of the Sleipner plume in the Eclipse simulator with the addition of vertical pathways chimneys and N-S high permeability sand bodies within the Sand Wedge and Utsira Formation units. Small variations in the topography of the reservoir surfaces can also have a large impact on the CO_2 lateral distribution, therefore a detailed structural uncertainty assessment capturing seismic interpretation and depth conversion uncertainties would be suggested to develop a robust prediction model.

VIII. References

Alnes, H., Eiken, O. and Stenvold, T. (2008). Monitoring gas production and CO_2 injection at the Sleipner field using time-lapse gravimetry. *Geophysics*, **73**:6, P. WA155-WA161.

Alnes, H., Eiken, O., Nooner, S., Sasagawa, G., Stenvold, T. and Zumberge, M. (2011). Results from Sleipner gravity monitoring: updated density and temperature distribution of the CO_2 plume. *Energy Procedia*, **4**, 5504-5511.

Andersen, O. (2017). Simplified models for numerical simulation of geological CO_2 storage. Phd thesis, University of Bergen, 290p.

Armitage, P. J., Faulkner, D. R., Worden, R. H., Aplin, A. C., Butcher, A. R. and Iliffe, J. (2011). Experimental measurement of, and controls on, permeability and permeability anisotropy of caprocks from the CO_2 storage project at the Krechba Field, Algeria. *Journal of Geophysical Research*, **116**, B12208.

Arts, R., Eiken, O., Chadwick, A., Zweigel, P., van der Meer, B. and Kirby, G. (2004). Seismic monitoring at the Sleipner underground CO_2 storage site (North Sea). *Geological Society, London, Special Publications*, 233(1), 181-191.

Arts, R., Chadwick, A., Eiken, O., Thibeau, S. and Nooner, S. (2008). Ten years' experience of monitoring CO_2 injection in the Utsira Sand at Sleipner (offshore Norway). *First Break*, **26**, 65–72.

Baklid, A., Krobøl R. and Owren, G. (1996). Sleipner Vest CO_2 disposal, CO_2 injection into a shallow underground aquifer. *SPE*, 36600, 269-277.

Bickle, M., Chadwick, A., Huppert, H.E., Hallworth, M. and Lyle, S. (2007). Modelling carbon dioxide accumulation at Sleipner: Implications for underground carbon storage. *Earth and Planetary Science Letters*, **255**, 164-176.

Boait, F.C., White, N.J., Bickle, M.J., Chadwick, R.A., Neufeld, J.A. and Huppert, H.E. (2012). Spatial and temporal evolution of injected CO_2 at the Sleipner Field, North Sea. Journal of Geophysical Research, vol. 117, BO3309.

Bandilla, K.W., Celia, M.A. and Leister, E. (2014). Impact of Model Complexity on CO_2 plume modeling at Sleipner. *Energy Procedia*, GHGT-12, **63**, 3405-3415.

Cavanagh, A.J. and Ringrose, P. (2011). Simulation of CO_2 distribution at the In Salah storage site using high-resolution field-scale models. *Energy Procedia*, **4**, 3730–3737.

Cavanagh, A.J. (2013) Benchmark calibration and prediction of the Sleipner CO_2 plume from 2006 to 2012. *Energy Procedia*, **37**, 3529–3545.

Cavanagh, A.J. and Haszeldine, R.S. (2014) The Sleipner storage site: Capillary flow modeling of a layered CO_2 plume requires fractured shale barriers within the Utsira Formation. *International Journal of Greenhouse Gas Control*, **21**, 101-112.

Cavanagh, A.J. and Nazarian, B. (2014) A new and extended Sleipner Benchmark model for CO_2 storage simulations in the Utsira Formation. *Energy Procedia*, **63**, 2831-2835.

Cavanagh, A.J., Haszeldine, R.S. and Nazarian, B. (2015) The Sleipner CO_2 storage site: using a basin model to understand reservoir simulations of plume dynamics. *First Break*, **33**, 61-68.

Carruthers, D. and Ringrose, P. (1998). Secondary oil migration: oil-rock contact volumes, flow behaviour and rates. *In:* Parnell, J. (ed.). Dating and Duration of Fluid Flow and Fluid-Rock Interaction. *Geological Society*, London, Special Publications, **144**, 205-220.

Chadwick, R.A., Zweigel, P., Gregersen, U., Kirby, G.A., Holloway, S. and Johannessen, P.N. (2004a). Geological reservoir characterization of a CO_2 storage site: The Utsira Sand, Sleipner, northern North Sea. *Energy*, **29**, 1371-1381.

Chadwick, R.A., Arts, R., Eiken, O., Kirby, G.A., Lindeberg, E. and Zweigel, P. (2004b). 4D seismic imaging of an injected CO_2 plume at the Sleipner Field, central North Sea. In: Davies, R.J., Cartwright, J.A., Stewart, S.A., Lappin, M. and Underhill, J.R. (eds.) *3D Seismic Technology: Application to the Exploration of Sedimentary Basins.* Geological Society of London, Memoirs, **29**, 311-320.

Deegan, C. E. and Scull, B. J. (1997). A proposed standard lithostratigraphic nomenclature for the Central and Northern North Sea. Report of the Institute of Geological Sciences, No. 77/25. Bulletin of the Norwegian Petroleum Directorate, No. 1.

Eidvin, T., Riis, F. and Rundberg, Y. (1999). Upper Cainozoic stratigraphy in the central North Sea (Ekofisk and Sleipner fields). *Norsk Geologisk Tidsskrift*, **79**, 97-128.

Eidvin, T., Riis, F., Rasmussen, E.S. and Rundberg, Y. (2013). Investigation of Oligocene to Lower Pliocene deposits in the Nordic offshore area and onshore Denmark. *NPD Bulletin*, **10**, 1-46.

Eiken, O., Ringrose, P., Hermanrud, C., Nazarian, B., Torp, T.A. and Høier, L. (2011). Lessons Learned from 14 years of CCS Operations: Sleipner, In Salah and Snøhvit. *Energy Procedia*, **4**, 5541-5548.

England, W.A., Mackenzie, A.S., Mann, D.M. and Quigley, T.M. (1987). The movement and entrapment of petroleum fluids in the subsurface. *Journal of the Geological Society*, **144,** 327-347.

Flett, M.A., Gurton, R.M. and Taggart, I.J. (2005). Heterogeneous saline formations: Long-term benefits for geo-sequestration of greenhouse gases. *Proceedings of the 7th International Conference on Greenhouse Gas Control Technologies* (GHGT-7), v. I, 501-510.

Furre, A.K. and Eiken, O. (2013). Dual sensor streamer technology used in Sleipner CO_2 injection monitoring. *Geophysical Prospecting*, European Association of Geoscientists and Engineers, 1-14.

Furre, A.K., Kiær, A. and Eiken, O. (2015) CO_2-induced seismic time shifts at Sleipner. Interpretation, vol. 3, no. 3, pp. SS23-SS35.

Furre, A.K., Eiken, O., Alnes, H., Vevatne, J.N. and Kiær, A.F. (2017). 20 years of monitoring CO_2-injection at Sleipner. *Energy Procedia*, **114**, 3916 – 3926.

Fyfe, J. A., Gregersen, U., Jordt, H., Rundberg, Y., Eidvin, T., Evans, D., Stewart, D., Hovland, M. and Andresen, P. (2003). Oligocene to Holocene. *In* Evans, D., Graham, C., Armour, A. and Bathurst, P., (eds). *The Millennium Atlas: petroleum geology of the central and northern North Sea*. London: The Geological Society of London. 279-287.

Galloway, M. E., Garber, J. L., Xijin, Liu and Sloan, B. J. (1993). Sequence stratigraphic and depositional framework of the Cenozoic fill, Central and Northern North Sea Basin. *Petroleum Geology of Northwest Europe* (Ed. J. R. Parker), Proceedings of the 4th Conference, The Geological Society, London, 33-43 p.

Galloway, W. E. (2002). Palaeogeographic setting and depositional architecture of a sand-dominated shelf depositional system, Miocene Utsira Formation, North Sea Basin. *Journal of Sedimentary Research*, 72, 476-490.

Gasda, S.E., Wangen, M., Bjørnara, T.I. and Elenius, M.T. (2016). Investigation of caprock integrity due to pressure build-up during high-volume injection into the Utsira formation. *Energy Procedia*, **114**, 3157-3166.

GCCSI (2017). The Global Status of CCS: 2017. *Global CCS Institute*, Docklands, Victoria, Australia, www.globalccsinstitute.com

Gregersen, U., Michelsen, O. and Sørensen, J. C. (1997). Stratigraphy and facies distribution of the Utsira Formation and the Pliocene sequences in the northern North Sea. *Marine and Petroleum Geology*, **14**, 893-914.

Gregersen, U. and Johannessen, P.N. (2007). Distribution of the Neogene Utsira Sand and Hutton Sand, and the succeeding deposits in the Viking Graben area, North Sea. *Marine and Petroleum Geology*, **24**, 591–606.

Hantschel, T. and Kauerauf, A.I. (2009). Fundamentals of Basin and Petroleum Systems Modeling. Springer, 476p.

Harper, T.R. and Lundin, E.R. (1997) Fault seal analysis: reducing our dependence on empiricism. In: Møller-Pedersen, P. & Koestler, A. G. (Eds.) Hydrocarbon Seals: Importance for Exploration & Production, NPF Special Publication, 7, Elsevier, 149-165.

Harrington, J.F., Noy, D.J., Horseman, S.T., Birchall, D.J. and Chadwick, R.A. (2008). Laboratory study of gas and water flow in the Nordland Shale, Sleipner, North Sea. *In:* Grobe, M., Pashin, J. and Dodge, R. (Eds.) *Carbon Dioxide Sequestration in Geological Medi*a. AAPG Special Publication, in press.

Head, M.J., Riding, J. B., Eidvin, T. and Chadwick, R. W. (2004). Palynological and foraminiferal biostratigraphy of (Upper Pliocene) Nordland Group mudstones at Sleipner, northern North Sea. *Marine and Petroleum Geology*, **21**, 277-297.

Hermanrud, C., Andresen, T., Eiken, O., Hansen, H., Janbu, A., Lippard, J., Bolås, H.N., Simmenes, T.H., Teige, G.M.G. and Østmo, S. (2009). Storage of CO_2 in saline aquifers – lessons learned from 10 years of injection into the Utsira Formation in the Sleipner area. *Energy Procedia*, **1**, 997-2004.

Hermanrud, C., Teige, G.M.G., Iding, M., Eiken, O., Rennan, L. and Østmo, S. (2010). Differences between flow of injected CO_2 and hydrocarbon migration. *In*: Vining, B.A. And Pickering, S.C. (eds). *Petroleum Geology: From Mature Basins to New Frontiers – Proceedings of the 7th Petroleum Geology Conference*, 1183-1188.

Hubbert, M.K. (1953). Entrapment of Petroleum under Hydrodynamic Conditions. *AAPG Bulletin*, Vol. 37, No. 8, 1954-2026.

IEA. (2016a). CO_2 Emissions from Fuel Combustion – 2016 edition. *Key CO_2 Emissions Trends*. International Energy Agency (IEA), Paris.

IPCC (2005). Underground Geological Storage. Chapter 5, 195-276 p. In *IPCC Special Report on Carbon Dioxide Capture and Storage*. Prepared by Working Group III of the Intergovernmental Panel on Climate Change [Metz, B., O. Davidson, H. C. de Coninck, M. Loos, and L. A. Meyer (eds.)]. Cambridge University Press, Cambridge, United Kingdom and New York, NY, USA, 442 pp.

Justwan, H. (2006). The Petroleum Systems of the South Viking Graben, Norway. Phd thesis, University of Bergen, 37 p.

Kemp, S.J., Bouch, J. and Murphy, H.M. (2001). Mineralogical characterization of the Nordland Shale, UK Quadrant 16, Northern North Sea. British Geological Survey Comissioned Report, CR/01/136.

Kennett, C. (2008). Evaluation of internal geometries within the Miocene Utsira Formation to establish the geological concept of observed CO_2 responses on 4D seismic in the Sleipner area, North Sea. MSc Petroleum Geoscience, Imperial College London, 66 p.

Kirby, G. A., Chadwick, R. A. and Holloway, S. (2001). Depth mapping and characterisation of the Utsira Sand Saline Aquifer, Central and Northern North Sea. British Geological Survey Commissioned Report, CR/01/218., 26 p.

Kiær, A. F., Eiken, O., & Landrø, M. (2016). Calendar time interpolation of amplitude maps from 4D seismic data. Geophysical Prospecting, 64(2), 421-430.

Lindeberg, E. (1997). Escape of CO_2 from aquifers. *Energy Conversion and Management*, 38, S235- S240 p.

Nelson, P.H. (2009) Pore-throat sizes in sandstones, tight sandstones, and shales. *AAPG Bulletin*, **93**:3, 329-340 p.

Nielsen, H.M., Herrera, P.A., Ashraf, M., Ligaarden, I., Iding, M., Hermanrud, C., Lie, K., Nordbotten, J.M., Dahle, H.K. and Keilegavlen, E. (2011). Field-case simulation of CO_2-plume migration using vertical-equilibrium models. *Energy Procedia*, **4**, 3801-3808.

Ringrose, P. S. (2017). Principles of sustainability and physics as a basis for the low-carbon energy transition. *Petroleum Geoscience*, **23**, 287-297.

Ringrose, P.S. (2018). The CCS hub in Norway: some insights from 22 years of saline aquifer storage. *Energy Procedia*, **146**, 166-172.

Rundberg, Y. (1989). Tertiary sedimentary history and basin evolution of the Norwegian North Sea between 60ºN - 62º N – an integrated approach. Unpublished Dr. Ling thesis. University of Trondheim, Norway, (Reprinted 1991 in report of the Institute for Geology and Rock Mechanics, University of Trondheim, Norway, No. 25).

Rundberg, Y., & Eidvin, T. (2002). Significance of Oligo-Miocene tectonism in the reconstruction of sedimentary and oceanographic history of the northern North Sea. In A. Hurst (Ed.), Onshore–offshore relationships on the Nordic Atlantic margin (Vol. 2) (pp. 175–176). Abstracts and Proceedings of the Norwegian Geological Society (Norsk Geologisk Forening).

Senior, W.J., Kantorowicz, J.D. and Wright, I.W. (2010). Geological storage of carbon dioxide: an emerging opportunity. *In*: Vining, B.A. And Pickering, S.C. (eds). *Petroleum Geology: From Mature Basins to New Frontiers – Proceedings of the 7th Petroleum Geology Conference*, 1165-1169.

Slatt, R. M. (2006). Stratigraphic Reservoir Characterization for Petroleum Geologists, Geophysicists and Engineers. *Handbook of Petroleum Exploration and Production*, Volume 6, 478 p.

Singh, V.P., Cavanagh, A.J, Hansen, H., Nazarian, B., Iding, M. and Ringrose, P.S. (2010). Reservoir Modeling of CO_2 plume behavior calibrated against monitoring data From Sleipner, Norway. *SPE 134891*, 19.

Sorkhabi, R., and Tsuji, Y. (2005). The place of faults in petroleum traps. In: Sorkhabi, R., and Tsuji, Y. (Eds.) Faults, Fluid Flow and Petroleum Traps. AAPG Memoir, 85, 1-31.

Springer, N. and Lindgren, H. (2006). Caprock properties of the Nordland Shale recovered from the 15/9-A-11 well, the Sleipner area. *In* GHGT-8: 8th International Conference on Greenhouse Gas Control Technologies, Trondheim, Norway, June 19–22. Elsevier, Oxford, 6.

Valberg, E. (2014). Time-lapse seismic interpretation of injected CO_2 plume at the Sleipner Field, North Sea. MSc thesis, University of Tromsø, 114p.

Vavra, C.L., Kaldi, J.G. and Sneider, R.M. (1992). Geological Applications of Capillary Pressure: A Review. *The American Association of Petroleum Geologists Bulletin*, **76**, 840-850.

Watsend, L. (2012). Vertical flow of CO_2 in the Utsira Formation. MSc in Petroleum Geoscience, University of Bergen, 86 p.

Williams, G. and Chadwick, A. (2017). An improved history-match for layer spreading within the Sleipner plume including thermal propagation effects. Energy Procedia, 114, 2856 – 2870.

Williams, G., Chadwick, A. and Vosper, H. (2018) Some thoughts on Darcy-type flow simulation for modelling underground CO_2 storage, based on the Sleipner CO_2 storage operation. *International Journal of Greenhouse Gas Control*, **68**, 164-175.

Williams, G. and Chadwick, A. (2018). Chimneys And Channels: History Matching The Growing CO_2 Plume At The Sleipner Storage Site. Fifth CO2 Geological Storage Workshop, *EAGE*. 1-5p.

Ziegler, P. A. (1981). Evolution of sedimentary basins in north-west Europe. *In*: Illing, L. V. and Hobson, G. D. (eds). Petroleum geology of the continental shelf of North-West Europe. London: Heyden and Son. 3-39.

Zweigel, P., Hamborg, M., Arts, R., Lothe, A., Sylta, Ø. and Tømmerås, A. (2000). Prediction of migration of CO_2 injected into an underground depository: reservoir geology and migration modelling in the Sleipner case (North Sea). Fifth International Conference on Greenhouse Gas Control Technologies, Cairns, Australia, 6 p.

Zweigel, P., Arts, R., Lothe, A.E and Lindeberg, E. (2004). Reservoir geology of the Utsira Formation at the first industrial-scale underground CO_2 storage site (Sleipner area, North Sea). In: Geological Storage of Carbon Dioxide for Emissions Reduction, S. Baines, J. Gale and R. Worden, Eds., London, Geological Society, pp. 165-180.

Appendix 1 – Input Parameters (SPE 134891)

SPE Utsira Table					
Formation properties	**Symbol**	**Units**	**Assumed reference case properties**	**Range**	**References and comments**
Seabed temperature	T_s	°C	7	6,1-7,2	Institute of Marine Research (Norway), 11.05.10.
Geothermal gradient	dT/dz	°C/km	35.6		Lindeberg et al. 2000.
Hydrostatic gradient	dP_H/dz	MPa/km			Assumed hydrostatic equilibrium (pgh)
Lithostatic gradient	dP_L/dz	MPa/km	17		Assumed lithostatic gradient based on typical values (poro=0.36; rho=2700 kg/m3)
Total Utsira Fm area	A	km^2	26100		Chadwick et al. 2002.
Total reservoir thickness	h_{res}	m	255	50-300	Assumed value derived from well log 15/9-A16 (CO2 injector); Range: Zweigel et al. 2000.
L9 model area	A	km^2	18		Defined as model area (3 x 6 km)
Top L9 depth	Z	m TVD SS	817.3	802,2-840,5	Defined by seismic depth map
L9 thickness	h_{L9}	m	11,3	3,5-26,3	Defined by seismic depth map
Intrashale thickness	h_{sh}	m	6.5		Intrashale between layer 8 and 9
Caprock porosity	φ_{cap}	%	35	34-36	Springer and Lindgren (2006)
Caprock permeability	k_{cap}	md	0.0010	0,00075-0,0015	Springer and Lindgren (2006)
Caprock threshold pressure	P_{th}	MPa	1.7		Springer and Lindgren (2006)
Utsira porosity	φ_{frm}	%	36	27-40	Lothe and Zweigel, 1999; Holloway et al. 2000
Utsira permeability	k_{xy}	md	2000	1100-5000	Lindeberg et al. 2000.
Utsira anisotropy	k_v/k_{xy}	[/]	0.1		Assumed based on general petroleum reservoir analogue data, e.g. Ringrose et al. 2005.
Shale porosity	φ_{sh}	%	34	31-38	Zweigel et al. 2000; Yang and Aplin 2004. Porosity in shales is very uncertain and controlled by clay content and effective stress.
Shale permeability	k_{sh}	md	0.0010	0,00075-0,0015	Assume same as caprock, but has a large uncertainty. Springer and Lindgren, 2006.
Assumed coordinates of L9 injection point	l_{xyz}	[/]	x: 438516; y: 6,47121e+06		z: bottom of layer 8 (L89 model) or layer 9 (L9 model)
Injection perforation length	l_{perf}	m	38		Hansen et al. 2005
Depth to top perforation	l_{depth}	m TVD MSL	1010.5		Hansen et al. 2005. Interval is 1010,5-1013 m TVD MSL
Injected mass	M				Defined by exp function/table based on seismic
Injection period	t_{inj}				Defined by exp function/table based on seismic
Injection rate	r_{inj}				Defined by exp function/table based on seismic
CO2 phase behaviour					Defined by PR EOS (tuned Cpen 4.5)
Critical gas saturation	S_{gcrit}	[/]	0.02		
Connate water saturation	S_{gmax}	[/]	0.89		
Residual gas saturation	S_{resid}	[/]	0.21		
Interfacial tension factor	IFT factor	[/]	0.0625		IFT factor at the top of the model. Fluid conversion factor = IFT(hw) x Cos θ / IFT(ma) * cos θ, where hw is hydrocarbon water interface; ma is mercury air interface, and θ is wetting angle for the respective systems
CO2 viscosity	μ_{CO2}	mPas	6.00E-02		NIST data. Defined by PR EOS (tuned Cpen 4.5)
CO2 density	ρ_{CO2}	kg/m^3	760		Alnes et al. 2008.
Porewater salinity	W_{NaCl}	ppm	33500		Assumed. Seawater EOW calculator.
Porewater viscosity	μ_W	Pas	8.00E-04	0.00079-0.000875	CREWES fluid property calculator. Assumed salinity of 33,500 ppm and pressure of 8.1 MPa. Temperatures taken from PVT range: 31 and 37 deg C.
Porewater density	ρ_W	kg/m^3	1020		Bickle et al. 2007.